UNIVERSITI TEKNOLOGI MARA

SYNTHESIS AND CHARACTERIZATION OF Z-SCHEME SILVER CARBONATE WITH CADMIUM SULFIDE FOR ENHANCEMENT OF PHOTOCATALYTIC DEGRADATION OF METHYL ORANGE UNDER VISIBLE LIGHT

OMMY MADINA BINTI ABDUL HALIM

MSc

July 2026

UNIVERSITI TEKNOLOGI MARA

SYNTHESIS AND CHARACTERIZATION OF Z-SCHEME SILVER CARBONATE WITH CADMIUM SULFIDE FOR ENHANCEMENT OF PHOTOCATALYTIC DEGRADATION OF METHYL ORANGE UNDER VISIBLE LIGHT

OMMY MADINA BINTI ABDUL HALIM

Thesis submitted in fulfilment
Of the requirements for the degree of
Master Of Science
Applied Chemistry

Faculty of Applied Science

July 2026

CONFIRMATION BY PANEL OF EXAMINERS

I certify that a Panel of Examiners has met on 04 March 2026 to conduct the final examination of Ommy Madina Abdul Halim on her Master of Science thesis entitled "Synthesis and Characterization of Z-Scheme Silver Carbonates with Cadmium Sulfide for Enhancement of Photocatalytic Degradation of Methyl Orange Under Visible Light" in accordance with Universiti Teknologi MARA Act 1976 (Akta 173). The Panel of Examiners recommends that the student be awarded the relevant degree. The Panel of Examiners was as follows:

Mohd Lokman Ibrahim (PhD)
Associate Professor
Faculty of Applied Sciences
Universiti Teknologi MARA
(Chairman)

Zul Adlan Mohd Hir (PhD)
Associate Professor
Faculty of Applied Sciences
Universiti Teknologi MARA
(Internal Examiner)

Nurfatehah Wahyuny Che Jusoh (PhD)
Associate Prof
Malaysia-Japan International Institute of
Technology Universiti Teknologi
Malaysia
(External Examiner)

PROFESSOR DR HJH ZURAEDA IBRAHIM
Dean
Institute Postgraduate Studies
Universiti Teknologi MARA

Date: 13 July 2026

AUTHOR'S DECLARATION

I declare that the work in this thesis was carried out in accordance with the regulations of Universiti Teknologi MARA. It is original and is the results of my own work, unless otherwise indicated or acknowledged as referenced work. This thesis has not been submitted to any other academic institution or non-academic institution for any degree or qualification.

I, hereby, acknowledge that I have been supplied with the Academic Rules and Regulations for Postgraduate, Universiti Teknologi MARA, regulating the conduct of my study and research.

Name of Student	:	Ommy Madina Binti Abdul Halim
Student ID. No.	:	2023956629
Programme	:	Master of Science (Applied Chemistry)
Faculty	:	Applied Sciences
Thesis Title	:	Synthesis and Characterization of Z-Scheme Silver Carbonates with Cadmium Sulfide for Enhancement of Photocatalytic Degradation of Methyl Orange Under Visible Light
Signature of Student	:	
Date	:	July 2026

ABSTRACT

Methyl orange (MO) is an anionic azo dye commonly used in food, textile, leather, and paper industries. However, its discharge into the environment causes serious concerns due to its toxicity, mutagenicity, carcinogenicity, and high stability, which make it difficult to degrade by conventional methods. Among various alternatives, photocatalytic degradation has emerged as an effective approach for removing MO. Silver carbonate (Ag_2CO_3) has demonstrated excellent photocatalytic activity due to its abundant active sites, but the rapid recombination of photogenerated electron–hole pairs limit its efficiency. To overcome this, the construction of Z-scheme heterojunction systems has been proposed, offering improved charge separation and strong redox potential. Cadmium sulfide (CdS), with its suitable band gap energy, is a promising candidate for coupling with Ag_2CO_3 to form such heterostructures. Therefore, this study focuses on synthesizing CdS-loaded Ag_2CO_3 photocatalysts via a facile precipitation method and evaluating their photocatalytic performance in the degradation of methyl orange.In addition, the modified photocatalyst were characterized by using X-ray diffraction (XRD), Field Emission Scanning Electron microscopy (FESEM), Transmission-electron Microscopy (TEM), X-ray Photoelectron spectroscopy (XPS), Photoluminescence (PL), Fourier Transform Infrared (FTIR), and Ultraviolet-visible Diffuse Reflectance Spectroscopy (UV-Vis DRS). The mass ratio of CdS was varied from 5 to 15 wt% and denoted as x-ACD, namely 5 ACD, 10 ACD and 15 ACD. XRD and FTIR analyses the confirmation of the successful preparation of the Ag_2CO_3/CdS composite, where CdS incorporation alters peak intensities due to good dispersion and strong interaction between components, especially evident in the 10ACD sample. In addition, the FESEM mapping and TEM image reveals the same pattern which the Ag_2CO_3/CdS composite exhibits well-dispersed Cd and S elements on Ag_2CO_3 with modified morphology, where the 10ACD sample shows optimal distribution leading to higher active sites and improved surface accessibility. With the good dispersion of both photocatalyst, 10ACD exhibits the lowest PL intensity that illustrates the effective electron hole recombination. Hence, the photocatalytic performance of MO over different ratio loaded on silver carbonates were in following order: 10ACD (94.38%) > 15ACD(83.28%) > 5ACD (80.56%) while Ag_2CO_3 and CdS obtained 75.22% and 81.61% respectively. The optimum performance was ascribed to the 10 ACD with the higher photocatalytic activity and appropriate band gap energy at 2.05 eV as reported with UV-Vis DRS. As the proposed mechanism for the MO, it successfully illustrated that hydroxyl radical on the surface was the main active species in the reaction which align that CdS has lower negative valence band (VB) and endow more hole with high oxidizing ability. Moreover, XPS analysis revealed that the binding energies of 10ACD were blue shifted compared Ag_2CO_3 highlights the function of electron donor while CdS acts as electron acceptor simultaneously due to the 10ACD showed the reduced binding energy than the pure CdS. As a conclusion, this study elucidates the synergistic interfacial interaction between Ag_2CO_3 and CdS in constructing an efficient Z-scheme heterojunction photocatalyst, leading to enhanced photocatalytic degradation of organic pollutants in wastewater, in alignment with the Sustainable Development Goal of clean water and sanitation (SDG 6).

ACKNOWLEDGEMENT

Alhamdulillah, all praises to Allah, the Most Gracious and Most Merciful, for granting me the strength, patience, and perseverance to complete this thesis. This journey has been a challenging yet rewarding experience, and it would not have been possible without the support, encouragement, and guidance of many individuals and institutions.

First and foremost, I extend my deepest gratitude to my supervisor, Dr. Mohammad Saifulddin Mohd Azami, Ts. Dr Zuliahani Ahmad and Ts. Dr Md Uwaisul Qarni for his invaluable advice, constructive feedback, and constant motivation throughout this journey. Their guidance has not only shaped this research but also inspired me to grow as a researcher and individual.

To my beloved family Abah, Abdul Halim Salleh, and Ibu, your unconditional love, prayers, and sacrifices have been the foundation of my strength. Your endless doa, financial support, and unwavering encouragement, which cannot be fully expressed in words, have carried me through every step of this journey. To my wonderful siblings, Nur Atiqah, Mohammad Safuan, Intan Sapura, and Muhammad Syafiq thank you for always being there for me, cheering me on, and believing in me. To my adorable nieces and nephews, Syahadah Afiya, Aafiy Syaheed, Aariz Syaheed, and Iman Suhayl, you have been a source of light and joy during this journey.

To my dearest friend who feels more like a sister, Nurul Shafiqah Hazelin, you are truly a gift from Allah SWT. You have been my constant companion through every laugh, every tear, and every storm I've faced along this journey. Our bond goes beyond friendship; it feels like a connection destined for eternity. Your unwavering support, endless patience, and contagious laughter have turned the darkest days into moments of hope and strength. In you, I found not just a friend, but someone who stands by me like family, who believes in me when I'm struggled to believe in myself, and who celebrates every step of my journey as if it were her own. Thank you for being my rock, my cheerleader, and my sister in all but blood.

To my amazing friends who have also been a source of motivation and encouragement: Zurita Jaafar, Dr Afiq, Dr Raihan, Syuib, Aien, Isa, Aliff Haikal, Nadia, Batrisya, Nabila, Hamidah, Nonis, Ain, Syamimi, Syazwani, Rahil, Nureel, Nadiah, Dr. Siti Nurlia, Ts. Dr. Abu Hassan, Dr. Muhammad Faiz Pa'suya. I am truly grateful for your support, kind words, and belief in me throughout this journey. To my research team, Araucat , Assoc. Prof Dr Wan Izhan Nawawi - you have been instrumental in shaping me into a better researcher. Your guidance, teamwork, and willingness to share knowledge have been invaluable throughout this academic journey.

Finally, to everyone who has directly or indirectly contributed to this journey—your kindness, encouragement, and belief in me have left an indelible mark on my heart.

This thesis is dedicated to all of you who have been part of this remarkable journey. May it serve as a reminder that every step, no matter how challenging, brings us closer to our dreams.

TABLE OF CONTENTS

LIST OF TABLES

LIST OF FIGURES

LIST OF SYMBOLS

Symbols

%	Percentage
ºC	Degree Celcius
θ	Theta
λ	Wavelength
cm	Centimeter
eV	Electron Volt
g	gram
g L^{-1}	Gram per liter
h	Hour
K	Kelvin
M	Molar
min	Minute
mg L^{-1}	Milligram per liter
nm	Nanometer
µm	Micrometer
s	Second
t	Time
T	Temperature
W	Watt

LIST OF ABBREVIATIONS

Abbreviations

Ag_2CO_3	Silver Carbonates
Ag_2SO_4	Silver Sulphate
Ag_2PO_4	Silver Phosphate
$AgNO_3$	Silver Nitrate
ACD	CdS Loaded Silver Carbonate
5 ACD	5% of CdS ; 95% of Silver Carbonate
10ACD	10% of CdS ; 90% of Silver Carbonate
15ACD	15% of CdS ; 85% of Silver Carbonate
AOPs	Advance Oxidation Processes
AB1	Acid Black 1
BOD	Biochemical Oxygen Demand
BCC	Body Centred Cubic
CdS	Cadmium Sulfide
CdSe	Cadmium Selenide
CB	Conduction Band
CBM	Conduction Band Minimum
C_t	Concentration at time t
C_o	Initial concentration

DOE	Department of Environment
DB15	Direct Blue 15
E_f	Fermi Level
Eg	Energy Band Gap
e-	Electron
FTIR	Fourier Transform Infrared
FESEM EDX	Field Emission Scanning Electron Microscopy (FESEM) Energy Dispersive X-ray (EDX)
h	Planck Constant
h^+	Positive Hole
g-C_3N_4	Graphitic Carbon Nitride
I_{EF}	Internal Electric Field
IIWQ	International Initiative Water Quality
IP	Isopropanol
K_{LH}	Adsorption Coefficient of the Reactant
k_{app}	Apparent First Order Rate Constant
k_r	Reaction Rate Constant
LH	Langmuir Hinshelwood
MO	Methyl Orange

ME	Methanol
NHE	Normal Hydrogen Electrode
Na_2CO_3	Sodium Carbonates
pH_{ZPC}	Point Zero Charge
PL	Photoluminescence
PC	Potassium Chlorate
PI	Potassium Iodide
PC I	Photocatalyst I
PC II	Photocatalyst II
RR120	Reactive Red 120
RhB	Rhodamine B
$SrTiO_3$	Strontium Titanate
SDG	Sustainable Development Goals
TEM	Transmission Electron Microscopy
TiO_2	Titanium Dioxide
UV-Vis/DRS	Ultraviolet Visible Diffuse Reflectance Spectroscopy
VB	Valence Band
VBM	Valence Band Maximum

XRD	X-Ray diffraction
XPS	X-ray Photoelectron Spectroscopy
WHO	World Health Organization
UNESCO	United Nations Educational, Scientific and Cultural Organization
ZnO	Zinc Oxide
ZnS	Zinc Sulfide

CHAPTER 1
INTRODUCTION

1.1 Research Background

The world is facing a critical problem for the good water quality that can affect the living organism. Generally, the waters cover around 70% of the earth's surface which always be abundant but the quality of clean water in the environment is deteriorating. In this regard, UNESCO has reported in the International Initiative for Water Quality (IIWQ) that the limited source of clean water results from large amounts of untreated or inadequately treated wastewater that has been released into rivers, lakes, aquifers, and coastal waters (Glassmeyer et al., 2023). Recent research by Shetty et al., (2023), the rapid industrialization, urbanization, and large population growth in developing countries, is the biggest cause of the accumulation of toxic environmental pollution. As a consequence, Water Scarcity statistically demonstrated that the clean water is inaccessible to around 1.1 billion people globally, and water is deficient for at least one month of the year for a total of 2.7 billion. This emphasized that the critical need to balance human well-being and environmental hazards associated with exposure to contaminants in water.

Among the various contaminants, dyes and heavy metals are the most persistent in water, their synthetic source and complex structure lead to the biodegradation problem (Raninga et al., 2023). Textile, ceramic, refining, chemical, pharmaceutical, and many other industries produce effluents containing heavy metals such as mercury, copper, lead, chromium, and dyes likes methylene blue, methyl orange, methyl red, naphthalene black, and many others. According to Khan et al., (2023), dye molecules consist of chromophores which give them colour while auxochromes helps to enhance the dye's colour. The wavelength of light absorbed by the chromophores and auxochromes contributes to the various colours produced by the dyes. Most of synthetic dyes are highly hazardous, carcinogenic and discovered will increase the biochemical oxygen demand (BOD) and chemical oxygen demand (COD) levels which risk to human health. Therefore, most of researchers have studied several approaches including chemical, biological and physical treatment to solve the wastewater treatment issues.

Methyl orange (MO) is one of the most popular dyes and extensively utilized in dyeing and textiles industries (Kishor et al., 2021; Liu et al., 2020). In untreated textile effluents, the concentration of MO dye can reach up to 500 ppm, which may severely pollute various water ecosystems due to its carcinogenic and mutagenic nature. Specifically, MO dye is an anionic azo dye and a part of xenobiotic substance that can poses to the major ecological impact even at low concentrations exposure (Aljuaid et al., 2023). In addition, MO dyes also non-biodegradable because of its complex aromatic structure and xenobiotic characteristics. As a result, it is difficult for MO dyes to degrade by using biological treatments or conventional techniques such as coagulation–flocculation, adsorption, and membrane filtration under ambient conditions because these methods would accumulate the contaminants rather than degrade the MO dyes. Therefore, advanced oxidation processes (AOPs) have been recognized as one of the most effective treatment options, as they not only achieve high degradation efficiency but also consider the practical considerations such as time and cost constraints.

Advanced oxidation processes (AOPs) are relatively new technologies that have been increasingly demonstrated to be effective for the degradation of pollutants through reactions with hydroxyl radicals (•OH). AOPs comprise six main approaches, namely electrochemical oxidation, Fenton-based reactions, radiation, photolysis, photocatalysis, and ozone-based technologies (Liu et al., 2023). Although their potential is well recognized, large-scale application is sometimes limited by factors such as energy requirements and operational costs. In the research by Kumar and Shah, (2021), all six types of AOPs have been reported to be efficient, as they degrade organic compounds into simpler and stable inorganic compounds such as water, carbon dioxide, and mineral ions with slight sludge production. The presence of hydroxyl radical (•OH) will acts as oxidizing agent in this reaction up until 2.80V as represented in Table 1.1. which assist to increase the enhancement of degradation of pollutant and produce water (H2O) and carbon dioxide (CO2). This oxidizing agent with oxidation power has been explored and proved by the Brillas, (2025) that the presence of hydroxyl radical (•OH) give the great attention and effective for the photocatalytic degradation application due to their very high oxidation potential, non-selectivity, and ability to mineralize pollutants completely. In practical applications, the system is simplicity, low cost, and wide applicability are often prioritized over maximum effectiveness to ensure feasibility and scalability especially in wastewater degradation and hydrogen (H2) generation.

Table 1.1

Oxidation agent with oxidation power (Krupińska, 2020)

Oxidant	Oxidation Power (V)
Iodine	0.54
Bromide	1.09
Oxygen (molecular)	1.23
Chlorine dioxide	1.27
Chlorine	1.36
Hypochlorite	1.49
Hydrogen peroxide	1.78
Ozone	2.07
Oxygen (atomic)	2.42
Hydroxyl radical	2.80

Kulkarni et al., (2023) reported that photocatalyst are compounds that have high ability to enhance the chemical reaction exposed to the light. Photocatalyst based semiconductor capable to be effective if it is enough light absorption and small band gaps which lower than 3eV. Recently, photocatalyst based semiconductor such as silver carbonate, titanium dioxide, zirconium dioxide, zinc oxide, zinc sulphide, cadmium sulphide, bismuth tungstate, and ferric oxide have been explored as excellent photocatalyst in order to degrade contaminants in wastewater (Kumari et al., 2023). Ag_2CO_3 is an outstanding photocatalyst due to unique characteristics which non-metallic p block elements. The hybrid of Ag^{4d} orbitals with O^{2p} orbitals introduced to the unoccupied s, p states of p block elements could effectively tune potentials of conduction band of Ag-based oxides. Therefore, despite its promising photocatalytic performance, Ag_2CO_3 suffers from several limitations such as poor photostability and rapid recombination of photogenerated charge carriers, which restrict its practical application. To overcome these drawbacks, modification through the formation of heterojunction with suitable semiconductors has been widely explored to enhance its stability and photocatalytic efficiency.

Apart from that, CdS is recognized as a promising photocatalyst candidate that can absorb visible light and narrow band gap (Sinar Mashuri et al., 2023). As a result, it has been used in a variety of applications, including solar cells, hydrogen generation, photodetectors, photodiodes, and capacitors. Since that, researchers have demonstrated CdS as the potential composite photocatalyst with other semiconductor. Due to the energy levels of CdS and Ag_2CO_3 are compatible, it highlights to be one of effective composites photocatalyst that can enhance photocatalytic activity and prevent the charge recombination (Elkodous et al., 2023). Additionally, CdS has a more negative conduction band edge than H^+ to H_2 reduction potential, a higher flat-band potential, and better electrochemical performance, making it an excellent electron donor material.

Hence, based on the suitable band gap energy alignment between CdS and Ag_2CO_3, it is a great combination of these two semiconductors which expected to form an efficient Z-scheme heterojunction system that able to improve the charge separation and remain the strong redox ability during the photocatalytic reaction. The synergistic interaction between CdS and Ag_2CO_3 would not only minimize the electron hole recombination but increase the visible light absorption range leads to the superior photocatalytic performance. Consequently, in this study CdS loaded Ag_2CO_3 were synthesized via simple precipitation method to prepare a novel and efficient photocatalyst for the degradation of methyl orange. Additionally, this work aims to provide the valuable insight by characterize and evaluated the synthesized material with the various advanced instrumental analysis as well as the parameter study such as effect of catalyst dosage, initial concentration and pH. Thus, this research is significant where it is designing the sustainable photocatalytic system for wastewater treatment aligned with the Sustainable Development Goal 6 (SDG6) Clean Water and Sanitation.

1.2 Problem Statement

Water pollution has become a critical environmental issue due to the continuous discharge of industrial effluents containing toxic organic dyes and hazardous pollutants into aquatic systems. These contaminants not only threaten aquatic life but also pose serious risks to human health due to their persistence and non-biodegradable nature. Therefore, the development of efficient and sustainable treatment technologies is urgently required to address this issue. As a new photocatalyst, Ag_2CO_3 has narrow band gap energy theoretically around ~2.32eV which has high degradation of various

dyes and good efficiency of redox reaction in the photocatalytic performance. Unfortunately, Ag_2CO_3 displayed unstable photochemical behaviour under visible light due to the photo corrosion that will deactivate the photocatalytic activity. According to the Singh et al., (2026) claimed that unstable photochemical behaviour refers to the tendency of certain materials, upon absorbing light energy (UV or visible), to undergo rapid and often irreversible chemical changes. This results in the generation of highly reactive and short-lived species, as the excited molecules are unable to return to their original ground state. Consequently, structural modifications such as bond cleavage, rearrangement, or degradation may occur.

In addition, CdS has also been reported to act as a photocatalyst for water treatment processes, with an appropriate band gap of ~2.4 eV that allows excellent solar absorption. However, photo-corrosion is a prevalent phenomenon and one of the major challenges when dealing with CdS-based photocatalysts, which limits their industrial application. Photocorrosion refers to the deterioration of a semiconductor photocatalyst, such as CdS and ZnO, under light irradiation. In this process, photogenerated holes oxidize the catalyst itself rather than the target pollutants, leading to structural damage and loss of activity (Zhang et al., 2025). This phenomenon significantly limits the long-term efficiency of photocatalytic systems. Research by Nasir et al., (2020) indicate that this problem occurs when sulfur ions are attacked by photogenerated holes and oxidized into elemental sulfur, photogenerated holes cause anodic corrosion when exposed to light and defects formed on the CdS surface during photocatalysis facilitate redox reactions on the surface under aerobic conditions. In this sense, the fabrication between Ag_2CO_3/CdS significantly to construct heterojunction photocatalyst. Heterojunction photocatalyst is a combination of two semiconductors that can be classified into three types which are type I, II and Z scheme heterojunction. Z scheme is mostly preferred and effectively discovered by many studies in which to retain strong redox potential between two semiconductors. A Z-scheme heterojunction operates through a unique charge transfer mechanism where the photogenerated electrons from the conduction band of one semiconductor recombine with the holes from the valence band of another semiconductor (Ghosh et al., 2024). This process preserves the highly reductive electrons and highly oxidative holes in their respective bands, thus maintaining strong redox ability.

As consequence, the coupling between CdS and Ag_2CO_3 in this study could enhance the optical response to the visible spectrum, which is likely attributed to the

formation of a Z-scheme heterojunction. To the best of our knowledge, no previous work has reported the combination of silver carbonate with cadmium sulfide as a photocatalyst. The proposed heterojunction mechanism is supported by the band gap alignment of CdS (~2.4 eV) and Ag_2CO_3 (~2.32 eV), as well as the improved photocatalytic activity observed in the degradation of methyl orange and other organic pollutants. While further advanced characterization would be necessary to fully confirm the charge transfer pathway, the present findings strongly suggest the occurrence of a Z-scheme effect in CdS/Ag_2CO_3 composites.

1.3 Research Objectives

The aim of this study is to synthesize the Z-scheme of silver carbonate (Ag_2CO_3) with cadmium sulfide (CdS) for enhancement of photocatalytic activity for the degradation of methyl orange. The set of goals of this study is described as follows:

a) To synthesize the Z-scheme Ag_2CO_3/CdS heterojunction via facile precipitation method for the photocatalytic degradation of methyl orange.

b) To characterize the synthesize Ag_2CO_3 with CdS with the various advanced instrumental analysis for the photocatalytic degradation of methyl orange include XRD, FESEM, TEM, XPS, PL, FTIR, UV-Vis DRS.

c) To evaluate the optimum ratio of the Ag_2CO_3 with CdS for the photocatalytic degradation of methyl orange such as initial pH, initial concentration, catalyst dosage as well as the scavenger test.

1.4 Research Question

i) Why does the facile chemical precipitation method influence the photocatalytic performance and structural properties of Ag_2CO_3/CdS composite ?

ii) Why do advanced instrumental analyses provide insights into the structural, morphological, and optical characteristics of the synthesized Ag_2CO_3/CdS photocatalyst for the degradation of methyl orange?

iii) What is the optimum ratio of synthesize silver carbonate and cadmium sulfide for the photocatalytic degradation of methyl orange?

1.5 Significance of Study

Due to its excellent characteristics, photocatalysis holds great promise as an efficient and sustainable oxidation technology for wastewater treatment. In this research, a modified Ag_2CO_3/CdS composite is proposed owing to its low cost, high stability, and environmentally friendly properties. Mehra et al ., (2023), reported that a visible light-driven modified Ag_2CO_3 photocatalyst could form a Z-scheme heterojunction, thereby enhancing photocatalytic performance for the degradation of sodium isobutyl xanthate and o-cresol. This previous finding provides supporting evidence for the potential formation of a Z-scheme heterojunction in the present Ag_2CO_3/CdS system.

Besides that, Z-scheme heterojunction helps to preserve the photogenerated electron by controlling the oxidation and reduction process. At the interface, first semiconductor is positively charged while second semiconductor is negatively charged. By that, electric field will be produced and band edge bending will be occurred. This would help the combination of photogenerated electron from second semiconductor to first semiconductor. According to Li et al ., (2022), it is worth to construct the Z-scheme heterojunction due to the effect of separation efficiency of electron hole recombination and redox ability of the modified catalyst.

This study expected to bring benefit to wastewater industries such as pharmaceuticals, cosmetic formulations, automotive and others with modified photocatalyst, Ag_2CO_3/CdS nanocomposites can be more reliable, effective and eco-friendly. Notwithstanding, the clean wastewater treatment also can be utilized simultaneously for the further application in industry such as hydrogen generation. It can consider as a new photocatalytic technology to provide insight for advancement in the field environment and energy as well as could financially profit the industrial sector.

In view of the above and significant role played by modified photocatalyst, Ag_2CO_3/CdS it is hoped that this option can replace other conventional method that less effective especially wastewater industries area and synergistic with sustainable development goals of clean water and sanitation (SDG 6).

1.6 Hypothesis

In this study, it was hypothesized that the preparation of carbonaceous materials like Ag_2CO_3 with CdS by facile chemical precipitation method was expected to create more defect site and more active site. It could enhance the photocatalytic performance. In addition, the presence of cadmium sulfide as the composite catalyst will improve the redox reaction efficiency and light harvesting ability due to the formation of Z-scheme heterojunction. As a consequence, the combination of silver carbonate and cadmium sulfide will have a synergistic effect between them that anticipate enhancing the efficiency towards the photocatalytic degradation of methyl orange. More importantly, the formation of a Z-scheme heterojunction between Ag_2CO_3 and CdS is anticipated to significantly enhance the redox reaction efficiency. Unlike conventional type-II heterojunctions, which often sacrifice redox potential for charge separation, the Z-scheme configuration enables the selective recombination of low-energy charge carriers while preserving highly reductive electrons and highly oxidative holes. This allows the system to maintain strong oxidation and reduction abilities simultaneously.

1.7 Research Scope and Limitation

The scope of this study included the preparation and characterization of Ag_2CO_3 which the parent catalyst while CdS as the composite catalyst, their photocatalytic enhancement of methyl orange (MO), the effect of loading for the best ratio between Ag_2CO_3 and CdS as the potential application for the efficient degradation as well as photocatalytic activity of MO. The details of the specific research scopes are follows:

1. Silver carbonates were synthesized using facile precipitation method with silver nitrate and sodium carbonate as the precursor. Meanwhile, the cadmium sulfide was synthesized by using facile chemical precipitation method and cadmium chloride together with sodium sulfide was used as the precursor. The modification of photocatalyst was carried out by varying the lower concentrations of cadmium sulfide from 5% to 15%. The modified photocatalyst also prepared by using simple precipitation method with the addition of distilled water and dried in the oven approximately 90^{o}C around 3 hours.
2. The optimum photocatalyst was confirmed by the advanced analysis such as XRD, FTIR, FESEM-EDX, XPS, PL, UV-Vis DRS, and TEM analysis. In this

part, each of analysis will specifically discussed the modified photocatalyst in terms of structural, crystallinity, the phase studies, vibrational spectroscopy, surface and internal microscopic morphology, optical properties for the determination of optical absorption as well as the band gap energies, surface chemical composition and optical excitation of electron hole study.

3. The Ag_2CO_3/CdS photocatalyst with the optimum CdS loading was identified and subsequently subjected to further evaluation of its photocatalytic efficiency. The screening process was conducted referred to the previous parameters in the literature to determine the optimum conditions such as effect of pH (1-11), catalyst dosage (0.0125 – 0.0375 g L^{-1}) and initial concentration (10-70 mg L^{-1}). In addition, the kinetic study also was evaluated by using Langmuir-Hinshelwood model to accommodate the reaction occurred at the solid-liquid interface. The reusability was analysed by running five-time repetitions of the experiment under same conditions. Moreover, the mechanism of photocatalytic degradation of MO over the catalyst was tested to determine the active species using methanol (ME), potassium chlorate (PC), potassium iodide (PI), and isopropanol (IP) which indicated as scavenger of photogenerated electron (e-), photogenerated holes (h+), hydroxyl radical absorbed on the catalyst (•OHsurface), and hydroxyl radical absorbed in the bulk solution (•OHbulk).
4. Despite that, there are limitation throughout this study where the photodegradation only focus on the methyl orange which is anionic dye rather than various dye include cationic dye such as methylene blue, pharmaceutical waste and real wastewater. It definitely different dyes has different conditions include the pH, concentration, catalyst loading and others. Furthermore, this research widely studied towards low ratio of cadmium sulfide (CdS) as the composite catalyst between 5 % to 15%. This is due to the characteristics of the CdS which is photo-corrosion and high toxicity which may increase the level of chemical oxygen demand (COD). Ultimately, the system for photodegradation of modified photocatalyst Ag_2CO_3/CdS nanocomposites will be limited for suspension mode only rather than immobilized mode. It was considered due to the immobilization system will construct high surface area and tends to lower photocatalytic activity.

1.8 Research Outline

This manuscript reports the research conducted on the synthesis of modified photocatalyst, Ag_2CO_3/CdS for the enhancement of photocatalytic degradation of methyl orange. This study is divided into five chapters, starting with the general introduction of the research background, the literature surveys from the previous research, followed by the results and summary from the current study.

In Chapter 1, general introduction was discussed on the environmental issues towards the wastewater problems. It is crucial to emphasize the critical need of the good water quality and balance human well-being as it is an environmental hazard. Dyes and heavy metal among the complex structure which leads to the biodegradation problem. Methyl orange was selected as the one of the model pollutants to be studied. Several methods were compared and mentioned as the consideration for the removal of methyl orange. Besides that, the potential of silver carbonate and cadmium sulfide as the photocatalyst for the degradation of methyl orange was highlighted. The problem statements of the currents research were stated which subsequently provide a clear objective in this research study. Moreover, research scope along with limitation was described to ensure this research was significant to be studied which meet the industry demands.

Chapter 2 or known as literature review highlighted the details information regarding photocatalysis, semiconductor based photocatalyst, methyl orange as the dyes contaminated in the wastewater problems, previous technology for the removal of dyes, modified catalyst composite morphology, expected heterojunction for the synthesize modified photocatalyst, Ag_2CO_3/CdS as well as the mechanism. All the findings in this chapter are accentuated and relevant along with the theoretical framework.

Chapter 3 covers the methodology which describes the chemicals and materials used in the research works, advance instrumentation used, the catalyst preparation. In addition, the details setup of catalyst characterization was mentioned as well as the experimental system, photodegradation analysis and several parameters study. Besides that, the procedure for the analysis calculations also included and discussed.

Chapter 4 thoroughly discussed the experimental results of the study which respect to the research objective. The performance of various ratio towards the synthesize modified photocatalyst, Ag_2CO_3/CdS was analysed. Physiochemical properties of all synthesize photocatalyst was explained by advanced instrumentation

such as XRD, FTIR, FESEM EDX, UV-Vis DRS, PL, XPS and TEM. After that, few parameters study was examined as the evidence for the modified Ag_2CO_3/CdS even at different conditions. The parameter study that has been explored include effect of concentrations, pH,catalyst loading, scavenger test and reusability.

Ultimately, chapter 5 consists of the conclusion and summarization of the study along with the future recommendations for the next research.

CHAPTER 2
LITERATURE REVIEW

2.1 Environmental Issue

Water and environmental sustainability are crucial for all living organisms and the Earth's future. All organisms of the ecosystem are interconnected, hence any degradation in one part affects the entire system. Water, being essential for life and irreplaceable stands out among environmental components. Preserving water and safeguarding it from pollutants is vital. Water pollution occurs when hazardous substances, usually chemicals or microorganisms contaminate a water stream, river, lake, ocean, aquifer, or other body of water, deteriorating the water quality and rendering it toxic to humans or the environment. Contaminated water sources pose risks to human consumption and agriculture, leading to scarcity for humans and the ecosystem. Research by Verre et al., (2026) has mentioned that UNESCO has mentioned that most of the significant challenges faced by humanity today are due to water scarcity and quality issues. As stated by Camara et al., (2019), water quality assesses for water use such as drinking, industrial, agricultural, recreational, and habitat include in physical, chemical, and biological criteria. Thus, water quality plays an important role for all living species, drawing attention from scientists, researchers, and water resource management to encounter these issues.

To address the water pollution, maintaining the water quality is a challenge task that needs to understand where the sources of pollution coming from whether point sources or nonpoint sources (J. Yang et al., 2020). Point source pollution refers to contamination that comes from a single source such as wastewater that released legally or illegally such as manufacturing, oil refinery, or wastewater treatment facility, as well as contamination caused by leaking septic systems, chemical and oil spills, and unlawful dumping (Arif et al, 2020). Research by Lin et al., (2022), it describes that non-point sources are refers to contamination that originates from dispersed sources. These may include agricultural or rainfall runoff, as well as debris blown into streams from the land. In Malaysia, Department of Environment (DOE) was responsible to monitor the water quality as the sampling frequency between four to six time a year. In situ measurement were conducted along the monitoring and it

needs to be aligned with the quality index which consider few parameters such as pH, temperature, dissolved oxygen, turbidity, conductivity, salinity and more as depicted in Figure 2.1.

According to the National Water Quality Standards (NWQS) for Malaysia, the classification of water quality is divided into five categories, namely Class I to Class V, based on several key physical, chemical, and biological parameters such as pH, dissolved oxygen (DO), biochemical oxygen demand (BOD), chemical oxygen demand (COD), ammoniacal nitrogen, and total suspended solids (TSS). Class I indicates pristine water quality that requires minimal or no treatment, suitable for water supply and very sensitive aquatic species, while Class V represents highly polluted water that is unsuitable for most purposes. As the class increases from I to V, the concentration of pollutants such as COD, ammoniacal nitrogen, and coliform count rises significantly, reflecting progressive degradation in water quality. This classification framework is essential in assessing the status of surface water and provides a practical guideline for determining its potential use and the level of treatment needed before utilization.

NATIONAL WATER QUALITY STANDARDS FOR MALAYSIA (cont.)

PARAMETER	UNIT	CLASS					
		I	IIA	IIB	III	IV	V
Ammoniacal Nitrogen	mg/l	0.1	0.3	0.3	0.9	2.7	> 2.7
Biochemical Oxygen Demand	mg/l	1	3	3	6	12	> 12
Chemical Oxygen Demand	mg/l	10	25	25	50	100	> 100
Dissolved Oxygen	mg/l	7	5 - 7	5 - 7	3 - 5	< 3	< 1
pH	-	6.5 - 8.5	6 - 9	6 - 9	5 - 9	5 - 9	-
Colour	TCU	15	150	150	-	-	-
Electrical Conductivity*	µS/cm	1000	1000	-	-	6000	-
Floatables	-	N	N	N	-	-	-
Odour	-	N	N	N	-	-	-
Salinity	ppt	0.5	1	-	-	2	-
Taste	-	N	N	N	-	-	-
Total Dissolved Solid	mg/l	500	1000	-	-	4000	-
Total Suspended Solid	mg/l	25	50	50	150	300	300
Temperature	°C	-	Normal + 2 °C	-	Normal + 2 °C	-	-
Turbidity	NTU	5	50	50	-	-	-
Faecal Coliform**	count/100 ml	10	100	400	5000 (20000)a	5000 (20000)a	-
Total Coliform	count/100 ml	100	5000	5000	50000	50000	> 50000

Notes :

N : No visible floatable materials or debris, no objectional odour or no objectional taste
* : Related parameters, only one recommended for use
** : Geometric mean
a : Maximum not to be exceeded

WATER CLASSES AND USES

CLASS	USES
Class I	Conservation of natural environment. Water Supply I – Practically no treatment necessary. Fishery I – Very sensitive aquatic species.
Class IIA	Water Supply II – Conventional treatment required. Fishery II – Sensitive aquatic species.
Class IIB	Recreational use with body contact.
Class III	Water Supply III – Extensive treatment required. Fishery III – Common, of economic value and tolerant species; livestock drinking.
Class IV	Irrigation
Class V	None of the above.

Figure 2.1 National Water Quality Standard for Malaysia
(National Water Quality Standards and Water Quality Index - Department of Environment, 2021)

As mentioned by World Health Organization (WHO), globally the water-related diseases affect approximately 3.4 million people every year, with children under the age of 5 being most susceptible (Osiemo et al., 2019). Malaysia, situated in Southeast Asia, is no exception. The country is fortunate to be abundant in both its diverse flora and fauna, as well as its rich water resources. Nevertheless, the incompetent management towards the water bodies and lack authoritative enforcement leads to the major water pollution problems. In the research by Yap et al., (2019) it reported on the contamination issue in Sungai Kim Kim, Johor Bahru due to the irresponsible activity releasing the toxic chemicals to the water bodies. DOE inspectors recognized the illegally dumped matter such as marine oil, which emits potentially hazardous methane and benzene fumes. Because of its hazardous nature, the oil is classified as scheduled waste and must be disposed of properly. As a consequence, approximately 2,000 individuals, including school students, were affected and required medical treatment in the Intensive Care Unit at Hospital Sultan Ismail, as illustrated in Figure 2.2.

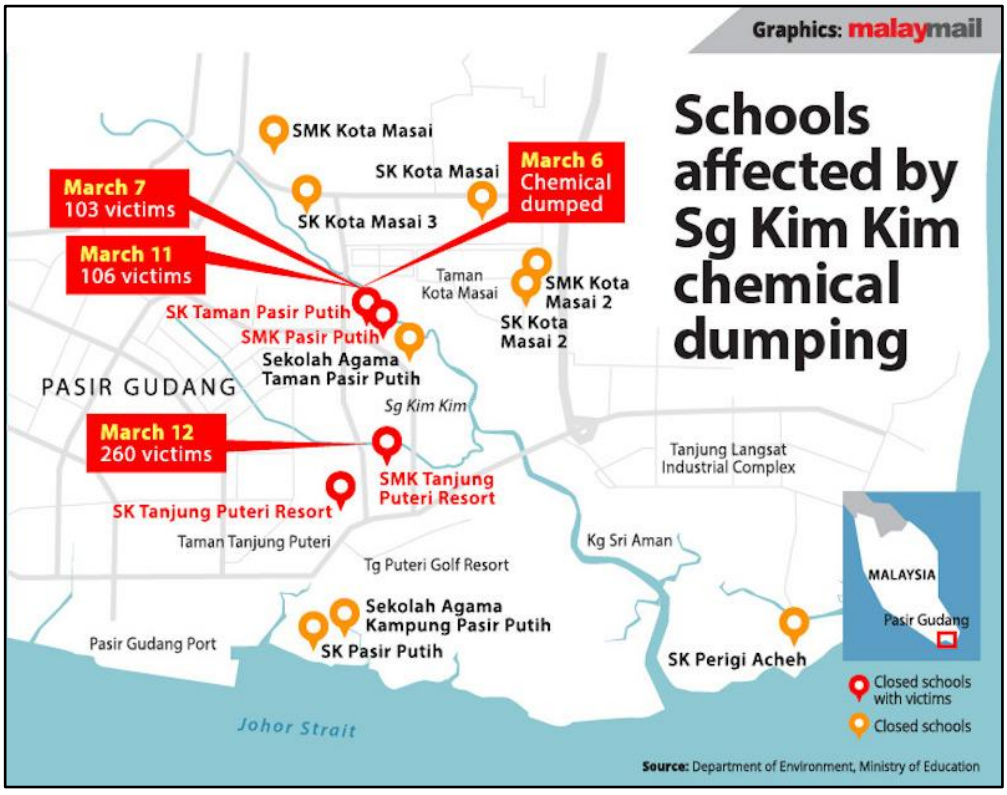

Figure 2.2 Water Pollution of Illegal Dumping in Sungai Kim Kim, Johor Bahru

(Ben Tan., 2019)

To fulfill the demands of the exponentially rising global population, industries and economic sectors have been enlarged to increase their production rate. According to Halepoto et al., (2022), the textile industry is one of the oldest industrial sectors that significantly contributes to economic growth but simultaneously generates a substantial amount of water pollution.Textile effluents comprise dyes, heavy metals, inorganic salts, surfactants, organic pollutants, oil, and grease. Textile effluents are disposed of on bare land or bodies of water, contaminating the soil and water (Khan et al., 2023). The improper disposal of textile effluents pollutes soil and water thus increase the level of COD level that can cause harm towards the aquatic life as well as human being. As illustrated in Figure 2.3, dyes from the textile industry exhibit high solubility in water and various organic solvents, making them difficult to remove from wastewater once discharged. Conventional methods are the most commonly to handle the textile industry even though longer time and costly. Therefore, production practices and strict environmental standards need to be considered. Uddin, (2021) emphasized the importance for all industrial sectors to promote research and innovation aimed at replacing and managing toxic chemicals and dyes, in order to make the resulting effluents more environmentally friendly.

Figure 2.3 Polluted water bodies by textile dyes industry (LaRose, 2017)

2.2 Wastewater Treatment Process

The most effective purification approaches to address water pollution problems are those that aim to achieve decontamination goals. Water purification refers to a series of processes aimed at removing contaminants and impurities from wastewater to achieve decontamination goals. Described by Crini and Lichtfouse, (2019), a purification can be divided into 5 successive steps which are : (1) preliminary treatment ; (2) primary treatment ; (3) secondary treatment ; (4) tertiary treatment ; (5) treatment of the sludge. Each purification process generally undergoes conventional wastewater treatment technologies, which consist of physical, chemical, and biological processes, as well as several operations to remove solids from the effluents, as illustrated in Figure 2.4 (Gkika et al., 2022). As reported by Ahmed et al., (2021), the physical treatment process represents a straightforward technological approach for eliminating insoluble coarse particles while maintaining the biochemical characteristics of the wastewater, since no chemical or biological agents are involved. Screening, sedimentation, adsorption, coagulation, and flocculation are commonly utilized in physical treatment processes. Nevertheless, this approach has certain limitations, such as excessive sludge production and the necessity for pH adjustment, which can complicate the overall wastewater treatment process.

Biological treatment of wastewater is considered an economical and relatively simple approach, operating through a combination of aerobic and anaerobic processes that utilize microorganisms to decompose organic pollutants effectively. According to Roy and Saha, (2020), biological treatment is a process that involves biodegradation and bleaching by using microorganisms, fungi, bacteria, yeast or algae. Despite that,

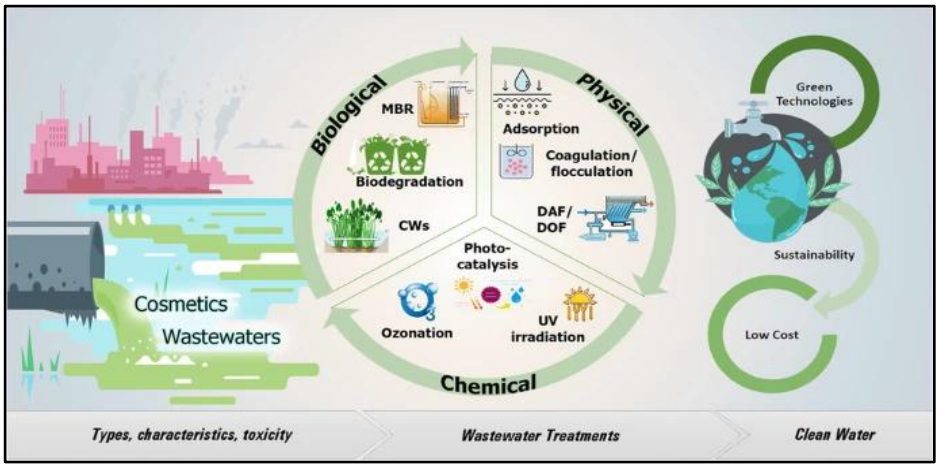

Figure 2.4 Conventional Wastewater Processes

it has some limitations that decrease the efficiency due to the flexibility in design operation. The biological method requires a large geographical area and, a diurnal cycle hence it needs greater time to function. As for the degradation of dyes, the colour removal is hardly possible and the complex chemical structure are recalcitrant to be degrade. Among the aforementioned approaches, chemical treatment such as Advances Oxidation Process (AOPs) are the most significant and outstanding methods which able to eliminate complex organic and inorganic pollutants as well as biological pollution. Garrido-Cardenas et al., (2020) has claimed that AOPs able to remove most of effluent approximately up to 98% which aligned with Sustainable Development Goals (SDGs).

AOPs of chemical treatments must be developed to bridge the gap between the treatability achieved through conventional physical and biological treatments and the day-to-day more stringent restrictions imposed by environmental legislation. The main advantage of this method compared to other conventional technologies is its ability to effectively degrade recalcitrant pollutants without generating additional waste. Over the years, the number of treatment processes has increased significantly with the advancement of hybrid and synergistic technologies based on various advanced oxidation processes (AOPs) (Goodarzi et al., 2023). The combinations of 6 types of AOPs, photocatalysis have helped to overcome the presence of refractory problems while also greatly improving the performance of AOPs (Dewil et al., 2017). Resultantly, photocatalysis from AOPs are the most selective by many researchers due to its significant outcomes.

2.3 Photocatalysis

Photocatalysis is the green technology process that utilizes light and semiconductor for wide applications such as degradation of dyes, water splitting, heavy metal removal and others. Successively, photocatalysis has been demonstrated in 1972 by Fujishima and Honda on the photocatalytic water splitting with titania or commonly known as TiO_2. Since that, many researchers have extensively studied and justified that photocatalysis process is the best alternative method for the various application as represented in the Figure 2.6 (Porcu et al., 2022). Correspond to the research by Ansari et al., (2018), photocatalysis over semiconductor is an advanced oxidation process that includes the irradiation of light energy with greater band gap of

semiconductor, its results the generation of photogenerated electron and positive holes. There are two simultaneous reactions will occur during photocatalysis process which are oxidation and reduction reaction. Oxidation reaction tends to help the photo-generated holes while the reduction reaction will help the photo-generated electrons. In general, photocatalysis process can be classified into two types which are homogeneous and heterogeneous. It is based on the reacting species and physical state of the catalyst.

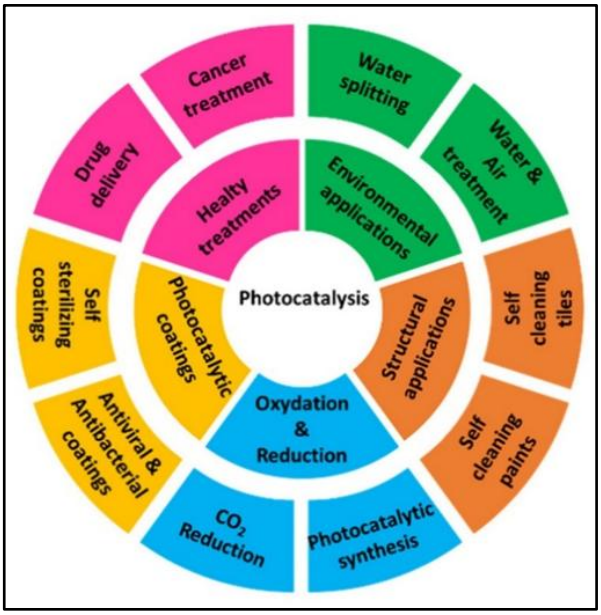

Figure 2.5 Applications in photocatalysis process (Porcu et al., 2022)

Homogeneous photocatalyst is when the photocatalyst and the reactant are in the same phase such as ozone and photo-Fenton system (Fe^{+} and Fe^{+}/H_2O_2). It is widely applied in various applications, where the reactive species (•OH), also known as hydroxyl radicals, play a crucial role (Panda et al., 2022) On the other hands, heterogeneous photocatalyst is when the photocatalyst and the reactant are in the different medium phase which frequently used in photocatalytic wastewater treatment. According to the (Kumar et al., 2021), it proved that for heterogeneous photocatalysis, semiconductors are favoured over other photocatalysts. The materials of heterogeneous photocatalyst are chemically stable, cost-effective, chemically and biologically inert, have high activity, resistant to poisoning and attrition, allow to be reused and are nonselective under various situation. Subsequently, the energy difference between valence band (VB) and conduction band (CB) or known as band

gap are crucial to be investigated. Specifically, the materials of photocatalysis reaction are restricted into three categories includes insulator (Eg<1.0 eV), semiconductor (Eg <1.5 – 3.0 eV) or conductor (Eg>5.0 eV), as demonstrated in Figure 2.7. Semiconductors can conduct electricity in the presence of light even at ambient temperature, which renders them ideal as photocatalysts (Ameta et al., 2018). Thus, semiconductor-mediated heterogeneous photocatalysis is a potentially environmentally friendly technology.

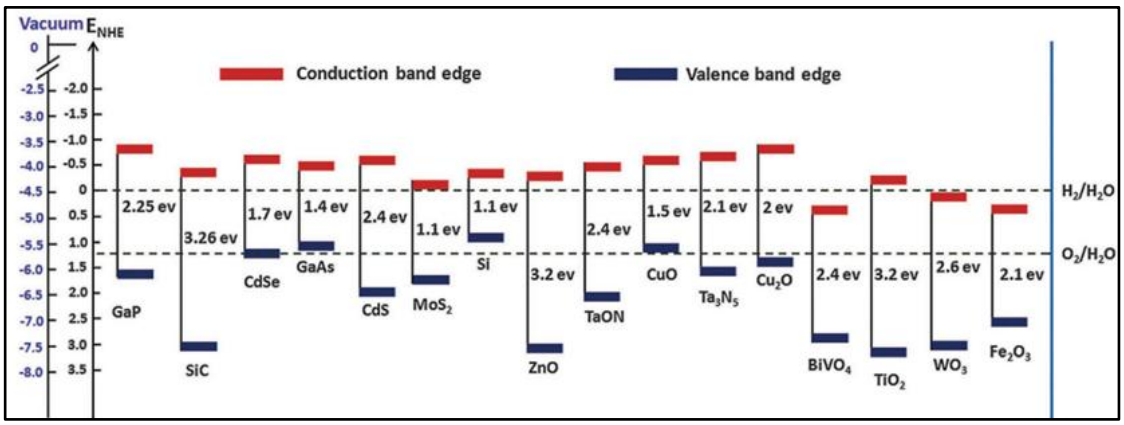

Figure 2.6 Types of materials that suitable for photocatalysis reaction (Pavlović et al., 2024)

2.3.1 Semiconductor Photocatalyst

The phrase photocatalyst is a combination of two words: photo, which refers to photons, and catalyst, which is a chemical that changes in its presence. Hence, photocatalysts are materials that when exposed to light it undergoes the changes in rate of a chemical reaction (Chimmikuttanda et al., 2022). Photocatalyst must be a semiconductor, as it has appropriate band gap that leads to the photo-excitation phenomenon, which allows a cross transition leading to the formation of an electron in the conduction band and a hole in the valence band.

To develop an efficient semiconductor photocatalyst capable of harnessing sustainable and safe solar energy, several key criteria must be satisfied. These include a low band gap for enhanced solar absorption, long-term stability characterized by non-toxicity and chemical inertness, high mobility of photogenerated charge carriers, and well-aligned conduction and valence band potentials relative to the redox potentials of water. Photocatalyst based semiconductor as like metal oxide has attracted the attention of many researchers recently. In the studied by (Vaya and Surolia, 2020), commonly titanium dioxide (TiO_2) and zinc oxide (ZnO) widely used due to their characteristic which are chemically inert, non-toxicity and construct high photocatalytic activity especially in the degradation of wastewater treatment. Besides that, sulfides photocatalyst also widely demonstrated to be efficient such as cadmium sulfide (CdS), zinc sulphide (ZnS), cadmium selenide (CdSe) and others. Figure 2.8 and Table 2.1 represented the common semiconductor that extensively used in wide application include degradation of dyes.

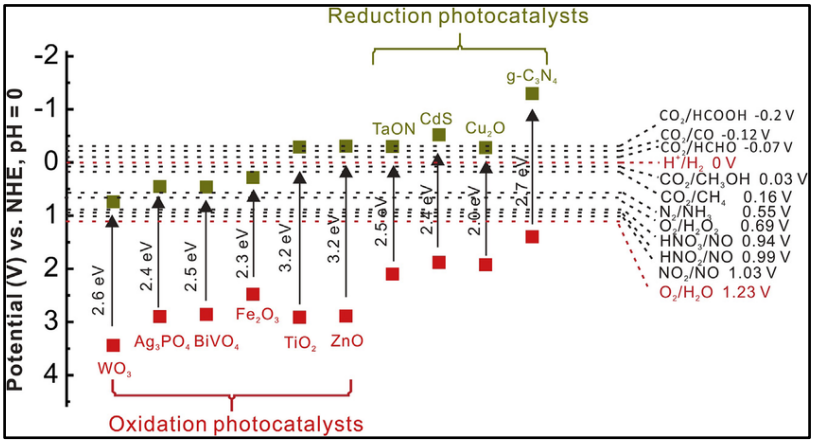

Figure 2.7 List of photocatalyst semiconductor that extensively used (Liao et al., 2021)

Table 2.1

List of photocatalyst and their band gap (Mo et al., 2026)

Photocatalyst	Band Gap (Ev)
CdS	2.4
Ag_2CO_3	2.3
Ag_2SO_4	3.0
Ag_2PO_4	2.43
g-C_3N_4	2.7

Generally, the general mechanism of photocatalysis has represented in the Figure 2.9, which based on the photoexcitation of semiconductor due to the absorption of electromagnetic energy under UV/visible light. According to the Saravanan et al., (2017), when the light energy in the form of photons fall on the surface of a semiconductor and irradiated with the equivalent or more than the bandgap energy of the semiconductor, the valence band electrons are excited and stimulated to the conduction band of the semiconductor. Along with the photogenerated electrons, holes will leave in the valence band of the semiconductor and oxidize donor molecules. Then, the holes will combine with water molecules to generate hydroxyl radicals which has strong oxidizing power that plays the important roles for the degradation of pollutants. Superoxide ions are formed when conduction band electrons combine with dissolved oxygen species. Redox reactions are initiated by the electrons. To produce the appropriate products, these holes and electrons might undertake successive oxidation and reduction processes with any species that might be adsorbed on the surface of the semiconductor (Mandade, 2021). Equation 2.1 to 2.5 summarized the photocatalytic mechanism that occur in an activated photocatalyst.

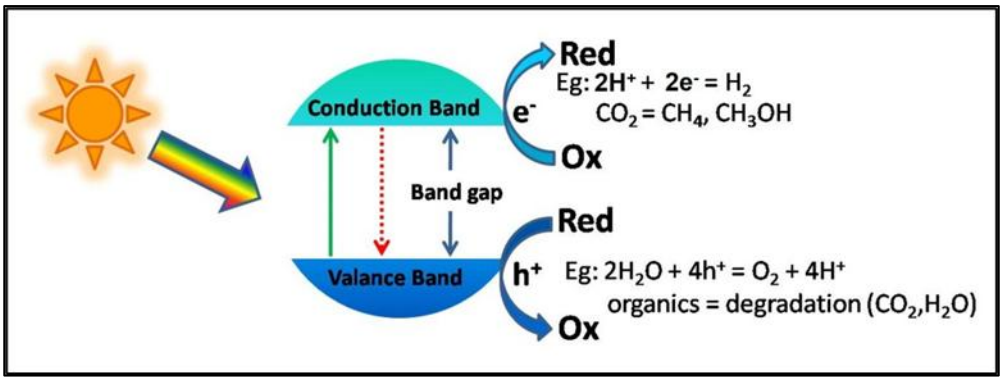

Figure 2.8 General mechanism of photocatalyst process (Langa et. Al., 2023)

$$\text{Photocatalyst} + h\nu \rightarrow e^- + h^+ \quad (2.1)$$

$$O_2 + e^- \rightarrow \cdot O_2^- \quad (2.2)$$

$$\cdot O_2^- + H_2O \rightarrow HO_2^\bullet \quad (2.3)$$

$$H_2O/OH^- + h^+ \rightarrow \bullet OH \quad (2.4)$$

$$\text{Organic pollutant} + \cdot O_2^- / HO_2^\bullet / \bullet OH \rightarrow CO_2 + H_2O \quad (2.5)$$

Anyhow, Zhu et al., (2023) has stated that if the photocatalytic degradation towards the pollutants is decrease as expected, this is due to the electrons was accumulated in the conduction band (CB) which leads to the high recombination of

charge carriers. Therefore, specific scavengers or selective semiconductor are crucial to reduce the rates of recombination together increase the photocatalytic activity. Kumar et al., (2021) explored that the excitation of photogenerated electron and holes towards the specific crystal facets of semiconductor enhances the reaction efficiency or rates of the photocatalyst. During the degradation process, selectivity is one of the most demanded towards the photocatalysts. The selectivity of photodegradation depends on several parameters, including appropriate band gap of the photocatalyst (Eg = 1.5–3.0 eV), the initial pollutant concentration, solution pH, light intensity, pore size, and surface charge. These factors influence the attraction, adsorption, and mineralization phases of photocatalysis and have been systematically studied (Ahmed and Mohamed, 2022).

The charge distribution and exposed surface area of photocatalysts play a crucial role in determining their selectivity towards pollutants of different polarities. In particular, pollutants bearing positive or negative charges interact with the photocatalyst surface primarily through Coulombic forces, which significantly affect adsorption efficiency and subsequent degradation pathways. This highlights the importance of tailoring the surface charge and morphology of photocatalysts to optimize selective adsorption and reactivity. Among the various candidates, silver carbonate (Ag_2CO_3) and cadmium sulfide (CdS) have attracted considerable attention because of their unique electronic structures and favorable band gaps, which not only facilitate efficient photodegradation of organic pollutants but also promote hydrogen evolution reactions. Previous studies have demonstrated that these materials can achieve enhanced photocatalytic activity by simultaneously offering strong light absorption, efficient charge separation, and selective interactions with pollutant molecules (Mehra et al., 2023; B. Tang et al., 2023).

2.4 Silver Oxosalts

Recently, the development of novel photocatalysts has gained increasing interest, with particular focus on metal halides and metal oxosalts due to their promising optical and electronic properties (Azami et al., 2022a; Ghazi et al., 2023a; He et al., 2019). Surprisingly, silver oxosalts such as silver carbonates (Ag_2CO_3), silver phosphate (Ag_2PO_4) and silver sulfate (Ag_2SO_4) exhibit well for the photocatalytic activity under light irradiation. It drawn intense study for silver oxosalts due to the

good oxidation photocatalyst related to the low negative valence band, which could contribute to the strong oxidation species for the photocatalytic efficiency. The different oxosalt groups can be term as XOy (X = C, P, S, As, and other p-block elements; y = 3, 4), which may couple to form other semiconductor networks with various metal ions, presenting a chance to produce unique as well for the effective photocatalysts. As studied by Jiang et al., (2017); M. Li et al., (2023); Teng et al., (2024), the silver oxosalts shown to be potential photocatalyst in the application of water splitting and photodegradation of organic pollutants. Likewise, due to their different crystal and electronic structures, which effect the energy band structure and charge carrier transfer efficiency, these photocatalysts have excellent photophysical performance and photocatalytic activity (Raeisi-Kheirabadi and Nezamzadeh-Ejhieh, 2020). Nevertheless, most of silver oxosalts photocatalyst have low stability due to the absence of sacrificial agent that can cause photocorrosion (Rafaie et al., 2023). Therefore, this silver oxosalts photocatalyst are hardly to be recycle which tends to increase the operating cost.

2.4.1 Silver Carbonates (Ag_2CO_3)

Silver carbonate (Ag_2CO_3) is a new photocatalyst that been discovered recently with the simple synthesize reaction between $AgNO_3$ and Na_2CO_3. It exhibits excellent responsiveness to visible light due to its narrow bandgap approximately around <2.3 eV. Represented in the Figure 2.10, the crystal structure of Ag_2CO_3 is monoclinic based on JCPDS 26-0339. However, despite the potential of Ag_2CO_3 for photocatalytic degradation under visible light, Ag_2CO_3 faces challenges in practical applications. It tends to be unstable and decompose under light irradiation because the photogenerated electrons reduce Ag^+ to Ag^0 (Murcia et al., 2020). Research by Lv et al., 2021 reported that Ag_2CO_3 was less study due to the low separation efficiency towards the photoinduced electron and holes and recyclability of long term catalytic activity. This would limit the photocatalytic application especially degradation of organic materials and toxic chemicals. To address this issue, constructing a heterojunction with other semiconductors offers a promising solution. Indeed, the construction of heterostructure semiconductors incorporating Ag_2CO_3 composites has been demonstrated to facilitate photo-carrier charge separation and significantly enhance photocatalytic performance.

Table 2.2 demonstrates the current research towards the heterostructure semiconductor with Ag_2CO_3 composites which the performance of degradation nearly 100%.

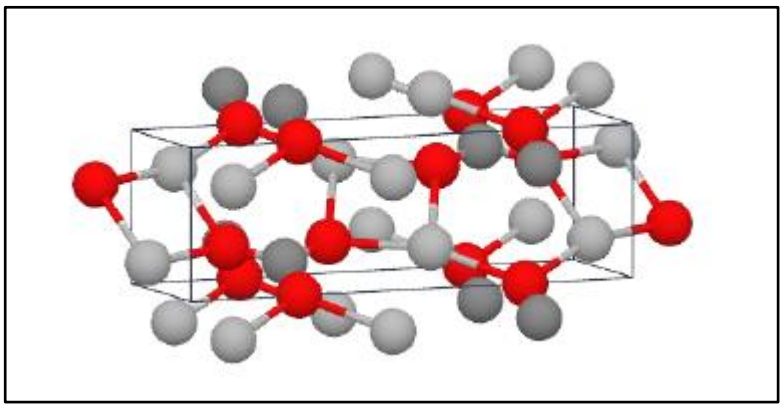

Figure 2.9 Simplified Unit Cell of Ag_2CO_3 (Ag – red ; C – dark grey ; O – grey)

Table 2.2 overview the recent research related to the Ag2CO3 based composite photocatalyst for the various model pollutant with the different conditions include the initial concentration and different light . Several synthesize method for the preparation the modified photocatalyst include in-situ precipitation, ion exchange and simple precipitation. The synthesis method is a crucial factor that directly affects the crystallinity, morphology, and surface area of the photocatalyst. These parameters strongly influence the separation of charge carriers and, consequently, the overall photocatalytic efficiency. Ag_2CO_3 based composite photocatalyst were compared with methyl orange (MO), rhodamine B (RhB), ethyl paraben (EP) and tetracyline (TC) at varying concentrations , light sources such as xenon lamp and visible light under different intensities with the irradiation time ranging from 10 to 100 minutes. Notably, the graphitic carbon nitride (g-C_3N_4) and CdS modifications were helps to promote the photocatalytic performance. The findings highlight Ag_2CO_3 based composite photocatalyst, particularly can increase the efficiency by coupling the semiconductor with other semiconductor to improve the charge separation as well as improve the light absorption.

Table 2.2

Current Research towards Ag_2CO_3 composites photocatalyst for the photodegradation of model pollutant

Photocatalyst	Preparation	Model Pollutant & Concentration	Operating Condition	Photocatalytic performance	Ref
Sulfate modified Ag_2CO_3	Simple precipitation	Orange G (10 mg L^{-1})	Vol = 25 mL; Visible Light 13W ; 0.0025g	94% OG removal after 30 min	(Ghazi et al., 2023a)
Ag_2CO_3	Simple precipitation	Ethyl paraben (5 mg L^{-1})	Vol = 25 mL; Xenon Lamp 100W; 0.0075g	90% EP removal after 30 min	(Petala et al., 2020)
g-C_3N_4/ Ag_2CO_3/graphene oxide	In-situ precipitation	Tetracyline (10 mg L^{-1})	Vol = 50 mL; Xenon Lamp 300W ; 0.0030g	81.6% TC removal after 60 min	(Liu et al., 2019)
BiOCl @CdS/ Ag_2CO_3	In-situ precipitation	Rhodamine B (15 mg L^{-1})	Vol = 50 mL; Xenon Lamp 1000W ; 0.025g	99% RhB removal after 100 min	(Fang et al., 2017)
g-C_3N_4/ Ag_2CO_3/AgBr	Ion exchange method	Rhodamine B (10 mg L^{-1}) Methylene Blue (10 mg L^{-1})	Vol = 100 mL; Xenon Lamp 350W ; 0.040g	99% RhB , 98% MB, 90% MO removal after 15 min	(Tang et al., 2017)
BiOCl/ Ag_2CO_3	In-situ precipitation	Methyl Orange (10 mg L^{-1})	Vol = 50 mL; Xenon Lamp 1000W ; 0.040g	97% RhB removal after 100 min	(Fang et al., 2016)
g-C_3N_4/ Ag_2CO_3	In-situ precipitation	Methylene Blue (10 mg L^{-1})	Vol = 50 mL; Xenon Lamp 500W ; 0.050g	81% MO removal after 20 min	(Tian et al., 2015)

2.4.2 Silver Phosphate (Ag_3PO_4)

Theoretically, Y. Liu et al., (2012) declare that the crystal structure of Ag_3PO_4 is a body-centered cubic (BBC) comprised of numerous isolated, regular PO_4 tetrahedral unit cells. The P-O bond distance is approximately 1.539 Å. Ag_3PO_4 belongs to the P4-3n space group and has a lattice parameter of around 6.004 Å. Greater application has been evolved especially for the wastewater treatment process includes degradation of phenol, dyes, pharmaceuticals waste and more. Researchers are increasingly focusing on Ag_3PO_4, which is regarded as a significant advance in the field of visible light responsive photocatalysts. Ag_3PO_4 has good photooxidative capability with a shorter wavelength approximately less than 530nm (Luo et al., 2014). In addition, as mentioned by Chen et al., (2015), the narrow band gap energy of Ag_3PO_4 is around +2.9eV vs normal hydrogen electrode (NHE, pH = 0) serve as an efficient for the strong oxidizing property as illustrated in the Figure 2.11. However, the high oxidation activity of Ag_3PO_4 can only be attained in the presence of electron sacrifice agents but the photo corrosion phenomenon will significantly limit the reuse efficiency of Ag_3PO_4 (C. Yu et al., 2022). Numerous of researcher has indicated that the Ag_3PO_4 exhibit good photocatalytic degradation towards the organic pollutant and photocatalytic for water splitting in both oxygen and hydrogen production.

Table 2.3

Current Research towards Ag_3PO_4 composites photocatalyst for the photodegradation of model pollutant

Photocatalyst	Preparation	Model Pollutant & Concentration	Operating Condition	Photocatalytic performance	Ref
Ag_3PO_4/Fe_3O_4/Chitosan	Ultrasonic assisted Precipitation Method	Methylene Blue (10 mg L^{-1})	Vol = 50 mL; Sunlight Irradiation ; 0.0300g	95% MB removal after 150 min	(Somasundaram et al., 2024)
Ag_3PO_4@g-C_3N_4	Workable Liquid Phase Deposition	Rhodamine B (100 mg L^{-1}) Methyl Orange (20 mg L^{-1})	Vol = 50 mL; Xenon Lamp 1000W ; 0.0010g	97.95% RhB, 98.34% MO removal after 120 min	(G. Huang et al., 2024)
Ag/ Ag_3PO_4/AgPMo	Hydrothermal & UV Reduction Method	Chromium(VI)- (0.08 mg L^{-1}) Tetracyline (30 mg L^{-1}) Methyl Orange (0.1 mg L^{-1}) Phenol (10 mg L^{-1}) Rhodamine B (10 mg L^{-1})	Vol = 50 mL; Xenon Lamp 300W ; 0.0500g	100% Cr (VI) ,97% TC, 92.7% MO, 47.6% RhB, 71.4% Phenol of removal after 90 min	(Fu et al., 2023)
Ag_3PO_4/CdS/Fe doped C_3N_4	Precipitation-Deposition Method	Phenol (50 mg L^{-1})	Vol = 100 mL; LED 35W ; 0.0050g	80% Phenol removal after 120 min	(Khan et al., 2021)
Pt- Ag_3PO_4/CdS/chitosan	Facile precipitation method	Methylene Blue (40 mg L^{-1})	Vol = 50 mL; Xenon Lamp 1000W ; 0.0010g	92% MB removal after 90 min	(Kiani et al., 2020)
AgBr–Ag_3PO_4/MWCNT	Chemical Precipitation Method	Basic Fuchin (20 mg L^{-1}) Basic Red 9 (20 mg L^{-1})	Vol = 50 mL; Xenon Lamp 500W ; 0.050g	97.8% BF, 98.8% BR9 removal after 60 min	(S. Wang et al., 2014)

In order to precisely explain the remarkable photocatalytic performance of Ag_3PO_4, (Li et al., 2019) conducted a detailed analysis and ascribed its superior activity to several key factors, which are outlined as follows. Firstly, the structure and distribution of conduction band minimum (CBM) of Ag_3PO_4 are important towards the electron transfer. Tetrahedral unit of PO_4 cause CBM to be dominated by Ag states in Ag_3PO_4. This will helps to completely occupied the d state in the valence band maximum (VBM). In addition, Ag_3PO_4 has a relatively isotropic distribution of CBM, which reduces the possibility of encountering photoinduced holes as compared to semiconductors with anisotropic distribution. Second, the inductive effect of PO_4^{3-} promotes the separation of electron-hole pairs. When the electron clouds are high and overlapping the PO_4^{3-} ions, it tends to draw the holes and reject electrons. This phenomenon effectively suppresses the recombination of photogenerated electron–hole pairs and consequently enhances the photocatalytic activity. Ultimately, native defects like Ag vacancies which effects the photocatalytic activity. These defects may cause to the photo corrosion phenomenon due to the Ag vacancies acts as shallow acceptor and contain high concentration in Ag_3PO_4. By functioning as capture traps for photogenerated holes, it can prevent charge carrier recombination, hence increasing the photocatalytic performance of Ag_3PO_4.

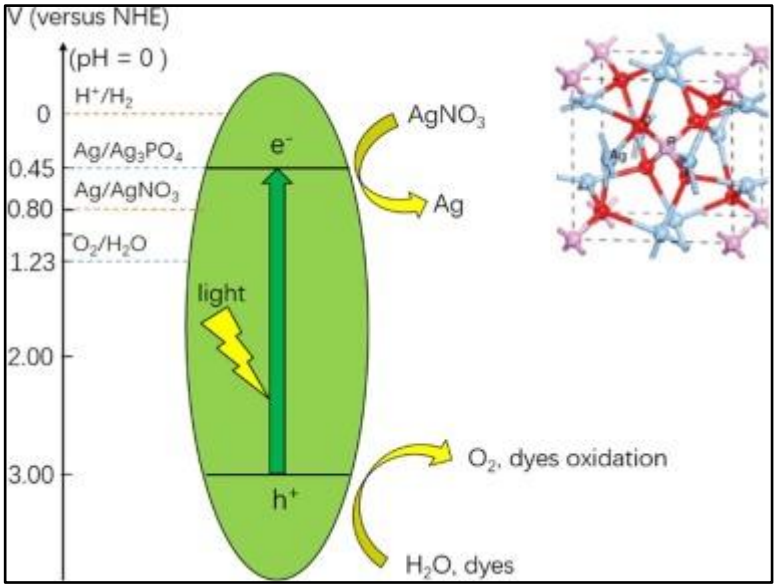

Figure 2.10 Schematic diagram and molecular structure of Ag_3PO_4 (Li et al., 2019)

Table 2.3 presents the recent studies towards the Ag_3PO_4 based photocatalyst for the various model pollutant with different synthesize method like chemical

precipitation, ultrasound-assisted precipitation and hydrothermal UV reduction were investigated. Among those model pollutant that has been compared in this literature review involve basic red (BR), rhodamine B (RhB), methyl orange (MO), methylene blue (MB) and chromium [Cr (VII)]. The degradation efficiencies were remarkably high towards the Ag_3PO_4/MWCNT which reach until 98.8% BR removal while Ag_3PO_4/g-C_3N_4 successfully achieve to degrade RhB at 97.6%. This table also conclude that the doping and hybridization such as Fe_2O_3 and Pt would significantly improve the photocatalytic activity for the potential Ag_3PO_4 based photocatalyst.

2.4.3 Silver sulfate (Ag_2SO_4)

Furthermore, silver sulfate (Ag_2SO_4) has demonstrated promising photocatalytic activity toward a wide range of model pollutants. However, its application remains relatively underexplored, as only a limited number of studies have been reported in the literature. As mentioned by Choo et al., (2016) , it claimed that Ag_2SO_4 has high cationic conductivity which helps to facilitate the rapid movement of cations. Hence, the photogenerated electron holes pairs are more effective that allows more charge in which reducing recombination as well increase the photocatalytic activity. Additionally, the core-shell structure based MSO_4 , (M = metal) exhibits the higher photocatalytic activity than the single core due to the good optical properties. Research by Zarghami et al., (2015) proved the significant optical properties and higher photocatalytic efficiency with $Ag@Ag_2SO_4$ nanoparticles for the degradation of methylene blue. Despite that, the utilization of Ag_2SO_4 was less selective could be due to the wide band gap energy approximately 2.8-3.8eV possess to the low absorption of the visible light region and high electron hole recombination. However, the band gap energy of Ag_2SO_4 can be modified based on the different method of synthesize and various type of oxosalts precursor. Figure 2.12 illustrated the crystal structure of Ag_2SO_4 is SO_4 based orthorhombic correlate with JCPDS 27-1403. Undeniable, Akhundi and Yangjeh, (2016), has successfully synthesize the novel g-C_3N_4/Ag_2SO_4 nanocomposites and achive to degrade Rhodamine B (RhB) about 99% within 390 min. These findings suggest that Ag_2SO_4 represents a promising alternative photocatalyst with the potential to enhance photocatalytic performance. The progress and recent developments in Ag_2SO_4-based composite photocatalysts are summarized in Table 2.4.

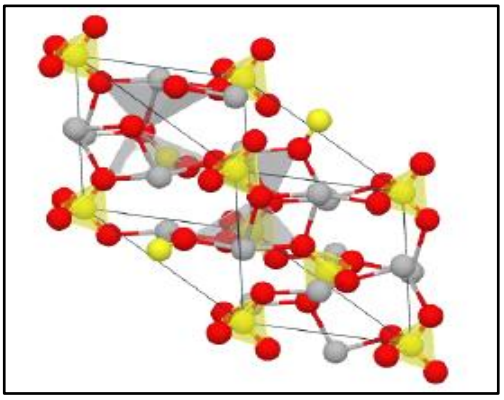

Figure 2.11 Simplified unit cell of Ag_2SO_4 (S – yellow, O- red, Ag-grey) (Shah et al., 2023)

Table 2.4 indicates the recent studies which focused on the Ag_2SO_4 based composite photocatalyst. Different synthesized was compared like microwave assisted, hydrothermal, impregnation and redox-precipitation preparation in which has been explored to enhance the photocatalytic performance. Among the studied, Ag_2S/Ag_2SO_4/Chitosan successfully degrade 99.9% RhB which show the highest efficiency within 60 minutes under sunlight irradiation. Moreover, $A_{g2}SO_4$/ZnO also demonstrates the significant photocatalytic activity by removing 99% IC and 100% of phenol under optimized conditions. Hence, these findings highlight the potential $A_{g2}SO_4$ as highly efficient photocatalyst for environmental remediation specifically in wastewater treatment applications.

Table 2.4

Current Research towards Ag_2SO_4 composites photocatalyst for the photodegradation of model pollutant

Photocatalyst	**Preparation**	**Model Pollutant & Concentration**	**Operating Condition**	**Photocatalytic performance**	**Ref**
Ag_2S/Ag_2SO_4/Chitosan	In situ Fabrication	Rhodamine B (20 mg L^{-1})	Vol = 50 mL; Sunlight Irradiation ; 0.0025g	99.9 % RhB removal after 60 min	(Zahedifar et al., 2024)
Ag@ Ag_2SO_4	Redox–precipitation reaction	Methyl Orange (10 mg L-1) Rhodamine B (10 mg L-1)	Vol = 80 mL; Xe lamp 300 W; 0.04 g	98% MO and RhB removal after 20 min	(T. Wei et al., 2017)
g-C_3N_4/ Ag_2SO_4	Fast microwave-assisted method.	Rhodamine B (25 mg L^{-1})	Vol = 250 mL; LED lamp 50 W; 0.1 g	99% RhB removal after 390 min	(Akhundi and Yangjeh, 2016)
Ag_2SO_4/ZnO	Impregnation method.	Indigo Carmine (IC) (10 mg L-1) Phenol (10 mg L-)	Vol = 150mL; Outdoor lamp 80 W; 0.15 g	99 % IC and 100 % phenol removal after 20 min and 300 min, respectively	(Choo et al., 2016)
Ag@ Ag_2SO_4/TiO_2	Facile Microwave Assited	Methylene Blue (20 mg L^{-1})	Vol = 150 mL; UV Lamp 30W ; 0.0020g	99 % MB removal after 90 min	(Zarghami et al., 2015)
Ag/ Ag_2SO_4/ZnO	Facile Microwave-Assisted Template-Free Hydrothermal Method	Rhodamine B (30 mg L^{-1})	Vol = 30 mL; Xe lamp 350 W; 0.03 g	97% RhB removal after 35 min	(Cao et al., 2015)

2.5 Cadmium Sulfide (CdS)

Cadmium sulfide (CdS) as an advanced nanostructured material that has been manifested by many researchers and has gained significant attention as a semiconductor recently. This is due to the favourable band positions, effective mass, strong quantum size effects and impressive photocatalytic activity when exposed to sunlight (Sharma et al., 2020). Cadmium sulfide (CdS) is classified as an n-type semiconductor and is considered one of the most prominent metal sulfides due to its suitable band gap, strong light absorption, and efficient charge carrier mobility. These features make it particularly attractive for applications in photocatalytic degradation. As mentioned by Mohan et al., (2021), CdS is a semiconductor with a band gap approximately around 2.42 eV and a maximum absorption peak of 514 nm wavelength, indicating that CdS can absorb visible and UV light wavelength. CdS is an effective photocatalyst which is noting that the the location of the CdS conduction band edge is lower than other common semiconductors such as TiO_2, ZnO, $SrTiO_3$ and more. Furthermore, CdS has remarkable as the great carrier transportation capability. This will enhance the photoinduced of electron and holes as well extend the photocatalytic performance. Hence, exploring the CdS and modified CdS catalytic behavior was very important to verify their efficiency in the field of photocatalysis and create the demand as the alternative for most of wastewater treatment.

CdS has two different crystal morphologies in the stable form which are hexagonal wurtzite and cubic-zinc blend. As demonstrated in the Figure 2.13, both of stable CdS structure, each of sulfur and cadmium ion is surrounded by four other ions. Theoretically, hexagonal structure has a cone morphology while cubic crystalline structure demonstrated an axial morphology. Hojjati-Najafabadi et al., (2024), has studied and discussed the mechanisms of CdS towards the photocatalytic activity. When the light being penetrated on the photocatalyst, holes and electrons will be excited from valence band to the conduction band. Higher energy from the electron was moved towards the CdS photocatalyst because the holes are less mobile. This leading to the higher photogenerated electron holes which indicate lower photocatalytic activity and describe the photo corrosion phenomena. It is an irreversible reaction, in which oxidation at the holes permanently converts CdS into sulfur and sulfate species, leading to photocorrosion and loss of photocatalytic activity.The chemical reaction has clearly indicated in the Equation 2.6 until 2.9 explained CdS photocatalyst works.

$$CdS \rightarrow e^- + h^+ \quad (2.6)$$

$$CdS + 4h^+ + 2H_2O + O_2 \rightarrow Cd^{2+} + SO_4^{2-} + 4H^+ \quad (2.7)$$

$$2O_2 \rightarrow Cd^{2+} + SO_4^{2-} + CdS \quad (2.8)$$

$$CdS + 2h^+ \rightarrow Cd^{2+} + S \quad (2.9)$$

Because of the presence of two holes and lack of oxygen, the photo corrosion of cadmium sulfide was altered and leads to the oxidation of sulfur. Therefore, CdS is appropriate photocatalyst in the visible light region due to its narrow band gap energy. Among the aforementioned above, CdS has extensive recombination which can retards the photogenerated electron holes and acute problem for the photo corrosion, this will affect the materials stability and recyclability. Therefore, coupling CdS with other semiconductors or developing CdS-based composites is an effective strategy to improve photocatalytic stability, while simultaneously enhancing overall photocatalytic performance. In consequence, the synthesized CdS with other materials have high chances to forms the heterojunction and the main focus of this research.

Research by Ravikumar et al., (2023) CdS was successfully developed for the removal of azo dyes under UV and solar light. In this study, CdS was doped with silver (Ag) to encounter the photo-corrosion issue that can inhibit the photocatalytic activity. The incorporation of Ag dopants reduces the band gap and decreases the nanoparticle size, which in turn suppresses charge recombination and significantly enhances the photocatalytic degradation efficiency towards diverse organic dye molecules. It shows around 93% of degradation with 3 different azo dyes include Reactive Red 120 (RR 120), Acid Black 1 (AB 1) and Direct Blue 15 (DB 15) dyes. After loading the CdS with Ag, the bandgap energy increased marginally from 2.30 to 2.41 eV. The bandgap of the Ag-incorporated material is almost enhanced and develops transitional phases in the energy gap. Ali et al., (2022) has validated the establishment of transitional phases

in the energy gap following silver replacement. As a consequence, increased electron-hole separation leads to improved photocatalytic activity.

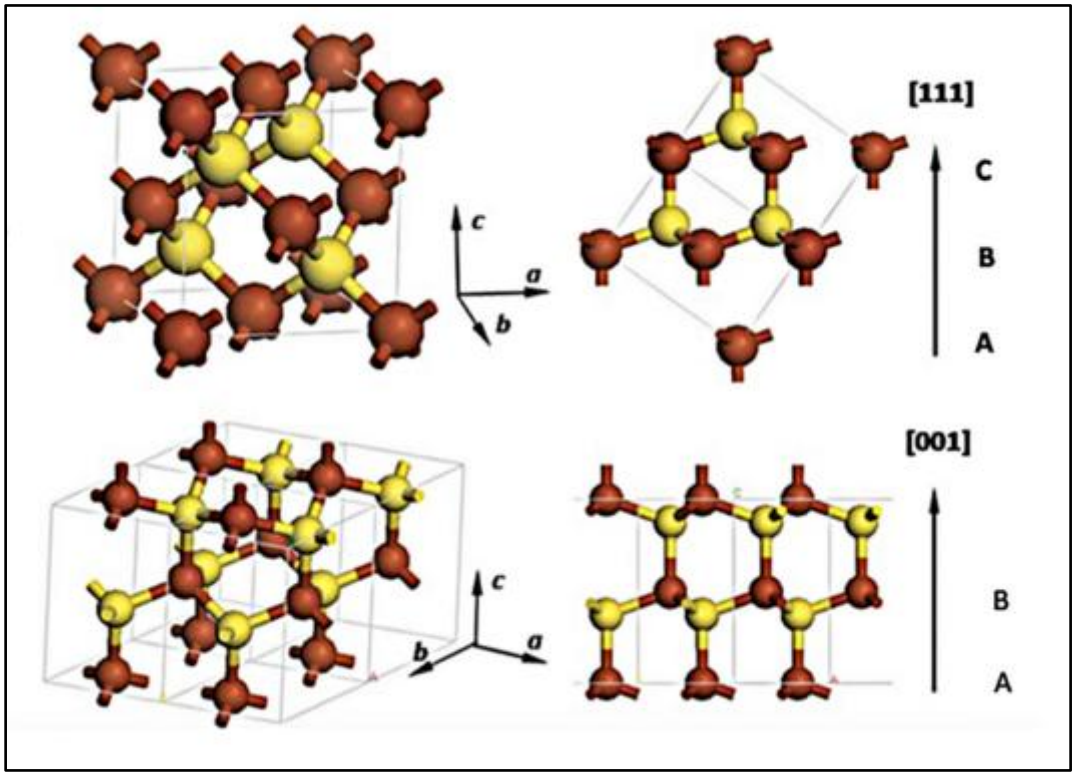

Figure 2.12 Crystal Morphology of CdS Zinc-blende (cubic) and wurtzite (hexagonal)
(Mao et al., 2024)

Table 2.5

Current Research towards CdS composites photocatalyst for the photodegradation of model pollutant

Photocatalyst	**Preparation**	**Model Pollutant & Concentration**	**Operating Condition**	**Photocatalytic performance**	**Ref**
Ni-doped CdS/ZnTe	Facile co-precipitation method	Methylene Blue (25 mg L^{-1}) Methyl Orange (25 mg L^{-1}) Rhodamine B (25 mg L^{-1})	Vol = 100 mL; Hg lamp 400W ; 0.0025g	98.74% MB, 99.71% MO and 95.04% RhB removal after 45 min	(Kamran et al., 2024)
rGO-CdS	Hydrothermal Method	Naphthol Blue Black (20 mg L^{-1})	Vol = 100 mL; UV light ; 0.0200 g	95% NBB removal after 120 min	(Priya et al., 2024)
TiO_2-CdS	Green synthesis	Congo Red (25 mg L^{-1}) Rhodamine B (25 mg L^{-1})	Vol = 100 mL; 300 W xenon lamp ; 0.0015 g	98.74% CR, 99.71% RhB removal after 45 min	(Rani et al., 2023)
CdS/ZnO	Hydrothermal and Deposition Method	Rhodamine B (10 mg L^{-1})	Vol = 100 mL; UV Lamp 120W ; 0.1000g	98.8 % RhB after 90 min	(Li et al., 2022)
Fe_3O_4/$BiVO_4$/CdS	Modified Solvothermal Reaction	Tetracyline (10 mg L^{-1})	Vol = 100 mL; 300 W xenon lamp ; 0.0010 g	87.37% TC removal after 90 min	(G. Xu et al., 2021)
CdS/$CuInS_2$	Hydrothermal Method	Hexavalent chromium (10 mg L^{-1})	Vol = 150 mL; 300 W xenon lamp ; 0.030 g	100% Cr(IV) removal after 60 min	(F. Deng et al., 2019)

2.6 Type of Heterojunction

To utilize maximum photocatalytic performance, it is highly necessary to modify the novel semiconductor photocatalyst, which is high photostability with the efficient visible light absorption. Most of the single photocatalyst such as CdS and Ag_2CO_3 will demonstrate less photocatalytic efficiency due to rapid recombination of photogenerated electron-hole pairs. According to Wen et al., (2022), a single photocatalyst is often unable to resist strong Coulombic interactions, which significantly limit charge separation and ultimately reduce overall photocatalytic efficiency. Apart from the rapid recombination, there are few crucial characteristics for an excellent photocatalyst such as sufficient redox capacity and broad sunlight absorption. For the redox ability, high conduction band (CB) and low valence band (VB) position resulting in wide band gap. Meanwhile, contemplating a broad absorption range, narrow band gap energy of single photocatalyst is more advantageous in the reaction. However, this condition cannot be reconciled at the same time. Hence, constructing heterojunction seems to solve it.

Heterojunction photocatalyst is when two semiconductors are joined together and the redox potential different archetypes are depicted in Figure 2.14A. From the thermodynamic standpoint, it is illustrated the reaction determines the driving force from the difference between the CB and VB potentials. To put it simply, the redox potentials energy difference is comparable to the gravitational potential energy difference.

As represented in Figure 2.14B and 2.14C, when a ball gets hit by a ball that has fallen from the higher altitude (refer Figure 2.14B), the initial acceleration and kinetic energy would be higher than when the ball get hit by a ball that falling down from lower altitude (refer Figure 2.14C). As a consequence, single photocatalyst perceived to have high redox ability which is high CB and deep CB position. It should be noted that high solar light absorption is required means low CB and VB location was recommended. Due to these two conditions, most of researchers are triggering and focusing their efforts on heterojunction photocatalyst (Xu et al., 2020).

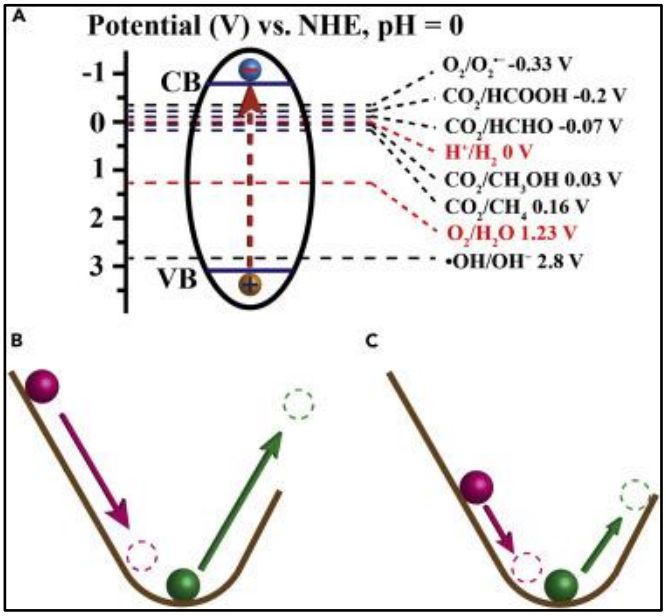

Figure 2.13 (A) Analogy between redox potential versus normal hydrogen electrode (NHE) at pH 0 ; the collision ball by another ball from (B) high altitude and (C) low altitude
(Tupikina et al., 2023)

2.6.1 Type II Heterojunction

Among the aforementioned approaches from the single photocatalyst, various types of heterojunctions have been garnered. Type II heterojunctions are the most prevalent and discovered by many researchers. Serpone et al., (1984) has successfully developed the electron transfer technique to avoid the charge photogenerated electron hole recombination. The interparticle electron transport was extended to the interparticle hole transfer when two linked semiconductors presented staggered band structures. In the presence of irradiation from both photocatalyst (photocatalyst I and photocatalyst II ; henceforth PC I and PC II), the photogenerated holes were transferred to the PC II to PC I, while the photogenerated electron were transferred from the PC I

to PC II as represented in the Figure 2.15. Aggregate from that, electron and holes gathered on PC II for reduction reaction and PC I for the reactions respectively. Hence, the photogenerated electron and holes were spatially separated.

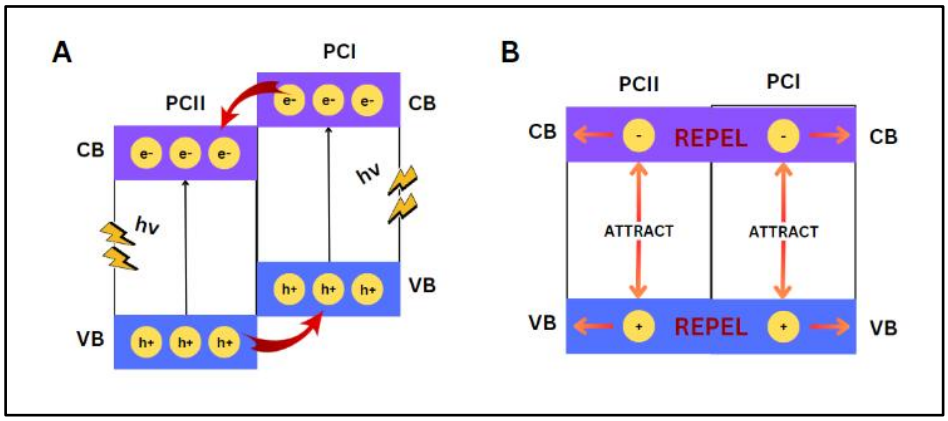

Figure 2.14 (A) Type II heterojunction ; (B) charge repel and opposite charge attract (Quan et al., 2026)

Although the type II heterojunction charge transfer mechanism is considered ideal and has inspired numerous investigations and discoveries, it still suffers from several limitations. It is due to the thermodynamic perspective; higher charge separation efficiency occurred with this type II heterojunction and leads to the decrease redox ability which is unfavourable for the photocatalytic process. As demonstrated in the Figure 2.15A, photogenerated holes would accumulate from VB at PC I will have high oxidation potential while photogenerated electron would collect from CB at PC II will have low reduction potential. Therefore, it may reduce the pushing force towards the photocatalytic activity mechanism. The reluctance process of the existing electrons in PC II will prevent the continuous flow of electrons from PC I in a dynamic standpoint. Simultaneously, repulsion process will be occur in PCI and any electron that will transfer from PCII will prevent the spatial charge transfer from being obtained. Concurrently, the electrostatic attraction between electron and holes at PC I will prevents the electrons from continuously moving from PCI to PCII as shown in the Figure 2.15B. This scenario could be the same with the charge attraction that exists in PCII where the holes are continuously prevent from transferred from PCII to PCI. Hence, the photogenerated electron holes in this type II heterojunction are challenged to be achieved. The repulsive electrostatic forces are more apparent than those between two magnetic poles. The magnetic levitation train may be suspended due to the strong repelling force between two poles. As a conclusion, the charge-transfer process in type

II heterojunctions is challenging since it fails to separate photogenerated electrons and holes which lower heterojunction's overall redox capacity.

2.6.2 Z-scheme Heterojunction

The mechanism of standard Z-scheme heterojunction relies on two different semiconductors where one for the reduction process and the other for oxidation process (Jiang et al., 2018). As illustrated in the Figure 2.16, the reduction photocatalyst would have high CB position for the significant reduction capacity, on the other hand oxidation photocatalyst have a lower VB position as the high ability of oxidation respectively. Researcher by (Shabbir et al., 2024) has declared that Z-scheme heterojunction offers superb photocatalytic activity with numerous advantages that demonstrate great charge transfer. It is include (1) the strong oxidation and reduction abilities can be maintained simultaneously ; (2) the active site of oxidation and reduction could spatial separate ; (3) high redox power with efficient photogenerated charge carrier ; (4) a wide range of photocatalyst for various photocatalytic reaction and (5) increased the light harvesting.

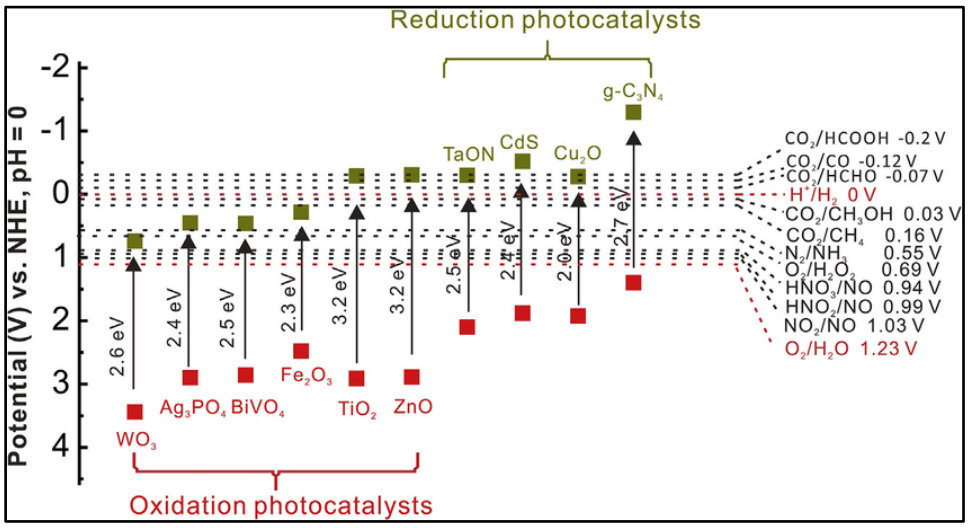

Figure 2.15 Standard Redox Potential of Photocatalyst (Sudha et al., 2026)

Z-scheme heterojunction can be classified into 3 categories commonly based on whether the charge carrier mediator is used and the type of mediator involved: (1) traditional Z-scheme photocatalysis in which utilized a reversible redox ion pair by using IO^{3-}/I^{-} or Fe^{3+}/Fe^{2+} to facilitate the charge carrier transfer; (2) all-solid state Z-scheme photocatalyst where the noble metal include Pt, Au or Ag act as electron

mediator to aid in charge transfer; (3) direct Z-scheme photocatalyst where the two semiconductor are closely coupling and the charge transfer occurs through an internal electric field as well as eliminating the need for any charge carrier transfer mediator (Sabzehmeidani et al., 2021).

2.6.2.1 Traditional Z-Scheme Heterojunction

Traditional Z-scheme photocatalyst was discovered by Bard since 1979 which mimic to the natural photosynthesis in plant. At that time, the exploration towards this study mainly to increase the efficiency of charge separation as well as maintained the strong redox ability. Theoretically, the mechanism of this traditional Z-scheme heterojunction is constructed by the hybridization of two photocatalyst with suitable shuttle redox ion mediator as example IO^{3-}/I^{-} or Fe^{3+}/Fe^{2+}. As depicted in the Figure 2.17, when light being penetrated to the photocatalyst, the photogenerated holes will be absorbed by electron acceptor (A) species in the CB of PC II whereas photogenerated holes in the VB of PC I are engendering by the electron donor species (D). Subsequently, the photogenerated electron in the CB of PC I and holes in the VB of PC II able to be maintained with high redox ability together spatially separated redox reaction sites. Thus, it leads to higher photocatalytic activity.

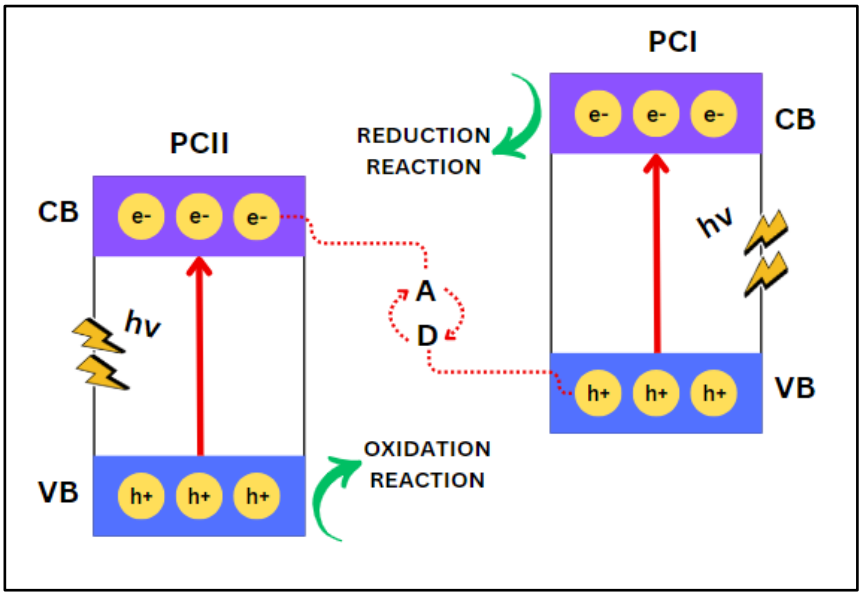

Figure 2.16 Schematic of charge transfer for traditional Z-scheme photocatalyst (Ebihara et al., 2021)

In spite of this system, it also has some drawbacks. The photogenerated electron holes with high redox power are indispensable by the shuttle redox ions pair which cause redox mediator-induced back reactions are thermodynamically advantageous and easily occur. Besides that, poor charge carrier transfer limited by ion pair diffusion, the solution very sensitive to the pH and light shielding effect where can contribute to the limited application of traditional Z-scheme photocatalyst (Jourshabani et al., 2020).

2.6.2.2 All Solid State Z-Scheme Heterojunction

As a traditional Z-scheme heterojunction, the mechanism will comprise the shuttle redox pairs to facilitate the charge transfer between both photocatalyst. However, for all-solid state Z-scheme heterojunction mechanism, an electron solid conductor will be transform or is used charge carrier transfer as a bridge as represented in the Figure 2.18. The first discovery of this system by Tada et al., (2006) has successfully synthesized CdS with TiO_2 and Au act as electron mediator. In addition, research by (Hou et al., 2022) has constructed $Ag@Ag_3PO_4/TiO_2$ and described that the selection of a relevant electron is very crucial because it help to transport the photogenerated carrier charge efficiently together to increase the stability of the photocatalyst.

Commonly, noble metal (NPs) such as Pt, Au and Ag have been used by many researchers as electron mediator for the development of all solid-state Z-scheme photocatalyst (X. Yu et al., 2020; M. Zhang et al., 2020). Besides that, additional conductive materials include fullerenes, carbon and graphene also promoting the alternative as electron mediator (Wu et al., 2017). Solid conductor though to be recommended rather than ionic redox solution because it able to avoid the reverse reaction and allow the photocatalyst recovery. Furthermore, this system of heterojunction can be operated whether in gas phase and liquid phase. Due to the solid conductor, it will increase the charge carrier transfer. But certain noble metal quite expensive and difficulties in terms of sintering effect that decrease the surface catalyst and interfere the surface structure.

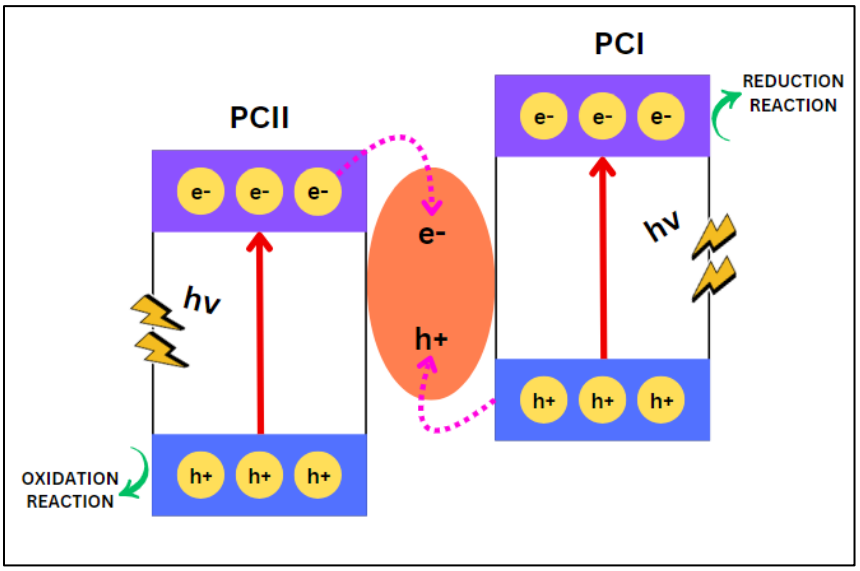

Figure 2.17 Schematic diagram of charge carrier in all solid state Z-scheme heterojunction photocatalyst
(Zhong et al., 2025)

2.6.2.3 Direct Z-Scheme Heterojunction

Until now, there is a lot of confusion over between the traditional Z-scheme as well as the all-solid state Z-scheme and show dissatisfactory due to their charge transfer. Therefore, direct Z-scheme has evolved without any intermediate whether redox couples or conductors. Zhu et al., (2018) has successfully fabricated the g-C_3N_4/TiO_2 as the direct Z-scheme for the photocatalytic degradation of organic pollutants as shown in the Figure 2.19. Basically, the charge mode of this scheme was investigated when the two semiconductors was contact to each other and the band structure was staggered It denotated that when two semiconductors have different operational, the charge redistribution and creation of internal electric field will be induce. Thus, it will give the major impacts towards the charge carrier's separation together with transfer of photogenerated electron hole pair (Jiang et al., 2018b; Low et al., 2019).

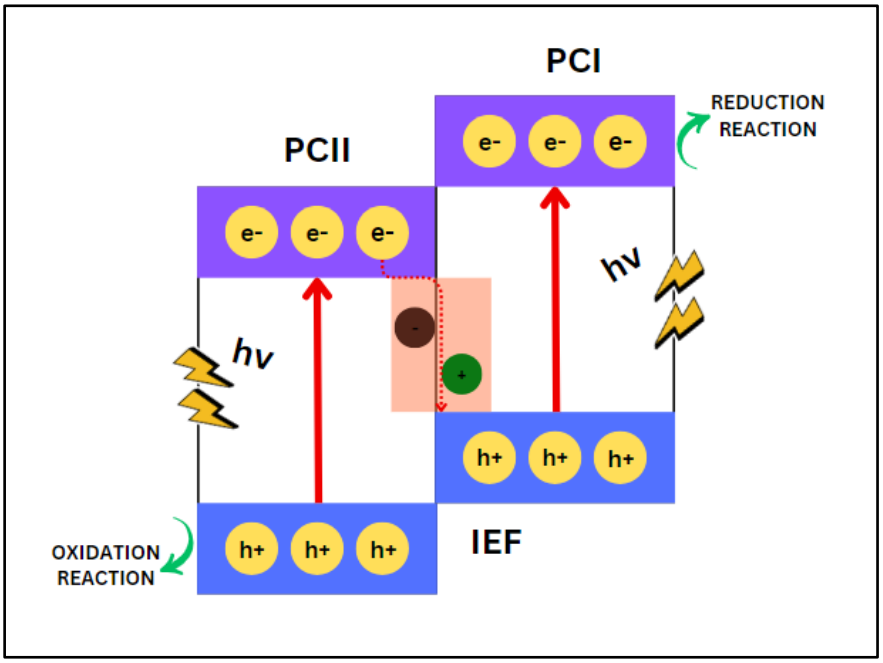

Figure 2.18 Schematic of charge carrier in direct Z-scheme photocatalyst (Zhang et al., 2019)

Direct Z-scheme fundamentally based on PC I has a higher position of VB and CB level with higher Fermi level (E_F) compared to PC II has a lower position CB and VB positions based on the Figure 2.20A. Electric field will be created within the band (Figure 2.20B), when PC I and PC II come into contact and free electron was transferred from the PC I to PC II. As a result, PC I is more positive at the interface while PC II is more negative. The presence of an internal electric field (IEF) , (Figure 2.20C) promotes recombination between photogenerated electron in PC II of CB and photogenerated holes in PC I of VB. The internal electric field is the additional potential barrier by the Coulomb repulsion and band bending as illustrated in the Figure 2.20D. Meanwhile, it will obstruct the transferred of photogenerated electron hole from PC I at CB to PC II to CB. Electron from PC I of CB and holes from PC II of VB can be maintained and spatially segregated together allows the reductive and oxidative for the photocatalytic processes. Hence, the IEF could prevent recombination between photogenerated electron in PC I of CB and photogenerated hole in PC II in VB ((Low et al., 2017; Q. Xu et al., 2018).

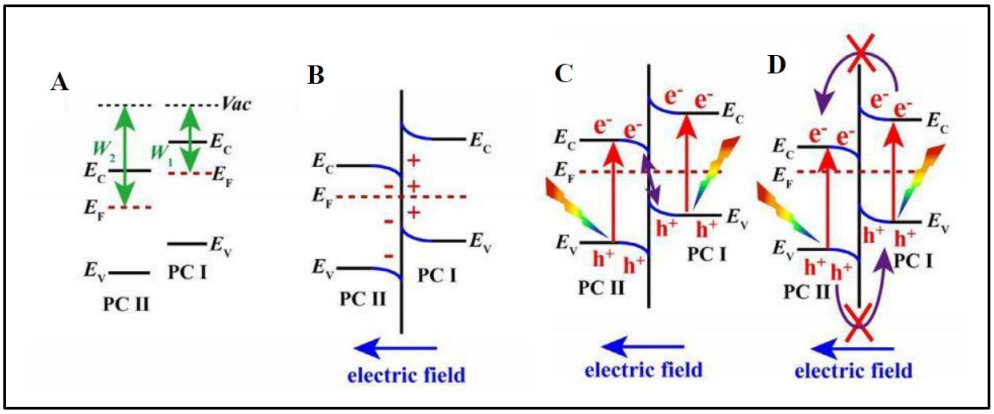

Figure 2.19 Schematic diagram of both photocatalyst with staggered band structure ; (A) before contact , (B) in contact , (C) photogenerated charge carrier transfer in direct Z-scheme, (D) photogenerated charge carrier in type II heterojunction
(Wang et al., 2023)

2.7 Clarification Method of Z-Scheme

Researcher has actively explored Z-scheme heterojunction and there are few methods to validate the Z-scheme mechanism, including : (1) evaluation XPS. According to Wang et al., (2019) that successfully prepared the direct Z-scheme of ZnO/CdS and proved by using XPS analysis. When the photocatalyst exposed to the light, the photogenerated charge carriers will be react and transfer, leading to shifts in the binding energy of constituent elements. When the binding energy increases means the electron loss, while a decrease it shows electron gain. These binding energy changes provide insight into the Z-scheme charge transfer mechanism. The next approach to validate the Z-scheme heterojunction is by ; (2) independently verified the photocatalytic processes like hydrogen (H_2) evolution and carbon dioxide (CO_2) reduction as the photogenerated electrons to retain the strong reduction ability (S. Tang et al., 2023). For the photocatalytic reactions, it can be confirmed through trapping test or also known as scavenger test to identify the active species involved in reactions such as oxygen (O_2) and degradation of model pollutant (Jia et al., 2016; J. Wang et al., 2017; J. Zhang et al., 2022). Additionally, (3), noble metal selective photo-deposition because the selective noble metal that has been deposited on the electro-rich area will exposed to the region containing electron. This could verified the Z-scheme charge carrier transfer pathway. Lastly, (4) analysing by characterization of UV-Vis DRS. It is a valuable tool because it provides the information about the optical absorption properties of each material which linked to the electronic structure of the photocatalyst involved. The wavelength of photocatalyst begins when it absorbs the light and corresponds to

the band gap energy (Eg). This can be determined from absorption spectrum where the onset of absorption indicate the minimum energy required to excite the electron from VB to the CB (F. Chen et al., 2018; Shao et al., 2019). According to Xia et al., (2024), from the absorption edge, the band gap can be calculated using Tauc plot which identified the position of the conduction band (CB) and valence band of semiconductor.

2.8 Photocatalytic Kinetic

Pseudo first order and Langmuir Hinshelwood (LH) is commonly described for the kinetic study for photocatalytic degradation to determine the influence of initial concentrations of the solution. The model of Langmuir Hinshelwood is typically for heterogeneous photocatalysis, explained based on substrate covered on the surface of catalyst and involve adsorption of the reactants (Kumar et al., 2008; Pourshaban-Mazandarani & Nasiri, 2024). When the reaction occurs on the surface of catalyst, it can be assumed that the reaction is directly proportional to the fraction of the surface that covered the substrate. At the point zero charge (pH_{pzc}), the surface catalyst is neutral but when the surface becomes positively charged, the organic pollutants will not adsorb on the catalyst surface. The presence between hydroxyl group and water on the same active sites cannot be neglected and Equation 2.10 expressed the model.

$$r = -\frac{dC}{dt} = k_r\,\theta = \frac{(k_r\,K_{LH}\,C)}{(1 + K_{LH}\,C + K_{H_2O}\,C_{H_2O})} \tag{2.10}$$

where r is the photooxidation rate of the reactant ($mgL^{-1}min^{-1}$), C is the concentration of the reactant (mgL^{-1}), t is the irradiation time, k_r is the reaction rate constant ($mgL^{-1}min^{-1}$), K_{LH} is adsorption coefficient of the reactant ($L^{-1}mg$), K_{H2O} is the solvent adsorption constant and C_{H2O} is the concentration of water. Commonly, C_{H2O} high concentration than C , and C_{H2O} remains throughout for every range of concentration. For all the experiments such as pH and amount of catalyst remain constant. Thus, Equation 2.11 were determined where the C is the variable for initial concentration.

$$r = -\frac{dC}{dt} = k_r\,\theta = \frac{(k_r\,K_{LH}\,C)}{(1 + K_{LH}\,C)} \tag{2.11}$$

Due to the formation of intermediates, interference in kinetic studies can takes place because the competition between adsorption and oxidation between photocatalytic reduction. Therefore, calculations should begin at the point where illumination starts as this allows ignoring changes like pH variation or intermediate formation at that moment. The concentration fraction then be used to derive the rate of photocatalytic reduction as Equation 2.12.

$$r_o = -\frac{dC}{dt} = k_r \left(\frac{K_{LH}\, C_o}{1 + K_{LH} + C_o} \right) \tag{2.12}$$

Where r_0 represents the initial photocatalytic oxidation rate ($mgL^{-1}min^{-1}$), C_o is the initial concentration (mgL^{-1}), K_{LH} is adsorption equilibrium constant ($L^{-1}mg$). When the chemical concentration C is very low, the equation can be simplified to an apparent first order reaction equation.

$$\ln\left(\frac{C_o}{C_t}\right) = k_r\, K\, t = k_{app}\, t \tag{2.13}$$

Based on the Equation 2.13, $k_rK=k_{app}$, C_t is the concentration at time t and Co is the initial concentration of the solution. In general, the initial oxidation rate can be conclude as below :

$$r_o = k_{app}\, C_o \tag{2.14}$$

$$\frac{1}{r_o} = \left[\frac{1}{k_r K_{LH}}\right]\left[\frac{1}{C_o}\right] + \frac{1}{k_r} \tag{2.15}$$

Where r_0 is the initial reaction rate, ($mgL^{-1}min^{-1}$), k_r is the reaction rate constant ($mgL^{-1}min^{-1}$), K_{LH} is adsorption coefficient of the reactant ($L^{-1}mg$), C_o is the initial concentration (mgL^{-1}). A linear relationship in a graph plotting ln (C_o /C) against time confirms that the photocatalytic activity follows a pseudo-first order kinetic model. The slope of the plotted graph corresponds to the first-order rate constant k.

2.9 Methyl Orange

Methyl Orange (MO) is a water-soluble azo dye that is widely employed in a variety of industries, including textile, paper, printing, and food and is mostly discharged in industrial wastewater. The structure of methyl orange dyes specifically due to the -N=N- azo bonds as illustrated in the Figure 2.21. According to Aljuaid et al., (2023), azo group is the stabilising dyes which able to form conjugated system which often helps to absorb visible light. Nevertheless, azo dyes and its by product are carcinogenic, mutagenic in high concentration and difficult to break down if releasing to the water stream. Furthermore, the molecular formula of methyl orange is $C_{14}H_{14}N_3NaO_3S$ and has been classified as anionic dyes in the group of sulfonic. Methyl orange has maximum absorption approximately around 465 nm with the molecular 327 g/mol. Generally, methyl orange as shown in the Figure 2.22 was suitable in laboratories as the pH indicator together with colouring agent. It is ascribed to the pH range of methyl orange between 3.1 until 4.4 which is efficient for the interaction study of strong acid and weak bases.

Figure 2.21 Methyl Orange Powder
(Hasni et al., 2026)

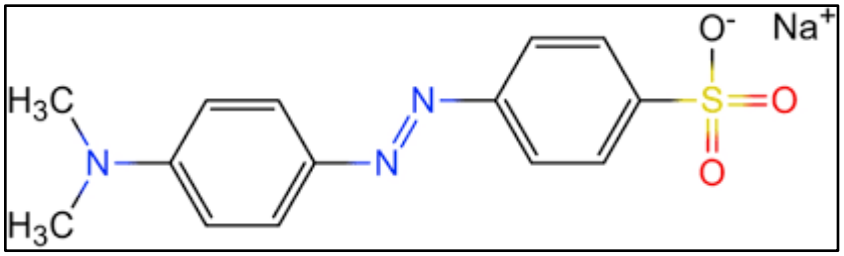

Figure 2.20 Chemical Structure of Methyl Orange
(Kostjukov, 2026)

CHAPTER 3
RESEARCH METHODOLOGY

3.1 Introduction

This chapter consists of several main parts including chemicals and materials, advanced instrumentation, experimental procedures, characterization, photocatalytic analysis, optimization and parameter study. Figure 3.1 represented the synthesize of silver carbonates as the parent's catalyst while cadmium sulfide as the composite catalyst. To mitigate the photo corrosion phenomenon for cadmium sulfide, low concentrations was focused on this research. Then, synthesized different ratio of silver carbonate and cadmium sulfide (95:5, 90:10 and 85:15) respectively. Next, the coupling between silver carbonate and cadmium sulfide were subjected to characterization analysis such as X-Ray diffraction (XRD), transmission-electron microscopy (TEM), Field emission scanning electron microscopy (FESEM), Fourier transform infrared (FTIR) spectroscopy, X-ray photoelectron spectroscopy (XPS) and Ultra-violet visible diffuse reflectance spectroscopy (UV-Vis/DRS) and Photoluminescence (PL). After that, photocatalytic testing was performed on the degradation of methyl orange as a model pollutant. Lastly, the proposed mechanism, the parameter study and reusability of photocatalytic degradation of methyl orange using modified catalysts were investigated.

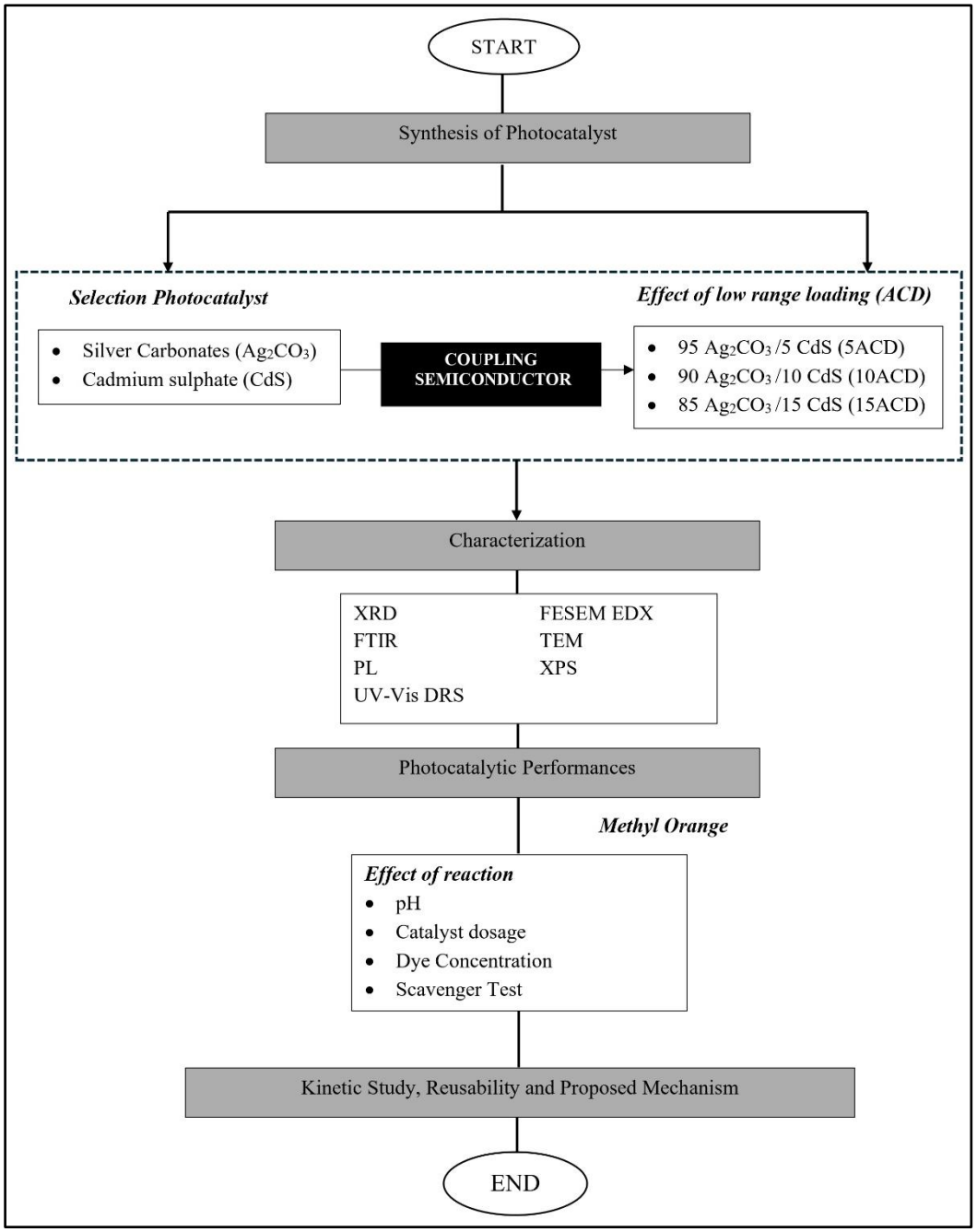

Figure 3.1 Research Methodology Flow Diagram

3.2 Chemicals and Materials

Table 3.1 indicate the chemicals and materials that involved in the experimental works. The chemicals used in this study include silver nitrate ($AgNO_3$) with a purity of 99.7% and analytical reagent (AR) grade, sourced from System. Sodium carbonate (Na_2CO_3), also of AR grade with 99% purity, and sodium sulfide (Na_2S) with 95% purity and CP grade were obtained from R&M Chemical. Cadmium chloride ($CdCl_2$),

with 98% purity and ACS grade, was supplied by Thermo Scientific. Methanol (CH_3OH) and isopropanol, both with 99% purity, were sourced from Merck and Qrec respectively, with methanol classified under ISO grade and isopropanol under AR grade. Additionally, potassium iodide (99% purity, ISO grade) was obtained from Merck, while potassium chlorate (99% purity, ACS grade) was supplied by Fisher. For the synthesized of silver carbonates, silver nitrate and sodium carbonate were used as the precursor. Meanwhile, the preparation of cadmium sulfide was prepared by cadmium chloride together with sodium sulphide . Besides that, the scavenger analysis was detected with isopropanol, methanol, potassium chlorate and iodide.

Table 3.1
List of Chemical

Chemical	Purity (%)	Grade	Sources
Silver Nitrate ($AgNO_3$)	99.7	AR	Systerm
Sodium Carbonate (Na_2CO_3)	99	AR	R&M Chemical
Cadmium Chloride ($CdCl_2$)	98	ACS	Thermo Scientific
Sodium Sulfide (Na_2S)	95	CP	R&M Chemical
Methanol (CH_3OH)	99	ISO	Merck
Isopropanol	99	AR	Qrec
Potassium Iodide	99	ISO	Merck
Potassium Chlorate	99	ACS	Fisher
Methyl Orange	89	ACS	Sigma Aldrich

3.3 Catalyst Preparation

In this study, the preparation step of catalyst includes of synthesize of silver carbonate (Ag_2CO_3), cadmium sulfide (CdS) and silver carbonate loaded on cadmium sulfide (ACD) at different ratio.

3.3.1 Preparation of Silver Carbonate (Ag_2CO_3)

Facile precipitation technique by Jiang et al., (2025) was employed for the synthesis of the parents' catalyst, silver carbonate (Ag_2CO_3). Approximately, 5.29 g of

$AgNO_3$ and 3.70 g of Na_2CO_3 was mixed with 30 mL of distilled water. To ensure the mixture are completely homogeneous, it was stirred around 30 minutes until light green precipitation formed. Then, the mixture was transferred in the oven and dried at 100^OC for 12 hours. Lastly, the obtained Ag_2CO_3 was grind and stored in the bottle sample.

$$2AgNO_3\ (aq) + Na_2CO_3\ (aq) \rightarrow Ag_2CO_3\ (s) + 2NaNO_3\ (aq) \qquad (3.1)$$

3.3.2 Preparation of Cadmium Sulfide (CdS)

Throughout this study, CdS nanoparticles was synthesized by using simple chemical mixing method with some modification based on Najm *et.al* (2020). Cadmium chloride ($CdCl_2$) together with sodium sulfide (Na_2S) was used as the precursor while deionized water and ethanol was be added to the solution as the capping agent. During the synthesis, 0.1 M of $CdCl_2$ and 0.1 M of Na_2S was dissolved in 50 mL of deionized water – ethanol with 50:50 ratio respectively. Then, $CdCl_2$ was added dropwise into Na_2S and the solution was continuously stirred until its homogeneous precipitation is obtained. The chemical reaction was shown in the Equation 3.1.

$$CdCl_2 + Na_2S \rightarrow CdS + 2NaCl \qquad (3.2)$$

The obtained precipitation was washed 4 times with deionized water and ethanol through centrifugation process at 6000 rpm for about 10 minutes to get high purity of prepared photocatalyst. As the result, the yellowish precipitation of CdS nanoparticles was collected and dried in the oven for overnight.

3.3.3 Preparation of Ag_2CO_3/CdS (ACD)

These nanocomposites of Ag_2CO_3/CdS were prepared using a modified simple mixing method at different ratios (95:5, 90:10, and 85:15) to explore the optimum photocatalyst composition for higher photocatalytic activity, as previously investigated by (Y. Liu et al., 2018). In this section, Ag_2CO_3 was act as parents' catalyst while CdS as the composite catalyst due to the photo corrosion and toxicity characteristics. Therefore, the ratio of CdS was only focused on the lower concentration to avoid the photo corrosion phenomenon at the surface of photocatalyst that have high possibility to retard the photocatalytic activity. The prepared Ag_2CO_3 and CdS was added together

with 40 mL of distilled water then it was sonicated around 10 minutes. Finally, the mixture was dried for 3 hours at 80ºC and ground into fine powder as Ag_2CO_3/CdS obtained.

3.4 Catalyst Characterization

The physiochemical properties of the synthesized catalyst were characterized by using several advanced instrumentations as mentioned below.

3.4.1 Structural, Crystallinity and Phase Studies

Research by Raja et al. (2022) deduced that XRD analysis is a non-destructive technique that helps reveal the phase purity, crystallinity, and optical properties of synthesized samples. The obtained diffraction peaks from the XRD analysis rely on the constructive interference of monochromatic X-rays with the crystalline structure. Each diffraction pattern created from the prepared samples corresponds to the intensity of the diffracted rays, atomic arrangement, and optical properties. Hence, the prepared Ag_2CO_3/CdS samples were evaluated using an XRD D500 (Bruker, Germany) with Cu-Kα radiation, at a scanning rate of 5 minutes in the 2θ range of 5° to 80°, as described by Długosz et al. (2025).

3.4.2 Functional group and Surface Characteristics Study

Fourier Transform Infrared (FTIR) Spectroscopy is a simple and cost-effective analysis used to verify the pure compounds present in the prepared Ag_2CO_3/CdS sample. The analysis depends on identifying the functional groups within the molecule, which vibrate when exposed to specific wavelengths of light. The wavenumber was set in the range of 400–4000 cm^{-1} using the KBr pellet method with a PerkinElmer FT-IR Spectrometer Frontier. Approximately 2 g of Ag_2CO_3/CdS sample was ground with potassium bromide (KBr) and compressed using a hydraulic press to form pellets, as demonstrated by P. Huang et al. (2026).

3.4.3 Optical Properties

UV-Vis DRS has gained prominence currently due to its flexibility with a wide range of samples in various states. This analysis is useful technique to evaluate the absorption of the samples surface and interior by the light reflection. Despite that, it may also be utilized to examine the structure and composition of the prepared samples (Zhang et al., 2025). Firstly, about 2.0 g of the prepared sample was pressed into pellet with applying 7-ton pressure, then was placed in a special holder to be characterized. Thus, the band gap of the samples can be estimated by Tauc Plot that between $(\alpha hv)^{1/n}$ and hv from the Kubelka-Munk according to the follow Equation 3.2,

$$(\alpha hv)^{1/2} = A(hv - Eg) \quad (3.3)$$

Where v is light frequency, h is Plank's constant, α is the absorption coefficient, Eg is direct band gap and A is proportionality constant. Based on this equation, the conduction band and valence band able to be calculated with Mulliken Electronegativity Theory as below Equation 3.3 and 3.4,

$$E_{VB} = X - E^{o} + 0.5\ Eg \quad (3.4)$$

Where, X is geometric means value of atomic electronegativity, E^{o} is energy free electron (4.50 eV), E_{VB} is valence band and Eg is direct band gap (calculated from Tauc Plot) and E_{CB} to determine the conduction band.

$$E_{CB} = E_{VB} - Eg \quad (3.5)$$

3.4.4 Internal Surface Morphology Study

The morphology and size of the synthesized catalyst was observed using TEM. The TEM characterization was carried out by employing JEOL JEM–2100F. For the TEM observations, a powder sample was dissolved in acetone and dropped onto the copper grid. This droplet was dried before subjected to morphological observation.

3.4.5 Surface Microscopic Study

In order to characterize the surface morphology and elemental composition of Ag_2CO_3/CdS samples, FESEM is an advanced technology that was performed. Firstly, the optimum prepared sample was ground and sieved by using Endecotts Ltd sieve with aperture sized of 150 μm to ensure the prepared samples are fully fine catalyst particles. Then, it was coated with gold and observed with LEO model 1530 FESEM at 3kV. The mechanism of FESEM analysis is based on the electrons with negative charge rather than light. According toSemnani, (2017), field emission is a source that generate for the electron with the strong electrical field gradient properties. These so-called primary electrons are focussed and deflected by electronic lenses within the high vacuum column to generate a narrow scan beam that bombards the item. As a result, each area on the item emits secondary electrons. The angle and velocity of these secondary electrons are related to the object's surface structure. Then, the secondary electrons are captured by a detector, which generates an electrical signal. This signal will be amplified and converted to a display or digital picture, which may then will be saved and processed. As revealed, this analysis was conducted in high vacuum since gas molecules tend to affect the electron beam while it is also suitable for backscattered electron that help in utilization of imaging.

3.4.6 Chemical Oxidation State Determination

In the research by Nossol et al. (2023) and Selva et al. (2023), XPS, also known as Electron Spectroscopy for Chemical Analysis (ESCA), is a technique based on the photoelectric effect, in which the core-level electrons of elements on the surface of the prepared sample are stimulated by a beam of monochromatic X-ray electromagnetic radiation. As a consequence, it is possible to detect not only the elemental composition but also the oxidation states, since each electron has a specific binding energy. Therefore, XPS is an ideal approach to examine the surface composition of the prepared Ag_2CO_3/CdS sample.The expected outcome for an ideal Ag_2CO_3/CdS sample in XPS analysis would be binding energy peaks corresponding to sp^2 carbons. To ensure the photocatalyst consisted of fine particles, the sample was ground and sieved with an aperture size of 150 μm. The prepared photocatalyst was then dried in an oven at 100

°C for 12 hours prior to analysis. Finally, the sample was sprinkled onto the surface of sticky carbon tape for analysis, with the base pressure maintained below 5.5×10^{-9} Torr.

3.4.7 Optical Excitation of Electron Hole Study

Photoluminescence (PL) is a methodology used to analyze the separation and recombination of photogenerated charge carriers when semiconductors emit spontaneous light under optical excitation. According to Chakrabartty et al. (2022), the excitation and intensity observed arise from the electron–hole recombination of the photocatalyst. The mechanism was studied by Kotb et al. (2023), who reported that when light with sufficient energy strikes a medium, photons are absorbed and electronic excitations occur. After these excitations decay, the electrons gradually return to their ground state. The emitted light is recognized as PL when radiative relaxation takes place. Hence, an increase in PL intensity indicates higher recombination of charge carriers, whereas a decrease in PL intensity suggests more effective charge carrier separation. This property is highly important for achieving efficient photocatalytic performance. In this study, the prepared sample was analyzed using a Perkin Elmer LS55 fluorescence spectrometer with an excitation wavelength of 325 nm. Approximately 0.2 g of the sample was compressed under 7 tonnes of pressure prior to analysis.

3.5 Preparation of Methyl Orange

The 100 mg L^{-1} stock solution of methyl orange was prepared by dissolving 0.056 g of methyl orange (89% purity) in 500 mL of distilled water to obtain the required concentration. The stock solution was then diluted with distilled water to the desired concentrations using a 100 mL volumetric flask.

3.6 Photocatalytic Degradation

The photocatalytic degradation of Ag_2CO_3/CdS was examined under 65W fluorescent lamp irradiation with approximately, 0.025g of optimum photocatalyst and methyl orange was used act as the model pollutant. Each of the cycle was took around 15 minutes adsorption-desorption equilibrium and 60 minutes with 15 minutes interval

for decolorization as completion methyl orange turn to colourless. To provide the sufficient oxygen along the photodegradation process, an aquarium pump model NS 7200 was used as an aeration source under 70 mL min^{-1} throughout the process. The percentage of the remaining of dye degradation was measured by spectrophotometer via HACH DR2000 with wavelength of 462 nm. Thus, it was obtained the absorbance reading to calculate the percentage degradation efficiency of dye (%) as the Equation 3.5 stated below. The calculation formula where D_0 is the initial absorbance of methyl orange concentration while D_i is the final absorbance of methyl orange concentration.

$$Degradation\ Efficiency\ (\%) = \frac{Do-Di}{Do} \text{ x } 100\ \% \qquad (3.6)$$

The photocatalytic degradation also was examined under different parameters to increase the efficiency of prepared samples, Ag_2CO_3/CdS in the degradation of methyl orange as the model pollutant. First of all, the effect of pH was adjusted with the series of pH solution of 1,3,6,9 and 11 at the fixed catalyst dosage (0.025g) and concentration (10 mgL^{-1}) during the photodegradation degradation reaction. With the optimum pH at the highest degradation, it was applied to the next parameter. Next, the effect of catalyst dosage also was studied (0.0125g, 0.01875g, 0.0250g, 0.03125g,0.0375g) with the best pH and 10 mgL^{-1}.

3.7 Kinetic Study

Research by Singh et al., (2023) mentioned that a linear fitting of ln (C_O/C_t) versus irradiation time was exhibited to study the kinetics of methyl orange. The linearity of the curves towards the synthesized photocatalyst indicates that the photodegradation reaction aligns with the pseudo-first order reaction kinetics and the rate expression as below,

$$-\frac{d[C]}{dt} = kC \qquad (3.7)$$

where k is the pseudo-first order rate constant. With the limit of $C=C_o$ which t=0, while C_o is the equilibrium concentration of the bulk solution, the integration of Equation 3.7 presents Equation 3.8,

$$ln\frac{Co}{Ct} = kt \quad (3.8)$$

The slope of the line is the first-order rate constant, k(h^{-1}). After that, the Langmuir Hinshelwood model was ploted ($\frac{1}{k}$ versus C_o) related to the equation as follows, where k_r is the reaction rate constant ($mgL^{-1}h$) and k_{LH} is Langmuir Hinshelwood adsorption equilibrium constant (L mg^{-1}).

$$\frac{1}{k} = \frac{1}{k_r k_{LH}} + \frac{c_0}{k_r} \quad (3.9)$$

3.8 Scavenger Test

Analysing the degradation mechanism towards the methyl orange with synthesized photocatalyst is a crucial procedure which able to examine the active species that generated in the photocatalytic degradation reaction. As a consequence, the effect of scavenger was performed in this study. Potassium chlorate (PC), methanol (Me), isopropanol (IP) and potassium iodide (PI) were used as a scavenger for the photogenerated electron (e-), holes (h^+), hydroxyl radical on the surface (•OHads), and hydroxyl radical in bulk ($•OH_{bulk}$) respectively (Merdoud et al., 2025).

3.9 Reusability Study

For the reusability study, the synthesized Ag_2CO_3/CdS was carried out. After dark adsorption, 60 min photocatalytic degradation process of methyl orange was performed and repeated four times. After each degradation process, the photocatalyst was separated from the solution of methyl orange by centrifugation and washed with ethanol three times. After that, the powder was dried for 4 hours at 70 °C and used again. To confirm no obvious changes in terms of functional group and structural properties of optimum photocatalyst, XRD and FTIR analysis was conducted comparing the fresh photocatalyst and spent photocatalyst.

3.10 Parameter Study

The effect of key operational parameters on the photocatalytic degradation of methyl orange (MO) was systematically investigated, including initial dye concentration, catalyst dosage, solution pH, and the point of zero charge (pH_pzc) of the

photocatalyst. The initial concentration of MO was varied at 10, 20, 30, 50, and 70 mg/L to evaluate its influence on degradation efficiency, while the catalyst dosage was adjusted to 0.01250 g, 0.01875 g, 0.02500 g, 0.03125 g, and 0.03750 g under identical conditions. The effect of pH was examined by varying the solution pH to 1, 3, 6, 9, and 11 using appropriate acidic and alkaline solutions. Additionally, the pH_pzc of the photocatalyst was determined to better understand its surface charge properties and interaction with MO molecules. All experiments were conducted under constant irradiation and reaction time to ensure reliable comparison of the results.

3.10.1 Effect of Initial Dye Concentration of Methyl Orange

To assess the photocatalytic performance of the Ag_2CO_3/CdS system, the influence of the initial methyl orange (MO) concentration was systematically examined. Hanafi & Sapawe, (2020) has discovered the study the changes in dye concentration can significantly affect the degradation efficiency, mainly due to their impact on light availability and reactive species generation. At elevated concentrations, the solution becomes more optically dense, which limits light penetration and reduces the activation of the photocatalyst surface, leading to lower production of reactive radicals such as •OH. This consequently decreases the degradation efficiency. On the other hand, at lower concentrations, improved light transmission enhances photon absorption by the photocatalyst, resulting in greater formation of reactive species and higher degradation rates under identical experimental conditions. Hence, MO concentrations ranging from 10 to 70 mg L^{-1} were employed to evaluate this effect.

3.10.2 Effect of Catalyst Dosage

The influence of catalyst dosage on the photocatalytic degradation of methyl orange (MO) using Ag_2CO_3/CdS was systematically examined. The quantity of photocatalyst is an important factor as it determines the extent of surface area and number of active sites available for the reaction. Increasing the catalyst dosage can improve degradation performance due to greater availability of reactive sites and enhanced formation of oxidative species (Rajesh et al., 2023). Nevertheless, when the dosage exceeds a certain level, the suspension may become too dense, causing light scattering and reduced light penetration, which limits the activation of the photocatalyst

(Yusoff et al., 2021)This condition can subsequently lower the overall degradation efficiency. In this study, the catalyst dosage was varied between 0.01250 g and 0.03750 g to identify the optimal amount for effective MO removal. The effect of catalyst loading was also considered together with initial dye concentration and solution pH to provide a more comprehensive evaluation of the photocatalytic behavior of the Ag_2CO_3/CdS system.

3.10.3 Effect of pH

According to Saint et al., (2025), the effect of solution pH on the photocatalytic degradation of methyl orange (MO) using Ag_2CO_3/CdS was systematically studied. The pH of the solution plays a significant role in influencing both the surface properties of the photocatalyst and the ionization state of the dye molecules. Variations in pH can alter the surface charge of the photocatalyst, which affects the electrostatic interactions between the catalyst and MO molecules, as well as the generation of reactive species during the photocatalytic process (Chen et al., 2024). Under highly acidic or alkaline conditions, the efficiency of degradation may be reduced due to unfavorable interactions or instability of reactive species. In contrast, an optimal pH range can enhance the attraction between the photocatalyst surface and dye molecules, leading to improved degradation performance. In this study, the pH was adjusted from 1 to 11 to evaluate its influence on MO removal. The results were further interpreted in relation to the point of zero charge (pH_pzc) to better understand the surface charge behavior of the Ag_2CO_3/CdS photocatalyst under different pH conditions.

3.10.4 Determination of the point of zero charge (pH_{pzc}) of the catalyst

The point of zero charge (pH_pzc) of the Ag_2CO_3/CdS photocatalyst was determined using the salt addition method. A series of 50 mL distilled water solutions with initial pH values ranging from pH 2 to pH 10 were prepared by adjusting with 1 M sodium hydroxide (NaOH) and 1 M hydrochloric acid (HCl). The initial pH (pH_0) of each solution was measured using a portable pH meter. Subsequently, 0.01 g of the photocatalyst was added into each solution, followed by the addition of 10 mL of 0.1 M potassium chloride (KCl) as an inert electrolyte to maintain ionic strength. The suspensions were then stirred continuously using a magnetic stirrer for 24 hours to allow

equilibrium to be reached. After that, the final pH (pH_f) of each solution was recorded. The difference between the initial and final pH values ($\Delta pH = pH_f - pH_0$) was calculated and plotted against the initial pH. The pH_pzc of the photocatalyst was determined from the point where ΔpH equals zero, corresponding to the intersection of the curve with the pH axis.

CHAPTER 4
RESULTS AND DISCUSSION

4.1 Introduction

This chapter reported the effect of cadmium sulfide loaded on the silver carbonates at the low ratio of concentrations. Consequently, the correlation between the characterization data and photocatalytic degradation for the modified photocatalyst were described in order to propose the mechanism. In addition, the specific kinetic study also was examined by Langmuir-Hinshelwood Model.

4.2 Effect of Cadmium Sulfide Loaded on Silver Carbonate

This section explained the effect of cadmium sulfide loaded on the silver carbonate and the synthesized photocatalyst were denoted as $AgCO_3$, CdS and ACD respectively. All synthesized photocatalysts were characterized with the XRD, FTIR, UV-Vis/DRS, FESEM, TEM, XPS and PL.

4.2.1 Structural, Crystallinity and Phase Studies

The XRD diffractograms of the synthesized Ag_2CO_3, CdS and modified photocatalyst with low ratio of composite CdS (5%, 10% and 15%) are represented in Figure 4.1. The pure Ag_2CO_3 clearly display the characteristics diffraction peaks at 2θ angles of 18.52°, 20.73°, 28.75° ,32.60°, 33.89°, 37.19°, 39.91°, 42.76° and 51.40° corresponding to crystalline planes of (020), (110), (011), (-110), (-130), (200), (031), (230) and (150) respectively, which indexed to (JCPDS 26-0339) as monoclinic phase which reported aligned by few researcher include (Ghazi et al., 2023b; Lv et al., 2021b). In addition, CdS exhibited well defined peaks as (JCPDS 41-1049), corresponding to the peaks of 25.06°, 26.67°, 28.40°, 36.96°, 43.91°, 48.10° and 52.23° which reflected at the plane (100), (002), (101), (102), (110), (103) and (112) respectively such as Iqbal et al., (2019). It was perceived that all the Ag_2CO_3 intensities were slightly decreased upon the subsequent loading of CdS. This significantly indicates that the combination of CdS and Ag_2CO_3 are successfully intact, suggesting the successful formation of a

stable heterojunction between both semiconductors. As a consequence, this structural stability promotes strong interfacial contact between CdS and Ag_2CO_3, which facilitates efficient charge transfer, reduces electron–hole recombination, and consequently enhances the photocatalytic activity. Furthermore, the unique peak has been strongly appeared for 10ACD at the 2θ = 43.91° compared to 5ACD and 15ACD, confirming the existence of multilayer between two photocatalyst that also demonstrated by Hussain et al., (2019). Hence, the reduced intensity of the (110) peak in the 10ACD photocatalyst can be attributed to the well dispersion of Cd and S on the Ag_2CO_3 surface. It is due to the good distribution of CdS nanoparticles leads to smaller crystalline domains, resulting in lower peak intensity compared to 5ACD and 15ACD. This finding has been claimed and discussed by the previous study towards the fibrous silica titania and the good dispersion of C and N by g-C_3N_4 (Azami et al., 2021).

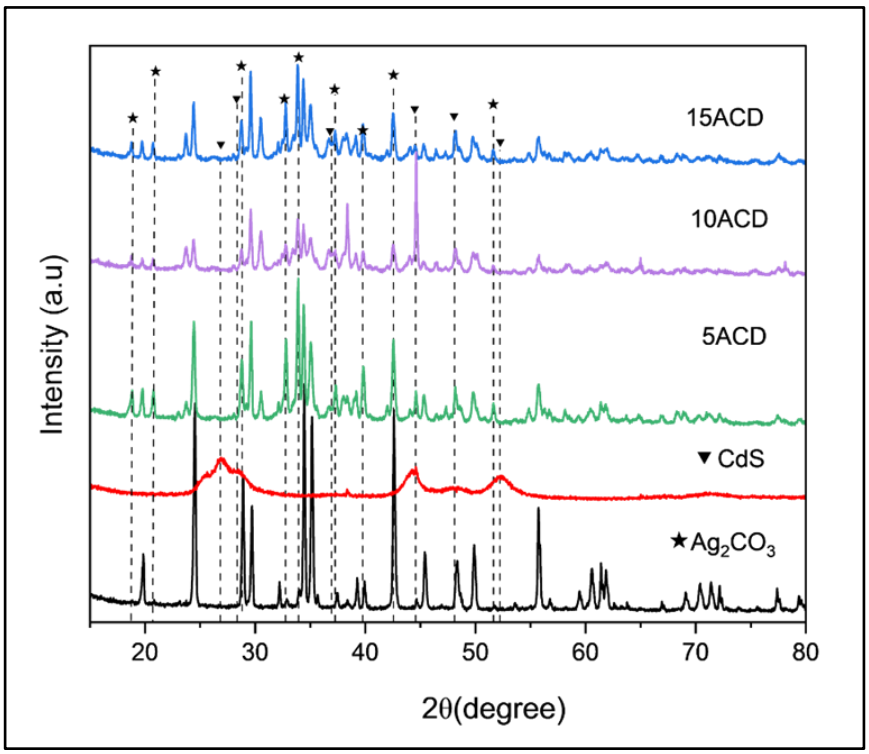

Figure 4.1 XRD diffractogram of all synthesized sample

4.2.2 Functional group and Surface Characteristic Study

Fourier transform-infrared (FTIR) analysis was reported to analyse the functional group and surface characteristics as illustrated in the Figure 4.2. The spectral pattern for Ag_2CO_3 exhibit absorption bands of CO_3^{2-} at the peak 1340 and 835 cm^{-1}.

The bands at 622 cm^{-1} correspond to Cd-S stretching band which indicates it was successfully synthesized but due to the lower concentrations that added into the Ag_2CO_3, the intensity of CdS peaks was less intangible for the modified photocatalyst, 5ACD, 10ACD and 15ACD. In addition, the bands at 3321cm^{-1} attributed to the bending vibration of O-H because of the adsorbed water on the surface CdS. The modified photocatalyst of 10ACD photocatalyst demonstrate the major peaks as the parents' catalyst, Ag_2CO_3 and CdS include absorption bands of CO_3^{2-} at 1340, 835 cm^{-1} and 622 cm^{-1} correspond to to Cd-S stretching band. These vibrations have been aligned by few of researchers such as a medium strong absorption peak at the of 651.62 cm^{-1} belonging to Cd-S stretching, 1373.13 cm^{-1} correspond to tris-amine C-N stretch and 880 cm^{-1} belongs to bending vibration of carbonate (S. Kumar & Sharma, 2016; Rey et al., 1991; Veerasingam & Venkatachalapathy, 2014). In addition, as shown in the Figure 4.2, noticeably the modified photocatalyst for 5ACD, 10ACD and 15ACD exhibit reduced intensity after the introduction of CdS materials towards the Ag_2CO_3 which demonstrated the shielding on the surface of Ag_2CO_3 bring out the major rearrangement. It is also observed by the Kamble et al., (2020) that the intensity of diffraction peaks of CdS nanoparticle has reduced compared to the bulk CdS due to the higher surface to volume ration of nanoparticles. Thus, 10ACD illustrate the lowest intensity among 5ACD and 15ACD due to the good dispersion of Cd and S element on the surface of Ag_2CO_3. It is also signifying with the XRD analysis which 10ACD shows the lowest intensity than 5ACD and 15ACD. Kurosawa et al., (2021) has explored that the lower XRD and FTIR peak intensities indicate good dispersion of Cd and S on the Ag_2CO_3 surface. Well-dispersed particles prevent aggregation and reduce crystallite size, lowering peak intensity. In FTIR, reduced intensity also shows strong interaction within the matrix and fewer exposed functional groups. This uniform dispersion enhances structural stability and photocatalytic performance.

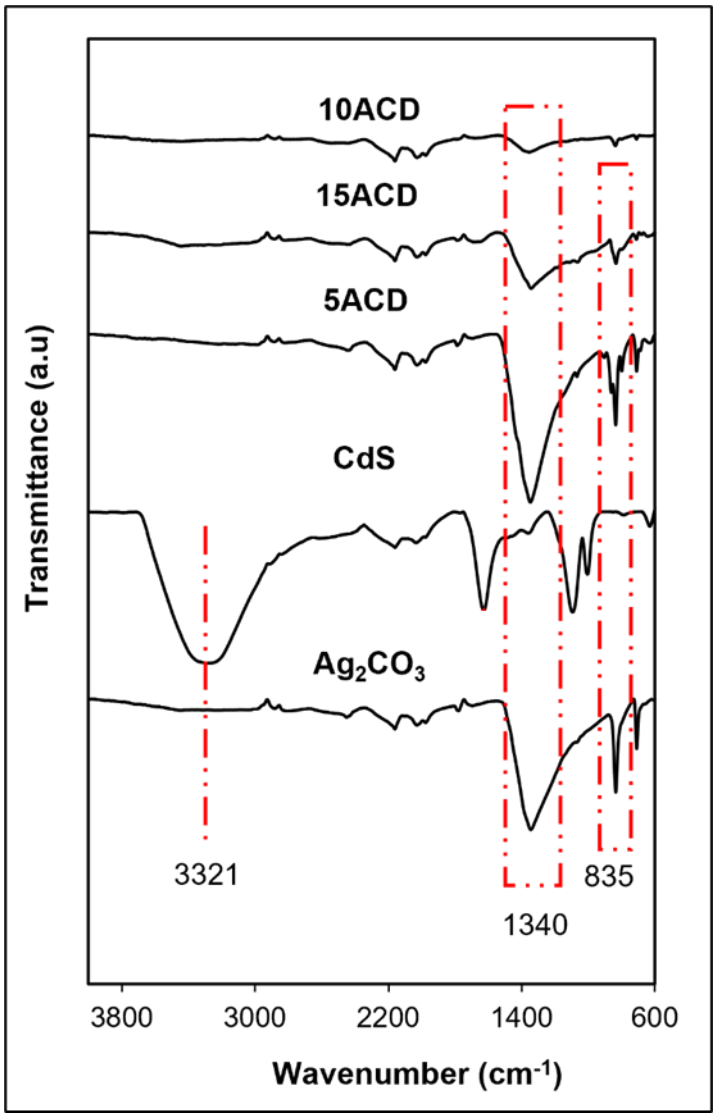

Figure 4.2 FTIR Spectra for all modified photocatalyst

4.2.3 Surface Microscopic Study

The morphology and elemental composition of synthesized photocatalyst were analysed by FESEM-EDX as portrayed in the Figure 4.3 and Figure 4.4 respectively. As illustrated in the Figure 4.3, the Ag_2CO_3 photocatalyst demonstrated a cylindrical rod like structure with different sizes and smooth surface at an average size of about 2µm. It is consistent reported by Zhu et al., (2017), that the synthesized Ag_2CO_3 has displays the rod-like structure with homogeneous smooth surface average size approximately 0.5–2 µm. Furthermore, the well distribution and uniform flower like structure was presented for the synthesized CdS photocatalyst like in the Figure 4.3 which is similar with the morphological structure reported in previous studies (Hojjati-

Najafabadi et al., 2024b; Wang et al., 2015). As can be seen by the naked eye, the morphology of modified photocatalyst at different ratio which 5ACD, 10ACD and 15ACD remained the same as the parents' catalyst and composite catalyst. The distribution of Cd as well as S on the surface Ag_2CO_3 respectively disparate by the ratio where 10 ACD has a well dispersed distribution which indicate high accessibility compared to the 5ACD and 15 ACD (Fatah et al., 2017). It can be correlate with the XRD and FTIR analysis when the peak intensity was slightly decreased upon the subsequent loading of CdS. Hence, this uniform dispersion of Cd and S on the surface of Ag_2CO_3 has delineated the spatial distribution and close contact of two photocatalyst which likely contributed to the good photocatalytic activity. The modified photocatalyst, 10 ACD was also verified with the appropriate percent and elemental composition by the elemental mapping, EDX as displayed in the Figure 4.3.

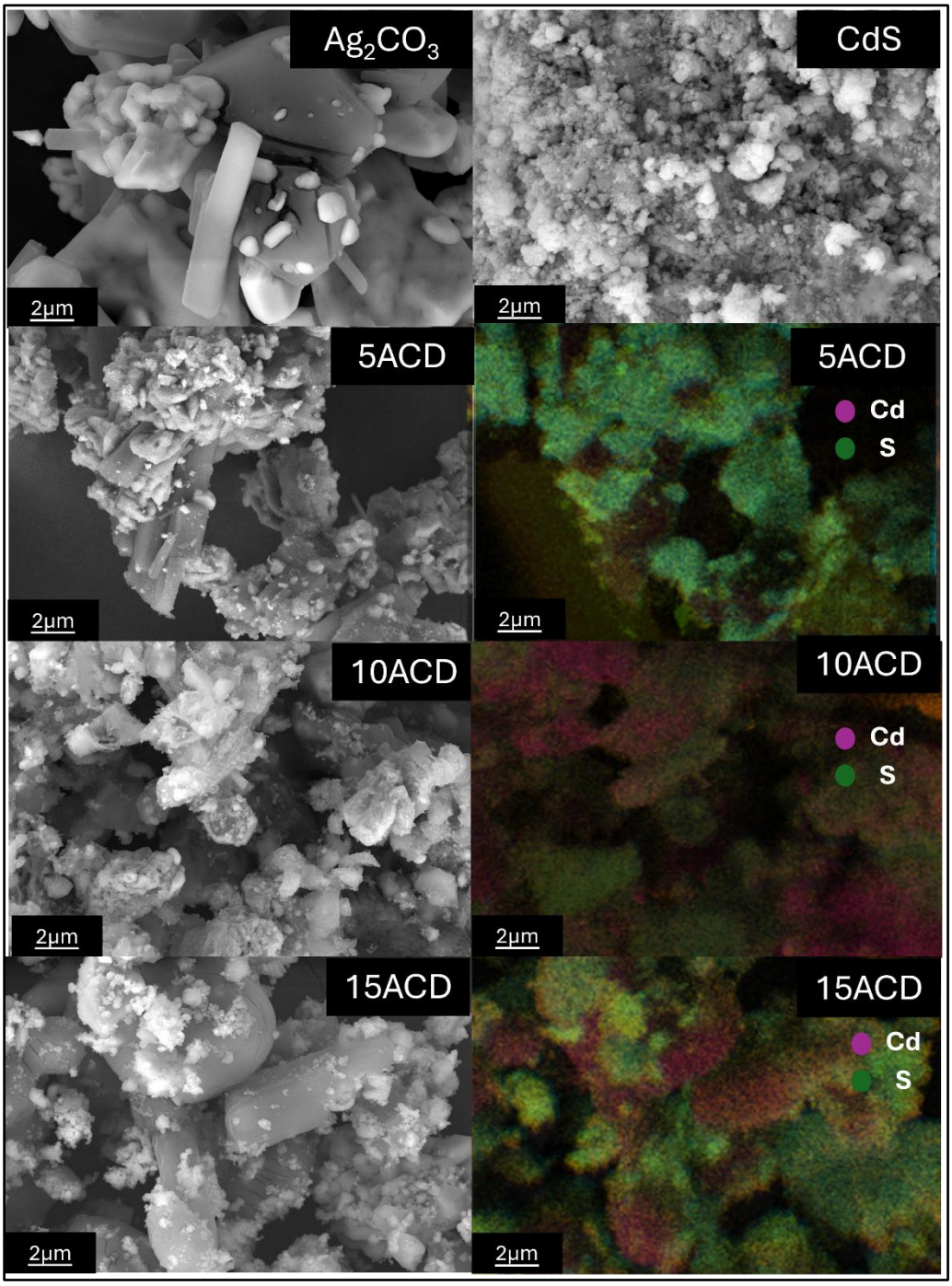

Figure 4.3 FESEM image of all the prepared sample with the elemental mapping of Cd and S

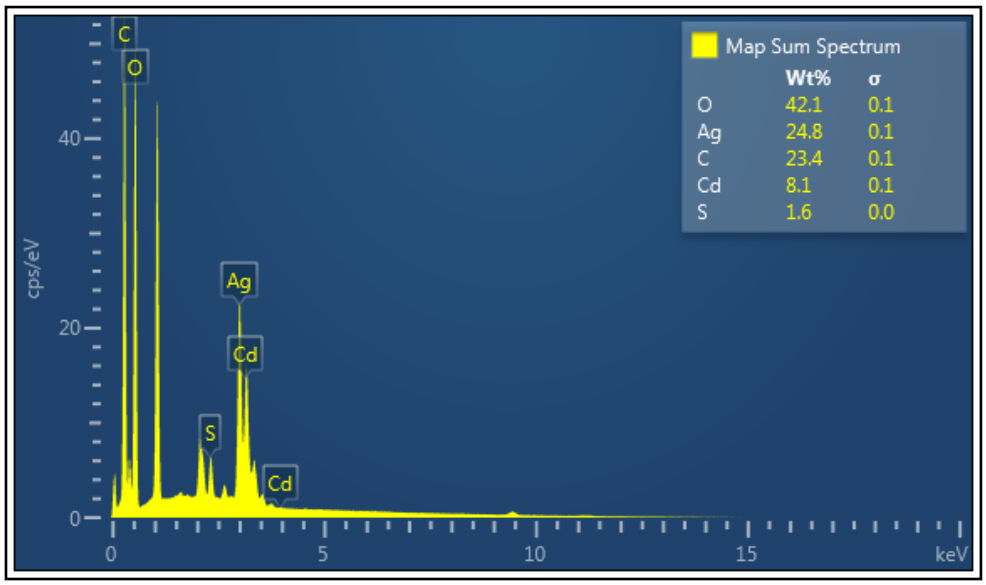

Figure 4.4 Elemental composition of 10ACD sample

4.2.4 Internal Surface Morphology

TEM analysis was performed to observe the morphological characteristics of and internal structure properties of synthesized photocatalyst which are Ag_2CO_3, CdS and the modified photocatalyst, 10ACD. The micrograph was illustrated as in the Figure 4.5 at magnification of 50K and 80K with a scale about 200nm, providing the high-resolution details of the samples. The TEM image of Ag_2CO_3 disclosed the cylindrical rod like structure with a relatively smooth surface proving this parents' catalyst has a well-defined morphology. The obtained Ag_2CO_3 powder has successfully exhibited consistent polyhedral rod-shaped particles, measuring approximately 2–4 μm in length and 0.3–0.6 μm in diameter as also similar represented by (Dostanić et al., 2017).These rods like structure appear interconnected by thin and flexible layers might be due to the simple precipitation method or the composite material deposition that indicated by (Bora & Mewada, 2017). On the other hand, the CdS sample exhibited well defined structure as flower like structure correlate as the FESEM Mapping analysis.

As demonstrated for the optimum sample, 10ACD, the TEM image at both 50K and 80K magnifications represents the dense packed and irregular shaped nanoparticles. As illustrated in the Figure 4.5, a large amount of well-defined of CdS with the flower like morphology which presented eventually when loaded with Ag_2CO_3. By this, it could clarified that both elements are randomly disperse with the uniform distribution suggesting the Ag_2CO_3 surface is loaded distribution by Cd and S from CdS as correspond to the Figure 4.4 elemental mapping. Furthermore, the increased contrast

and overlapping areas highlight the integration of CdS onto the Ag_2CO_3 surface resulting the composite material such as reported by Chen et al., (2016). Specifically, these structures features are often favourable in photocatalytic applications, as it helps to enhance the effective charge separation and increase the surface area for photocatalytic activity. It is consistently aligned with Nandiyanto et al., (2020) that has been systematically investigated and discussed the catalyst morphology as well as surface chemistry plays the important role on the enhancement of photocatalytic performance. As the overall, it observed that the size and shape of the particles were consistent with the results obtained from FESEM mapping analysis. Thus, it is aligns with the intended design of modified photocatalyst indicate the synthesize was successfully and integration of both photocatalyst. These findings provided essential insight that the 10ACD composite exhibit synergistic properties due to the intimate contact between two photocatalyst of Ag_2CO_3 and CdS.

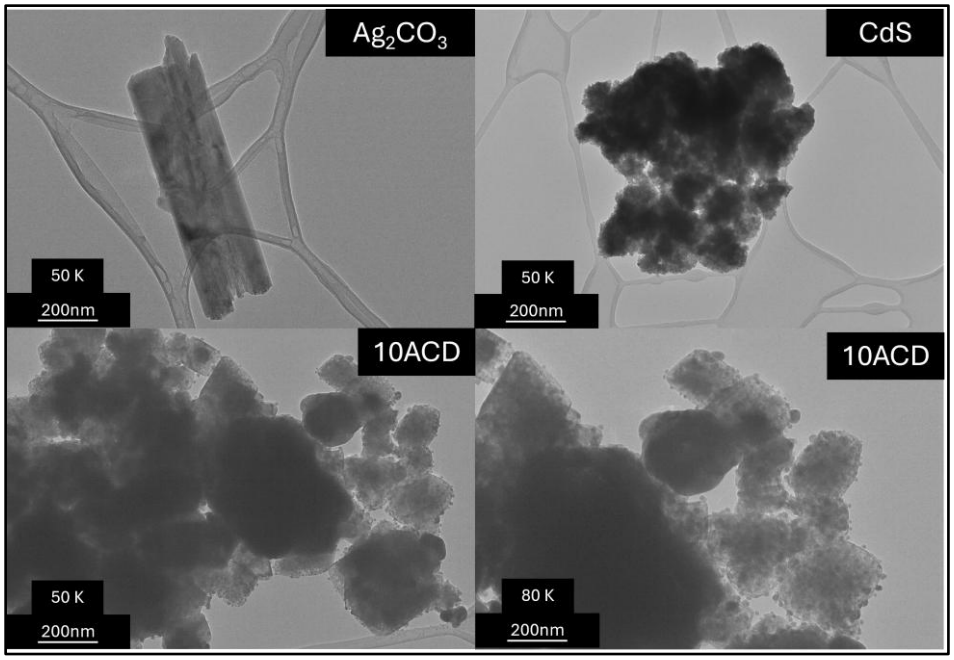

Figure 4.5 TEM analysis of (A) Ag_2CO_3 ; (B) CdS ; (C) Optimum modified photocatalyst of 10ACD at 50K Magnification ; (D) Optimum modified photocatalyst of 10ACD at 80K Magnification

4.2.5 Optical Properties

The UV-Vis Diffuse Reflectance Spectroscopy (DRS) analysis was used to determine the optical absorption properties and band gap energies of the synthesized sample as illustrated in the Figure 4.6. Each of the catalysts was revealed by Kubelka

Munk based on the coefficients of absorption defined as a purpose of incident photon energy according to the Equation 4.1. The extrapolation slope on the photon energy axis contributes to the value of band gap or binding energy for the photocatalyst.

$$(\alpha hv)^2 = A(hv - Eg) \quad (4.1)$$

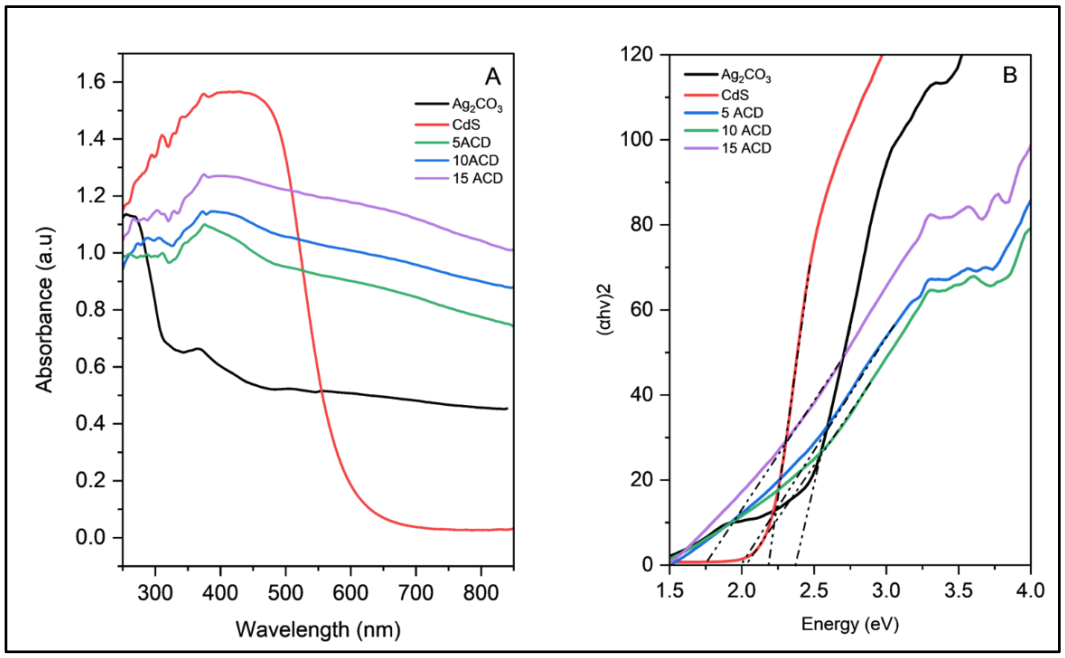

Figure 4.6 (A) Plot of Absorbance versus Wavelength for all catalyst ; (B) plot of transformed Kulbelka-Munk function versus energy of light of all synthesized sample

The values of band gap for the prepared photocatalyst were summarized in Table 4.1. The estimated optical band gap energy for pure Ag_2CO_3 was found to be 2.37eV while CdS exhibited lower band gap approximately 2.19 eV respectively, which are consistent with the values reported in the literature (Azami et al., 2022b; Heiba et al., 2023; J. Y. Li et al., 2020; Moghaddam et al., 2020; Teng et al., 2024b). The incorporation of CdS towards Ag_2CO_3 resulted in further band gap reduction, for 5ACD, 10ACD, 15ACD as represented to be 2.0 eV, 2.05 eV and 1.7 eV respectively. It is progressively reduced in band gap energy due to the addition of CdS onto the Ag_2CO_3 which undoubtedly caused by the interaction of both species contributes to the greatest interaction which could enhance the good photocatalytic activity under visible light irradiation. Yang et al., (2025) discovered that the combination of binary or ternary photocatalysts can significantly reduce the band gap energy. For instance, the band gap of ZnO/Ag_2CO_3 was successfully reduced from 3.14 eV to 2.97 eV, indicating the

greatest interaction of such combinations. This finding is in line with the significance of the present study. Besides that, it also was clarified and supported by other analysis such as XRD, FESEM Mapping and TEM analysis, when the higher dispersion and lower aggregation of its Cd and S elements would lead to greater photocatalytic efficiency. As a consequence, the potential charge transfer rate at the interfacial between both species would increase as well as indicate the modified photocatalyst are successfully synthesized with good light harvesting efficiency (Gan et al., 2021; Saeed et al., 2021).

Table4.1
Optical properties of synthesized photocatalyst

Photocatalyst	Band Gap (eV)
Ag_2CO_3	2.37
CdS	2.19
5ACD	2.00
10ACD	2.05
15ACD	1.70

4.2.6 Chemical Oxidation State Determination

Considering the above result to determine the surface chemical composition for the synthesized photocatalyst, XPS analysis was performed and the spectra resulted in the Figure 4.7 to Figure 4.9. The coexistence of element Ag, C, O, Cd and S from the survey scan spectra confirmed the successfully modified photocatalyst of 10 ACD heterostructure as represented in the Figure 4.7. Specifically, Figure 4.8A emphasized that the deconvoluted O 1s spectrum of Ag_2CO_3 shows in four peaks at 534.28, 532.78, 531.68 and 530.68 eV attributed to O-C-O bonds and the formation of oxygen vacancies (Vo) respectively in agreement with previous literature (Yin et al., 2022). The binding energies for 10 ACD were slightly blue shifted as compared to Ag_2CO_3 indicating the movement of the electron from Ag_2CO_3 to CdS and suggesting the role of Ag_2CO_3 as an electron donor. This shift also supports the formation of strong interfacial interactions between the O–C–O bonds in Ag_2CO_3 and the Cd and S elements in CdS. As studied by (Zhang et al., 2023), it would consequently promoting higher oxygen concentration on the photocatalyst surface. Similarly, the C 1s spectra of Ag_2CO_3 and 10 ACD was depicted in the Figure 4.8B. The deconvoluted peak of Ag_2CO_3 at 284.68, 285.38, 286.28, and 287.98 eV are correlated to the C-C bonds, C-H bonds, C-O bonds and C=O bonds respectively. These bonding assignments are consistent with previous

reports (An et al., 2020). The observed blue shifted which could attributed with the strong interfacial contact between two semiconductors of Ag_2CO_3 and CdS leading to the formation of interfacial bonds. Based on previous findings, such differences in the binding energies of constituent elements can effectively facilitate the establishment of a Z-scheme charge transfer mechanism (Wei et al., 2021).

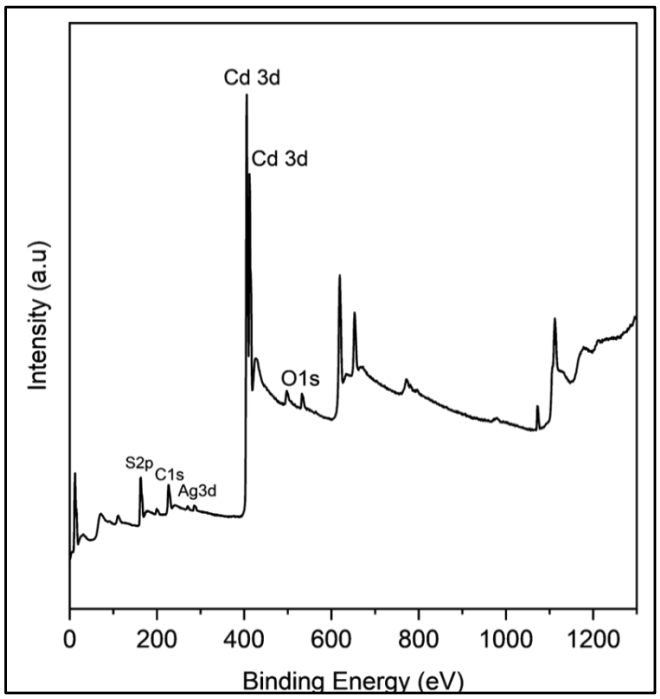

Figure 4.7 Wide scan spectra of 10 ACD samples

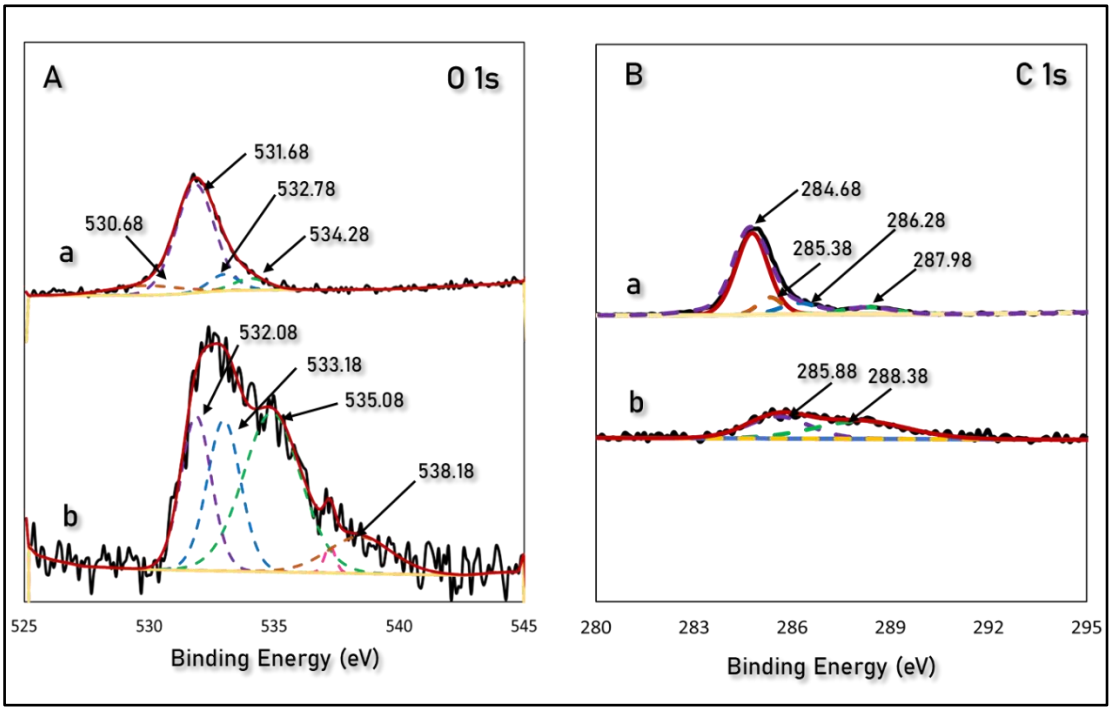

Figure 4.8 XPS spectra of (A) O 1s and (B) C 1s for (a) Ag_2CO_3 and (b) 10 ACD samples

Meanwhile, the Cd 3d spectra of CdS was deconvoluted to two important peaks as portrayed in the Figure 4.9. The binding energies of Cd 3d are determined in the Figure 4.9C around 406.41 and 411.98 eV correspond to Cd $3d^{5/2}$ and Cd $3d^{3/2}$ respectively, which attributed to the reported values (Lei et al., 2020). In comparison, the Cd 3d spectrum of 10ACD (Figure 4.9D) exhibited slightly lower binding energies at 405.58 and 411.56 eV, indicating a red shift relative to pure CdS. These peaks are also assigned to Cd $3d_{5/2}$ and Cd $3d_{3/2}$ (Alshammari et al., 2025; W. Zhang et al., 2025). The red shift confirms that CdS in the 10ACD composite photocatalyst acts as an electron acceptor, which aligns with the opposite binding energy shifts observed in the O 1s and C 1s spectra. This observation is in good agreement with previous findings by (Xie et al., 2025), who also reported similar energy band alignment behavior in CdS-based heterostructures. As demonstrated in the Figure 4.9C and Figure 4.9D, the photo corrosion properties of CdS, reducing the XPS intensity due to the high chances of electron recombination. Previous studies by (Dimitropoulos et al., 2024; Warren et al., 2023) has stated that the photo corrosion will affect the surface photocatalyst by altering the chemical composition of the surface and reduces the peak intensity. Hence, the modification of photocatalyst in the present of Ag_2CO_3 towards the CdS, support the electron mobility which Ag_2CO_3 role as the electron donor making the Cd easier to

detect than expected and increase the XPS intensity as depicted in the Figure 4.9D with the additional peak include 404.98, 408.58 and 412.98 eV. Furthermore, as the high resolution XPS spectrum of Ag 3d for 10 ACD, there are two important peaks approximately 367.86 and 373.83 eV could be ascribed to Ag $3d^{3/2}$ and Ag $3d^{5/2}$ level of Ag^{+} respectively as demonstrated in the Figure 4.9E. Meanwhile, Figure 4.9F describes the XPS spectrum of S 2p with 4 deconvoluted peak at 161.57 ,163.53, 163.83 and 165.09 eV which proves the possible bonds of S 2p $^{3/2}$ and S 2p ½. This XPS analysis was aligned with XRD, FESEM, TEM and previous studies where 10 ACD heterostructure was successfully constructed with strong interfacial interaction to expedite the transmission of photogenerated electron as well as promote the performance and stability of photocatalysis (Zulfiqar et al., 2021 ; Rosman et al., 2020).

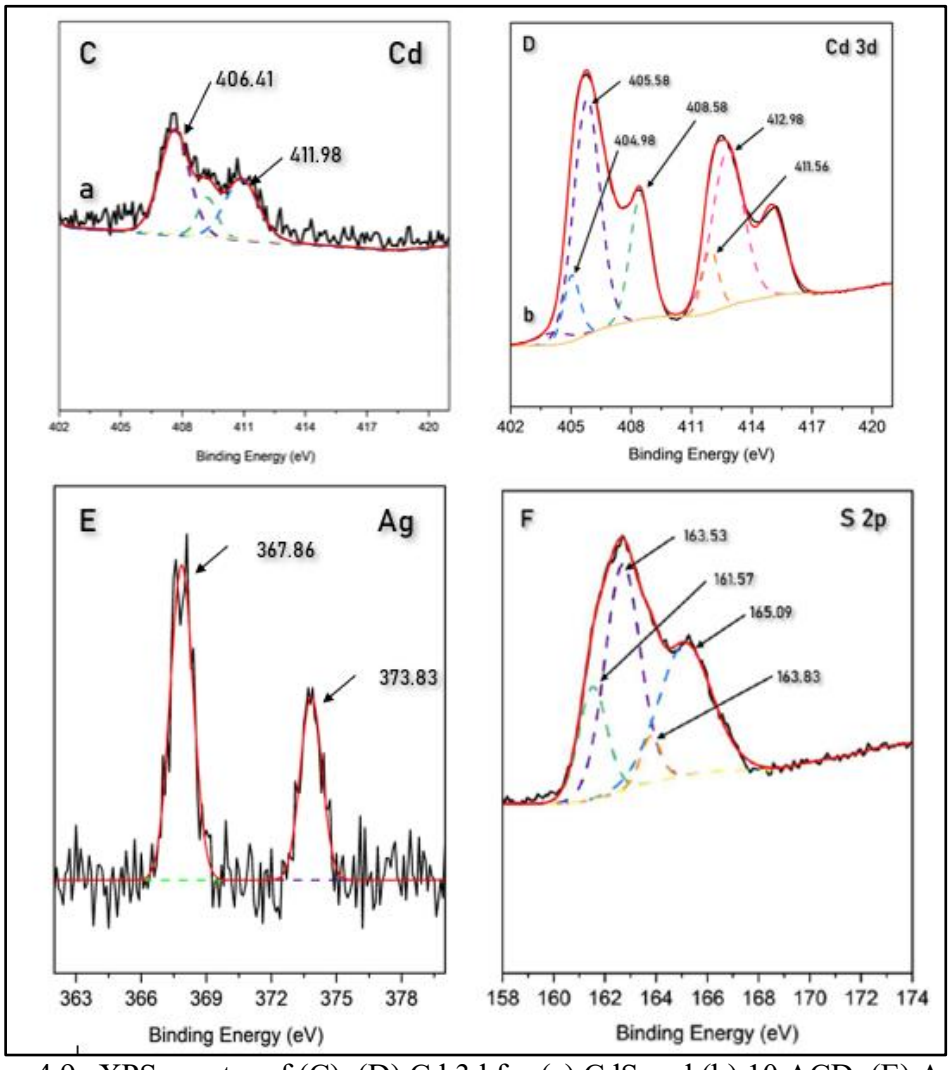

Figure 4.9 XPS spectra of (C), (D) Cd 3d for (a) CdS and (b) 10 ACD, (E) Ag 3d, and (D) S 2p for 10 ACD

4.2.7 Optical Excitation of Electron and Hole Study

In order to estimate the recombination rate of photogenerated charge pairs, photoluminescence (PL) spectroscopy is a non-destructive testing and powerful technique to be carried out as well to determine the defects materials that present in the photocatalyst. The photoluminescence spectra of Ag_2CO_3, CdS, 5ACD, 10 ACD and 15 ACD was represented in the Figure 4.10. As the parent photocatalyst, the UV peak at 713 nm of pure Ag_2CO_3 has been attributed to the near band-edge (NBE) transition which referred to the recombination of free excitons and different collision processes. As highlighted by (Le et al., n.d.; Roškaric et al., 2022), the enhanced fluorescence intensity reflects a higher recombination rate of photogenerated electron–hole pairs. It happens due to the small surface defects that has been associated towards the Ag_2CO_3.

As demonstrated in the Figure 4.10, the photoluminescence peak intensities of 5ACD, 10 ACD and 15 ACD were lower than those of parent photocatalyst, Ag_2CO_3 and CdS. Meanwhile, 10 ACD indicated the lowest photo photoluminescence peak intensity among all analysed samples. These results indicate that 10 ACD is the optimum condition which effectively inhibited the electron – hole recombination as well as increased the excitons lifetime and enhanced the photocatalytic performance of the composite photocatalyst. This relationship was aligned with the theoretical of photoluminescence spectrum, whereby when the semiconductor with the higher PL intensity exhibits low photocatalytic reactions due to the rapid electron hole recombination while those with the lower PL intensity illustrate high photocatalytic performance (Liqiang et al., 2006). Furthermore, 10 ACD also considered has well dispersion that has been associated between the combination of Ag_2CO_3 and CdS. It can be correlated with XRD, FTIR and FESEM Mapping analysis that synthesized of 10ACD has a well-defined dispersion and distribution that also supported by previous studies.

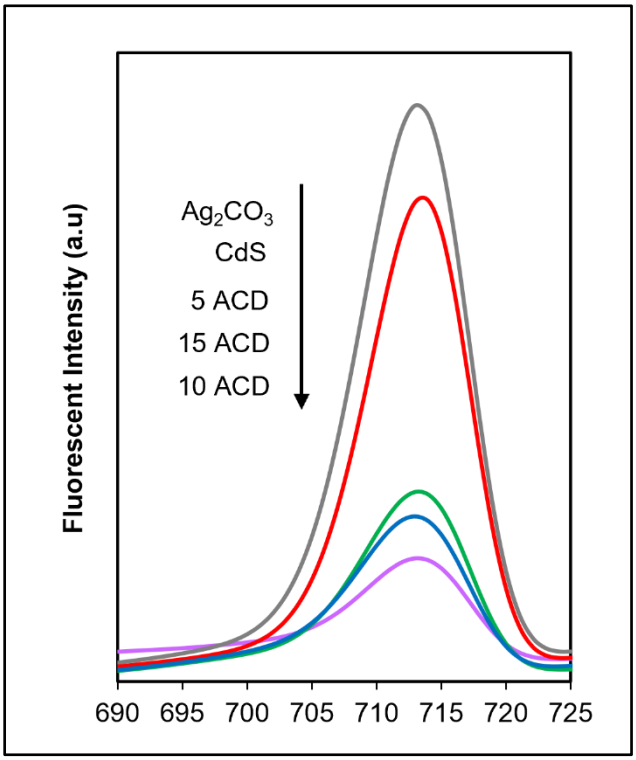

Figure 4.10 PL analysis of all prepared sample

4.3 Photocatalytic Performance and Kinetic Analysis

The photocatalytic performance of the synthesized samples included the parents' catalyst (Ag_2CO_3), composite catalyst (CdS) together with varied ratio of modified photocatalyst 5ACD, 10ACD and 15ACD was examined with visible-light driven towards the degradation of 10 mgL^{-1} methyl orange (MO) for 60 minutes and the results was depicted in the Figure 4.11. It clearly revealed that the modified photocatalyst of 10ACD has the highest photodegradation (94.38%) followed by 15ACD (83.28%) and 5ACD (80.56%) while Ag_2CO_3 and CdS obtained 75.22%, 81.61% respectively as supported in the Figure 4.12. Noticeably, the photocatalytic performance increased with the increasing wt% of CdS towards Ag_2CO_3 until an optimum loading was achieved. This behavior is attributed to the improved dispersion and interfacial contact within the 10ACD composite. Such a trend was further elucidated by (Azami et al., 2021b), who demonstrated that homogeneous dispersion of semiconductor components facilitates efficient charge separation and enhances photocatalytic efficiency. CdS definitely played the important role for the photodegradation as well as could help to reduce the band gap energy by creating more actives sites. As a consequence, these may improve the photogenerated electron hole

which better interfacial charge transfer. Research by (Jubeer et al., 2023) has clarified and proved with appropriate band gap energy, well dispersion of two photocatalyst and lower PL intensity would enhance the visible light harvesting thus boosting the photodegradation of organic pollutant. As a results, the ratio of 5ACD and 15ACD has a lower efficiency of photocatalytic performance due to the poor dispersion and interaction between materials of Ag_2CO_3 and CdS.

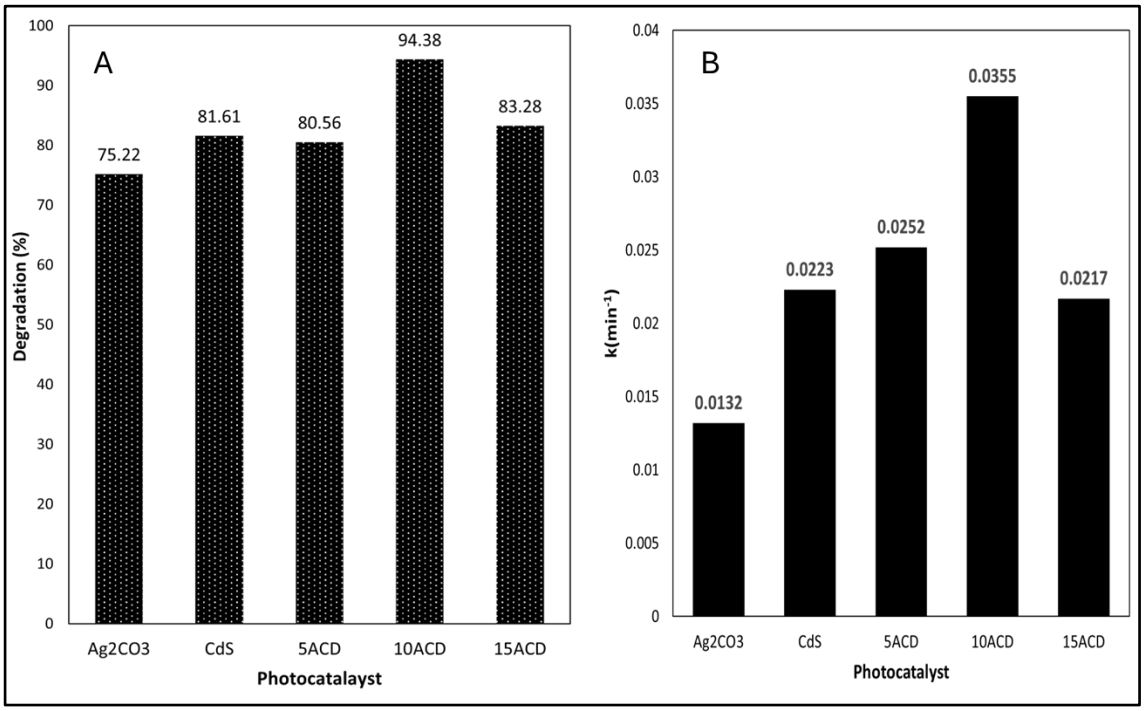

Figure 4.11 Photocatalytic Degradation of MO , (A) Percent degradation of MO ; (B) Degradation rate rate constant of MO (C_{MO} = 10 mg L-1, pH = 6, W = 0.0250 g L^{-1}, t = 1 h, 30°C)

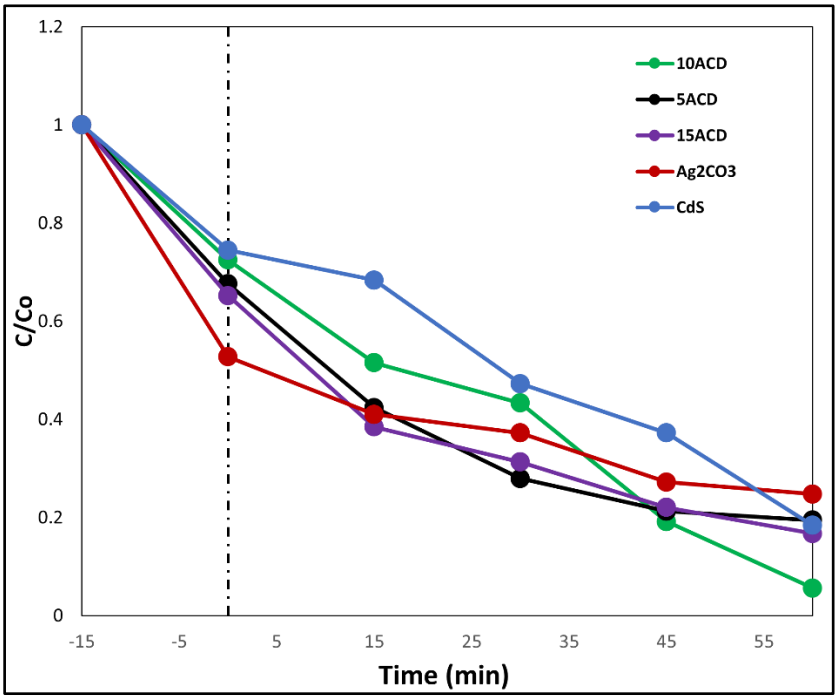

Figure 4.12 Photocatalytic degradation ; plot of C/Co against irradiation time (C_{MO} = 10 mg L^{-1}, pH = 6, W = 0.0250 g L^{-1}, t = 1 h, 30°C)

Photocatalytic performance definitely influenced by few parameters includes catalyst dosage, initial concentration of methyl orange (MO), pH, aeration flowrate and different light irradiation (Jabbar & Graimed, 2022). In this work, three parameter was conducted to maximize the optimum condition of modified photocatalyst for the photodegradation of MO. The initial concentration that has been examined in the range of 10 – 70 mg L-1 with the constant pH 6 and 0.0250 g L^{-1} as illustrated in the Figure 4.13A. Theoretically, as the increment initial concentration of model pollutant, the rate of photocatalytic activity is reduced. This can be attributed to the lower light absorption of photocatalyst. According to (Haleem et al., 2023) described that when the initial concentration increases, less light penetration will be occurred which due to the dye molecules were adsorbed on the surface photocatalyst. Thus, lower generation of reactive species for the degradation of dye as light is crucial in initiating the photocatalytic mechanism. Therefore, it was revealed at 10 mg L^{-1} was the optimum concentration of photodegradation towards methyl orange (MO).

Among the aforementioned approaches, catalyst dosage also significantly impacts the efficiency of photocatalytic degradation of model pollutant as it directly affects the availability of active sites for the reaction. The effect of catalyst dosage was inspected by varying values of 0.01250-0.03750 g L^{-1} over constant conditions at 10 mg L^{-1} and pH 6. As demonstrated in the Figure 4.13B, the highest degradation of methyl

orange (MO) was achieved at 0.0250 g L^{-1} with 94.38% catalyst dosage and aligned with the concept of photocatalytic activity. At lower catalyst dosages, the limited availability of active sites could hinder the degradation of pollutants, thereby reducing the overall photocatalytic efficiency (Ismael, 2021). Hence, the increasing catalyst dosage until optimum dosage would enhance the surface area for the photon absorption and pollutant adsorption whereby improve the degradation rate. Nevertheless, beyond the optimal dosage, the degradation consequently plateaus or even decrease due to the excess catalyst would block the light penetration as well will reduce the photon availability for the reaction. Moreover, at high concentrations can lead to the aggregation of photocatalyst particles thus lowering the effective surface area.

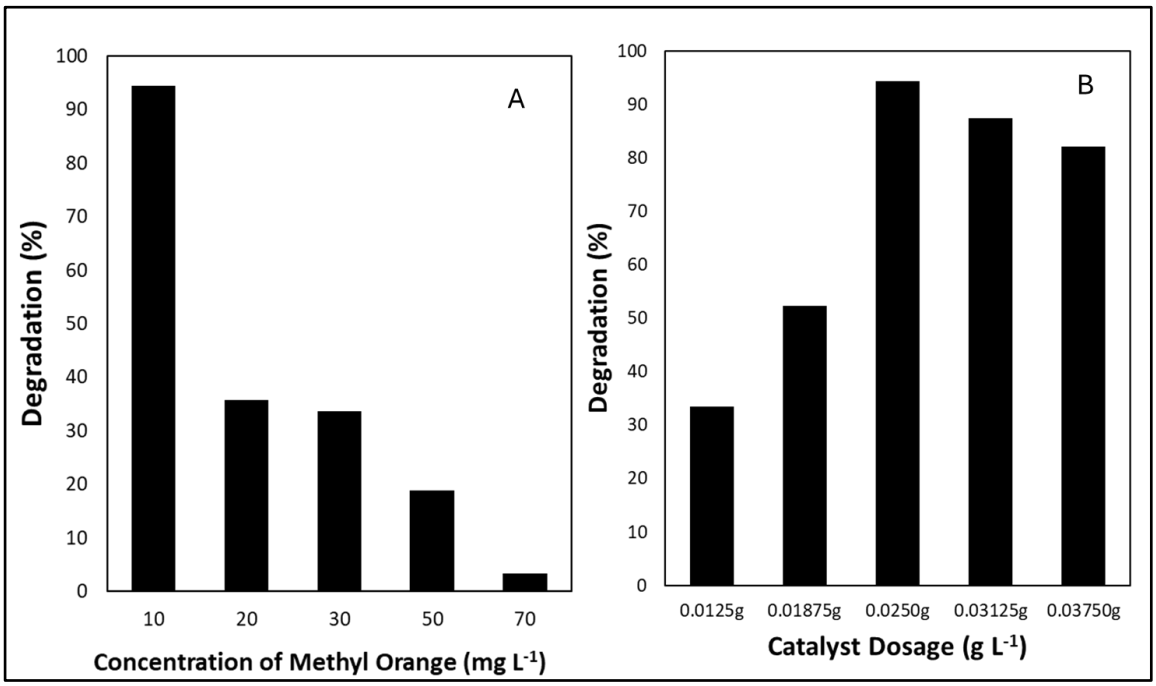

Figure 4.13 Photocatalytic degradation of MO, (A) initial concentration of MO (B) effect of catalyst dosage of 10ACD modified photocatalyst

Research by Rafiq et al., (2021) claimed that pH interferes the surface of the catalyst, the ionization of pollutants and the interaction between catalyst and target molecules. For the surface charge of the catalyst, the pH relative literally related towards pHpzc (point of zero charge). Point of zero charge describes to the pH where the surface charge of the catalyst has a neutral net charge (Zyoud et al., 2023). If the pH relative is below than the pHpzc , the catalyst surface it becomes positively charged while when the pH relative is more than the pHpzc , the catalyst surface it becomes negatively charged. It demonstrates that the charge of the surface catalyst is whether attraction or

repulsion towards the target pollutant molecules. Furthermore, most of the pollutants include dyes and organic molecules will change their charge state depending on the pH of the solution. In the acidic pH, the pollutants may be protonated whether positively charged or neutral compared to basic pH, the pollutant are often deprotonated which is negatively charged. Moreover, generation of reactive oxygen species such as hydroxyl radical are plays the important role in photocatalytic degradation. In acidic pH it will promote the generation of ●OH due to the oxidation potential. Additionally, the basic pH with the higher concentration of hydroxide ions (OH-) will produce more ●OH. However, excessive basicity can enhance to the recombination of radicals and retards the photocatalytic efficiency. Hence, at the acidic pH, a positively charged catalyst (pH<pHpzc) will attract negatively charged of methyl orange (MO) which promote to the degradation. At the basic pH, a negatively charged catalyst surface (pH>pHpzc) will repels charged of methyl orange (MO) thus reduce the degradation efficiency.

As indicated in the Figure 4.14A, the pH 3 was illustrated to be optimum photodegradation toward methyl orange until 98.02%. In addition, the point of zero charge (pHpzc) of this modified catalyst is 5.8 as illustrated in the Figure 4.14B, thus the catalyst is protonated which is positively charged as pH solution and below pHpzc value. As reported by (Acedo-Mendoza et al., 2020; Aljuaid et al., 2023b), methyl orange (MO) is an anionic dye that presence of N-H group which easily attract and construct strong electrostatic attraction between positively charge catalysts surface. This correlated that acidic condition is typically more favourable for MO degradation. Additionally, the presence of hydroxyl radicals throughout the photoreaction will destroy the MO molecules since no MO dye deposition occurs on the surface catalyst. The rivalry between hydroxide ions and MO ions in the system contributes to a poor reaction under alkaline conditions.

Furthermore, the kinetic analysis towards MO photodegradation was investigated based on the effect of initial concentrations in the range of 10–70 mg L^{-1} . Table 4.2 demonstrates that when the increasing initial concentrations, the lower k_{app} value was recorded. It proved that the system was suitable at low concentrations.

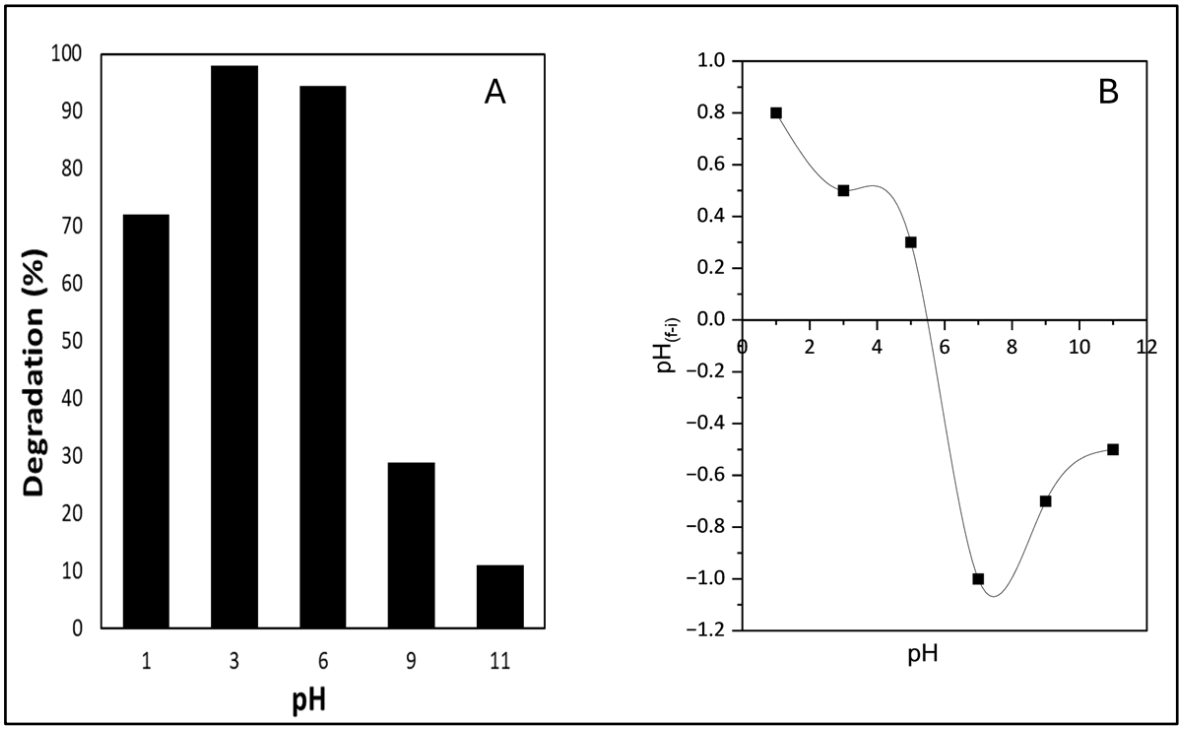

Figure 4.14 Photocatalytic degradation of MO, (A) effect of pH (B) The isoelectric point (pHZPC) of 10ACD

Table 4.2

Photodegradation at different initial concentrations of MO and pseudo first order rate constant values for MO degradation using 10ACD

Initial Conc. Co (mg L-$^{1)}$	**Rate, k_{app} (x10^{-3} min^{-1})**	**Initial Rate, r_o (x10^{-2} mgL^{-1} min^{-1})**
10	20.5	0.420
20	7	0.049
30	5.8	0.034
50	3.1	0.009
70	3.0	0.001

The linear plot of ln (C_o/C_t) vs irradiation time has represented in the Figure 4.15, which proved that the photodegradation of MO towards 10ACD follows the pseudo-first order kinetics model which discovered by the Langmuir -Hinshelwood model as (Cheng et al., 2022; H. Deng et al., 2025). The obtained values of k_r (the reaction rate constant) and K_{LH} (the MO adsorption coefficient onto the catalyst surface) were 0.0204 mg L^{-1} min^{-1} and -19.429 mg L^{-1} min^{-1} , respectively. It shows that the k_r is higher than K_{LH} which it well explained that MO adsorption on the surface catalyst throughout the reaction. As demonstrated in the Figure 4.16 the kinetic study also has been studied for the different catalyst dosage and different pH.

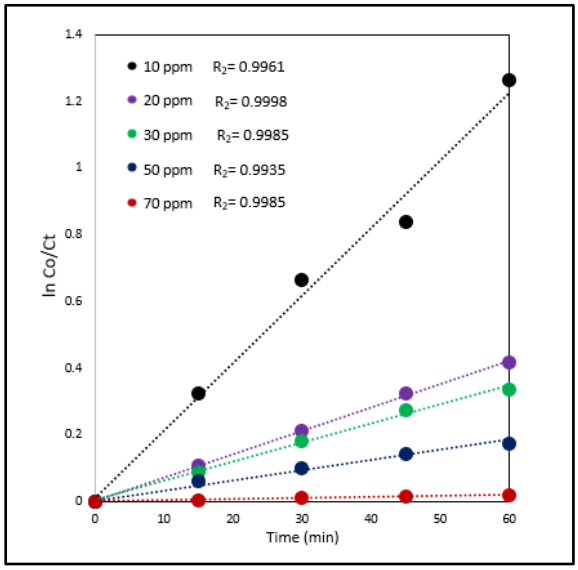

Figure 4.15 Photodegradation kinetic of MO over 10ACD at different concentrations (CMO = 10 mg L-1, pH = 6, W = 0.0250 g L-1, t = 1 h, 30ºC)

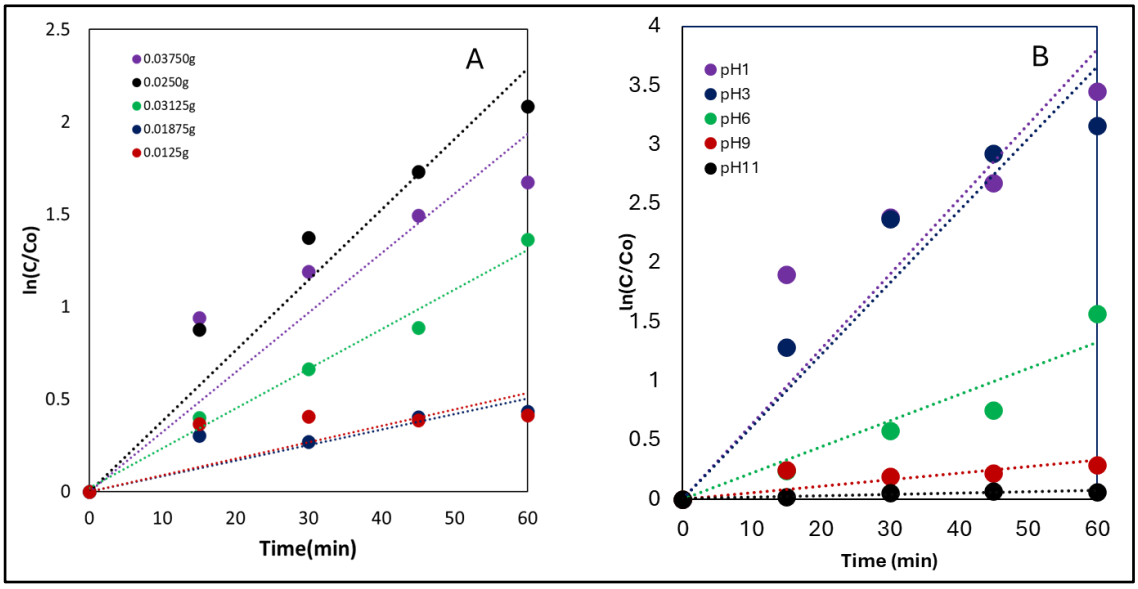

Figure 4.16 Photodegradation kinetic of MO over 10ACD at different catalyst dosage and different pH

4.4 Proposed Mechanism for Photodegradation of Methyl Orange

The scavenger test was clarified the active species and the reaction mechanism towards the photocatalytic activity of degradation of MO over the 10ACD as the optimum photocatalyst. Potassium chlorate (PC), methanol (Me), isopropanol (IP) and potassium iodide (PI) were used as a scavenger for the photogenerated electron (e-), holes (h^+), hydroxyl radical on the surface (•OHads), and hydroxyl radical in bulk ($•OH_{bulk}$) respectively. As illustrated in the Figure 4.16, the degradation of MO over 10 ACD markedly decreased after addition of potassium iodide which is 15.46%, demonstrating that the photogenerated of hydroxyl radical on the surface was the main active species in the reaction. Meanwhile, the electron (e-) illustrated a minor contribution (62.87%) in the photocatalytic reaction of MO with the existence scavenger of PC.

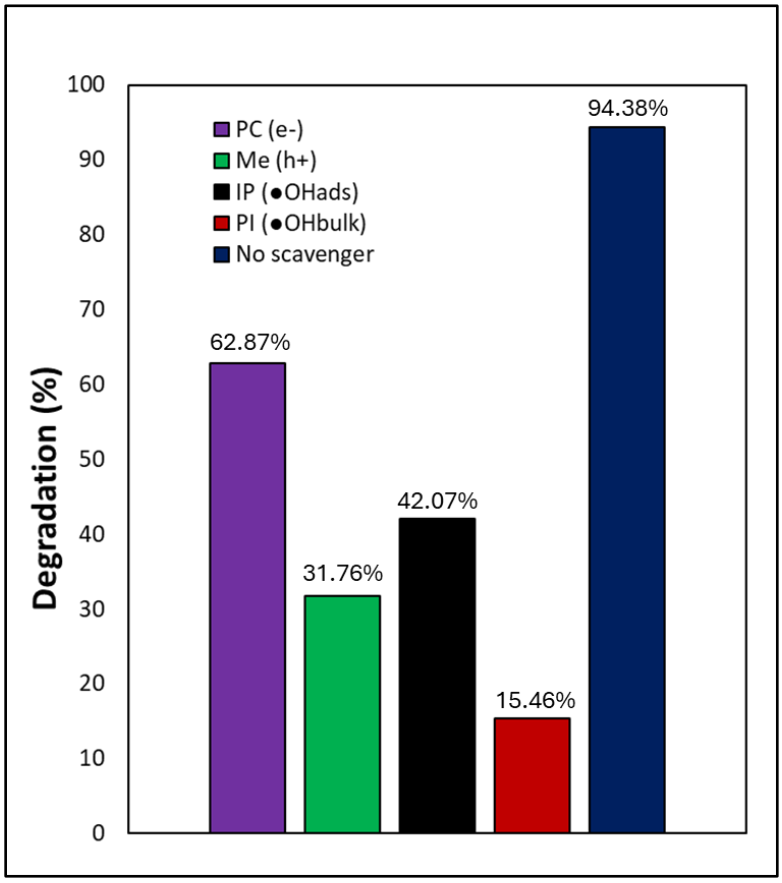

Figure 4.17 Scavenger effect on 10ACD for MO degradation under visible light (CMO = 10 mg L-1, pH = 6, W = 0.0250 g L-1, t = 1 h, 30ºC)

To illustrate the charge transfer mechanism of the modified photocatalyst heterostructure, the positions of valence band (VB) and conduction band (CB) could be calculated based on the UV-Vis analysis and electronegativity concepts. The empirical equation as described in the Equation 4.1 and 4.2.

$$E_{VB} = X - E^e + 0.5\ Eg \quad (4.1)$$

$$E_{CB} = E_{VB} - Eg \quad (4.2)$$

where E_{VB} and E_{CB} refers to the energy level of valence band and conduction band respectively, Eg is the semiconductor band gap, E^e is free electron energy on the scale of hydrogen approximately 4.5 eV while X signifies as the electronegativity of semiconductor. To determine the X value of electronegativity, the first ionization and the mean of electron affinity energy was used and it has been demonstrated in the Appendix 1. The X value has calculated for Ag_2CO_3 which are 6.15 eV. Based on the calculation as Equation 4.1- 4.2, the VB and CB value for Ag_2CO_3 are 2.84 eV and 0.47 eV. On the other hand, the X value also was calculated for the composite catalyst, CdS

which are 4.32 eV correspond to the VB and CB value at 0.92 eV and -1.23 eV respectively.

Based on the above analysis and discussion, a potential Z-scheme photocatalytic mechanism of modified photocatalyst, 10 ACD was proposed as schematically depicted in the Figure 4.16. Apart from that, the potential redox level (pH 5) of $O_2/\bullet O_2^-$ and of $H_2O/\bullet OH$ are -0.16 eV and 2.44 eV respectively. Among the aforementioned approaches, for the 10 ACD, the potential level of CB in Ag_2CO_3 is lower than the potential level of $O_2/\bullet O_2^-$ (-0.16 eV); hence, superoxide anion radical ($/\bullet O_2^-$) could not be formed by electrons (e^-) in Ag_2CO_3. The close contact gap between CB Ag_2CO_3 and VB CdS give the advantage for the photogenerated e^- from the CB Ag_2CO_3 to transfer as well to recombine with photogenerated h^+ in VB CdS which construct the crossing defect structure as the pathway for Z-scheme mechanism. In addition, the photogenerated e^- in the CB CdS would reduce the O_2 to $\bullet O_2^-$ radicals due to the CB CdS is more negative than the potential level of $O_2/\bullet O_2^-$ (-0.16 eV). Meanwhile, the photogenerated h^+ in the VB of Ag_2CO_3 will react with H2O in order to generate the ●OH radicals as the consequence for the position of VB Ag_2CO_3 2.84 eV photocatalyst is more positive than the potential level of $H_2O/\bullet OH$ (2.44 eV). As a consequence, the photogenerated h^+ from these two semiconductors play an important role in degrading the methyl orange to form H_2O and CO_2. It also aligned with the results of scavenger test where hydroxyl radical on the surface is the main active species in the reaction. As a conclusion, the low negative of VB energy of Ag_2CO_3 is expected to endow the

photogenerated h^+ with strong oxidizing ability and this well-made Z-scheme interface would promote the separation of the charge carrier rate.

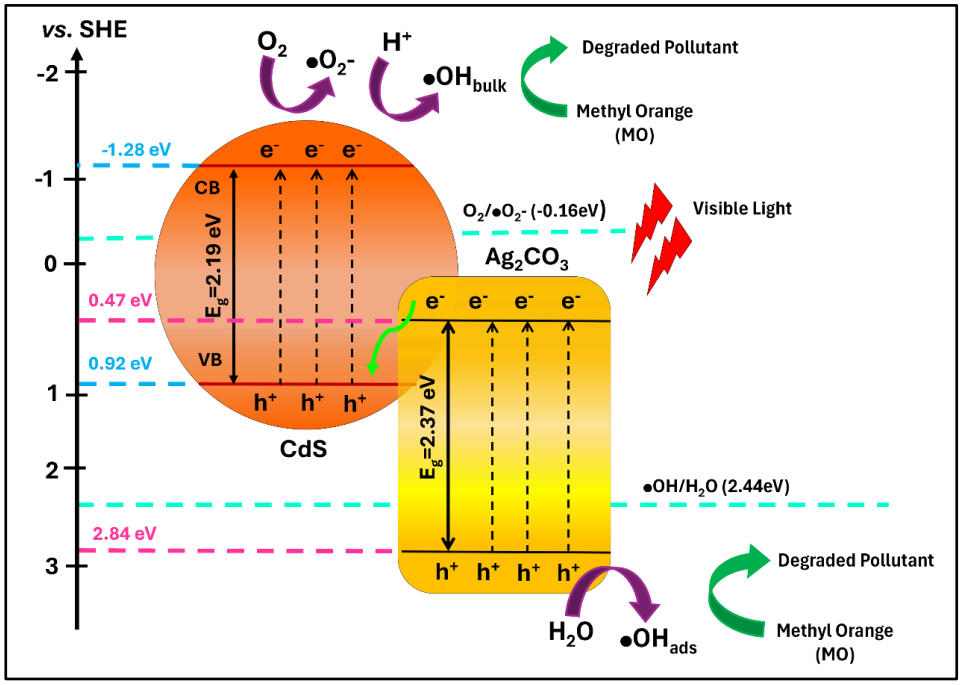

Figure 4.18 Schematic illustration of 10ACD for photocatalytic degradation of methyl orange under visible light irradiation

4.5 Reusability

The potential of catalyst to be recovered and reused in photocatalytic processes is a great concern which make it the synthesized photocatalysis an attractive method for wastewater treatment and reducing the operational cost. Hence, the reusability of photocatalyst was conducted as it is scrutinized for the practical used. Figure 4.18 was presented the stability of 10 ACD that has been experimented by repeating for five cycles. As clearly demonstrated in the Figure 4.18, the photocatalyst successfully remained active even after repeated for five cycles from 94.48% until 83.43 % with only lower reduction of percent degradation of MO and emphasized the efficiency of the photocatalyst. The efficiency of the photocatalyst could be retard due to the aggregation of the catalyst which make it low surface area and the accessibility of active site. Thus, these results reported that the catalyst are significantly photochemically stable and highly reusable. Besides that, as shown in Figure 4.19, there was no significant change observed in the XRD and FTIR spectra of the spent 10ACD catalyst compared to the fresh 10ACD, suggesting that the 10ACD structure remained chemically stable during the photodegradation process.

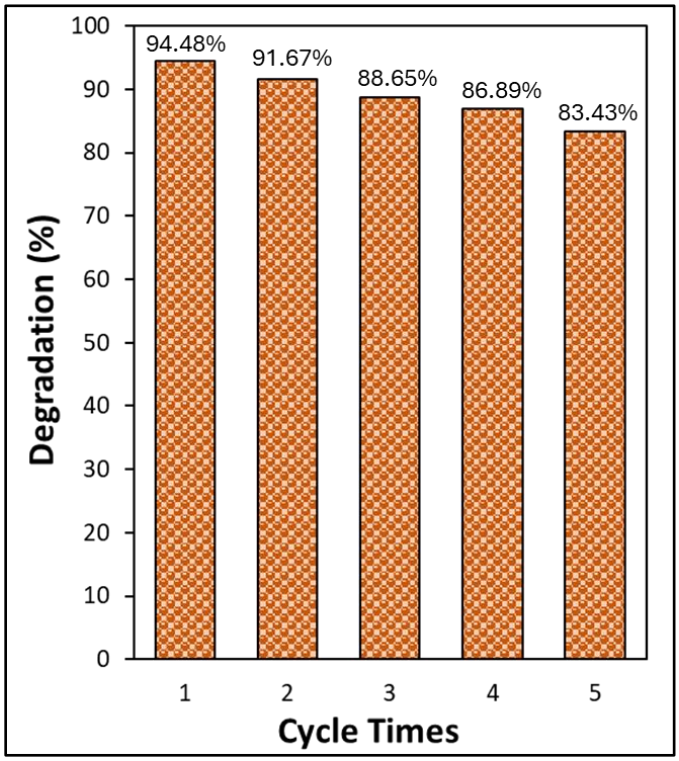

Figure 4.19 Photostability test within five cycle (CMO = 10 mg L-1, pH = 6, W = 0.0250 g L-1, t = 1 h, 30°C)

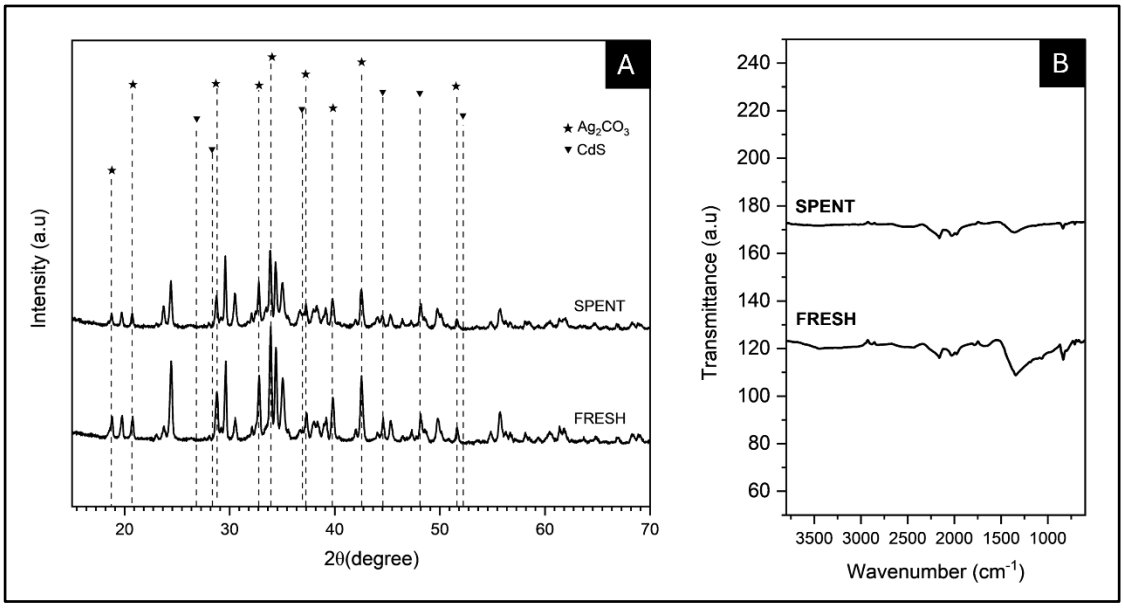

Figure 4.20 XRD and FTIR spectra of fresh 10ACD and spent 10ACD

4.6 Comparison Study with Other Semiconductor

A comparison study towards the photodegradation of methyl orange (MO) over various photocatalyst was tabulated in the Table 4.3. From the analysed results, it was observed that the combination of Ag_2CO_3 and CdS in the 10ACD photocatalyst

exhibited high photocatalytic efficiency for MO degradation. The performance of 10ACD was on par with other reported semiconductor catalysts, indicating its strong potential as an efficient and stable photocatalyst for the degradation of MO and other organic pollutants. Hence, this modified photocatalyst considered to produce an excellent photocatalyst for the photodegradation of MO and other model pollutant.

Table 4.3

Comparison of photocatalytic activity of MO over various photocatalyst

Photocatalyst	**MO concentration ($mg\ L^{-1}$)**	**Dosage ($g\ L^{-1}$)**	**Contact time (h)**	**Degradation (%)**	**Ref.**
$AgCO_3/CdS$	10	0.0250	1	94.38	This Study
C/ZnO	10	0.5000	5	87.80	Farag et al., (2024)
$Fe_3O_4@SiO_2@ZnO$	13.5	0.0500	4	96	Makota et al., (2024)
$Ag@Ag_2CO_3/Bi_2O_2CO_3$	30	1.000	1.5	93.60	(Y. Huang et al., 2024)
$Ag/MoO_3/TiO_2$	10	0.1200	5.5	95.6	Kader et al., (2022)
Co-ZnO	100	0.0500	2	93	Adeel et al., (2021)
TiO_2/MoS_2	20	0.500	1.2	94	(Kite et al., 2021)

4.7 Summary

In this study, all the photocatalyst such as Ag_2CO_3 ,CdS and the series of modified photocatalysts (5ACD, 10ACD and 15 ACD) were successfully synthesized by using facile precipitation method for the photocatalytic degradation of MO. Specifically, the results demonstrated that the presence of Ag_2CO_3 loaded on 10% of CdS (10ACD) photocatalyst possessed the optimum photocatalytic activity reach up until 94.38% of 10 mg L^{-1} MO under visible light irradiation. It is attributed to the strong interaction of Ag_2CO_3 with the well dispersion 10ACD on the surface photocatalyst in the present of Cd and S elements. This distribution elements leads towards the formation of oxygen vacancies and appropriate band gap approximately ~2.05eV thus enhanced the photocatalytic performance for the degradation of MO. In addition, the low negative of VB energy level of Ag_2CO_3 photocatalyst endowing the photogenerated h^+ and promote the more ●OH with the strong redox ability for the photocatalytic reaction. Therefore, with the optimum photocatalyst 10ACD, it gives the beneficial as well as successfully construct the Z-scheme mechanism which provide strongest redox ability in water remediation and encounter most of wastewater treatment in the industry. This indicate that these modified photocatalyst is synergistic and aligned with Sustainable Development Goals (SDGs).

CHAPTER 5
CONCLUSION AND RECOMMENDATIONS

5.1 Conclusion

In this study, the cadmium sulfide loaded on the silver carbonate were successfully synthesized via facile precipitation method. This modified photocatalyst of Ag_2CO_3/CdS was varied at different ratio (95:5, 90:10 and 85:15) respectively to explore the optimum of modified photocatalyst for higher photocatalytic activity. Experimentally, Ag_2CO_3 was act as parents' catalyst while CdS as the composite catalyst due to the photo corrosion and toxicity characteristics. Therefore, the ratio of CdS only was focussed on the lower concentration to avoid the photo corrosion phenomenon at the surface of photocatalyst that have high possibility to retard the photocatalytic activity.

The optimum sample was successfully characterized by few characterizations such as XRD, FTIR, FESEM EDX, TEM, PL, XPS and UV-Vis DRS. The XRD analysis confirms the successful formation of a stable Ag_2CO_3/CdS heterojunction with well-dispersed CdS particularly in the 10ACD sample enhancing interfacial contact, charge transfer, and overall photocatalytic performance as well it is align with the FTIR analysis where 10ACD illustrate the lowest intensity among 5ACD and 15ACD due to the good dispersion of Cd and S element on the surface of Ag_2CO_3. For the surface microscopic study and internal surface morphology, synthesized Ag_2CO_3 has displays the rod-like structure with homogeneous smooth surface and flower like structure was presented for the synthesized CdS photocatalyst. The distribution of Cd as well as S on the surface Ag_2CO_3 respectively disparate by the ratio where 10 ACD has a well dispersed distribution which indicate high accessibility compared to the 5ACD and 15 ACD. In addition, UV-Vis DRS summarize that the addition of CdS to Ag_2CO_3 led to a further decrease in the band gap. Specifically, the band gap values for 5ACD, 10ACD, and 15ACD were 2.0 eV, 2.05 eV, and 1.7 eV, respectively. This gradual reduction is due to the interaction between CdS and Ag_2CO_3, which promotes the enhanced photocatalytic performance under visible light irradiation. To estimate the recombination rate of photogenerated charge pairs, photoluminescence (PL) spectroscopy was carried out, 10 ACD indicated the lowest photo photoluminescence

which demonstrate the optimum condition which effectively inhibited the electron – hole recombination as well as increased the excitons lifetime and enhanced the photocatalytic performance of the composite photocatalyst. This trend has been strongly supported by the XPS analysis where the binding energies for 10 ACD were blue shifted as compared to Ag_2CO_3 which indicated the movement of the electron from Ag_2CO_3 to CdS which highlight the function as an electron donor while the CdS in the 10 ACD composite photocatalyst are roles as electron acceptor simultaneously aligned with the opposite energy banding shifts of O 1s and C 1s.

Experimentally, the study revealed that the modified photocatalyst of 10ACD has the highest photodegradation (94.38%) followed by 15ACD (83.28%) and 5ACD (80.56%) while Ag_2CO_3 and CdS obtained 75.22%, 81.61% respectively. Noticeably, the higher the wt% of CdS towards Ag_2CO_3, the photocatalytic performance was increased until an optimum reached. It is due to the highest number of surface defects and well dispersion in 10ACD modified photocatalyst which leads to the good interaction between of Cd and S element on the Ag_2CO_3. In addition, it was investigated in the scavenger test and proved in the proposed mechanism where hydroxyl radical on the surface was the main active species in the reaction. It is aligned that CdS has lower negative VB and endow more hole with high oxidizing ability as demonstrated by XPS analysis which suggesting the role of Ag_2CO_3 as an electron donor while CdS as electron acceptor. Hence, it progressively boosted the light harvesting ability, enhance the charge transfer and increase the efficiency of redox reaction for the photocatalytic degradation for the methyl orange and other model pollutant.

Photocatalytic performance influenced by few parameters includes catalyst dosage, initial concentration of methyl orange and pH to maximize the optimum condition of modified photocatalyst for the photodegradation of MO. For the effect of catalyst dosage, it successfully inspected with varying the values of 0.01250-0.03750 g L^{-1} and 0.0250 g L^{-1} reported to be optimum with the highest degradation until 94.38%. It is due to the conceptual mechanism when lower catalyst dosage, there might be insufficient of active sites for effective pollutant degradation while exceed optimal dosage, the degradation consequently decreases the photocatalytic degradation because of excesses catalyst would block the light penetration. This also can be attributed to the effect of initial concentrations where 10 mg L^{-1} was the optimum concentration of photodegradation towards methyl orange. When the initial concentration getting increased, less light

penetration will be irradiated to the photocatalyst thus lowering the generation of reactive species in the reaction and decrease the photocatalytic performance. Next, the pH 3 was examined to be optimum photodegradation toward methyl orange until 98.02%. It is because methyl orange anionic dye which present if N-H group that easily attract and construct strong electrostatic attraction between positively charge catalysts surface and negatively CR molecules. This is synergistic which acidic condition is typically more favourable for MO degradation. Ultimately, the kinetic study also was studied in this research for Ag_2CO_3, CdS together with 10ACD for the degradation of MO and it followed a psedo-first-order Langmuir Hinshelwood model. Next, the reusability study of the modified photocatalyst showed high efficiency when the reaction can be still stable after five cycles even at a slow degradation of MO. Moreover, the factual evidence from XPS and scavenger test supported with the reliable band gap energy of 10ACD between Ag_2CO_3 and CdS synergistic for the Z-scheme mechanism. It is helpful for the improvement in the interfacial charge transfer and the strong redox potential ability to speed up the photoactivity.

5.2 Future Works

In this research, the combination between Ag_2CO_3 and CdS were verified to enhance the properties and photocatalytic degradation of the modified catalyst towards the methyl orange. Therefore, this modified photocatalyst has a great potential and alternative than the conventional method as well could be extendable for the degradation of other pollutants including heavy metal, pharmaceuticals and organic pollutants. Furthermore, as an advancement of this research, modified photocatalyst can be utilized for other extended photocatalytic applications such as the generation of hydrogen production in water splitting, photoconversion of CO_2 into methanol and more. Additionally, referring to the previous technique, it is possible that the further modification of other semiconductors can be also implemented to create the dual - scheme heterojunction and generate the novelty of modified photocatalyst for various applications. Generally, this research has wide prospective to be scaled up until pilot scale as the real industrial application. However, the pilot scale commonly was executed using suspension mode which can caused treated wastewater in slurry form leads to the needed of filtration process. Thus, immobilization system can be efficient work as the alternative to overcome this problem.

REFERENCES

Abd Elkodous, M., El-Khawaga, A. M., Abouelela, M. M., & Abdel Maksoud, M. I. A. (2023). Cocatalyst loaded Al-SrTiO3 cubes for Congo red dye photo-degradation under wide range of light. *Scientific Reports*, *13*(1). https://doi.org/10.1038/s41598-023-33249-1

Acedo-Mendoza, A. G., Infantes-Molina, A., Vargas-Hernández, D., Chávez-Sánchez, C. A., Rodríguez-Castellón, E., & Tánori-Córdova, J. C. (2020). Photodegradation of methylene blue and methyl orange with CuO supported on ZnO photocatalysts: The effect of copper loading and reaction temperature. *Materials Science in Semiconductor Processing*, *119*, 105257. https://doi.org/10.1016/J.MSSP.2020.105257

Adeel, M., Saeed, M., Khan, I., Muneer, M., & Akram, N. (2021). Synthesis and Characterization of Co-ZnO and Evaluation of Its Photocatalytic Activity for Photodegradation of Methyl Orange. *ACS Omega*, *6*(2), 1426–1435. https://doi.org/10.1021/ACSOMEGA.0C05092/SUPPL_FILE/AO0C05092_LIVESLIDES.MP4

Ahmed, M. A., & Mohamed, A. A. (2022). Recent progress in semiconductor/graphene photocatalysts: synthesis, photocatalytic applications, and challenges. *RSC Advances*, *13*(1), 421–439. https://doi.org/10.1039/D2RA07225D

Ahmed, S. F., Mofijur, M., Nuzhat, S., Chowdhury, A. T., Rafa, N., Uddin, M. A., Inayat, A., Mahlia, T. M. I., Ong, H. C., Chia, W. Y., & Show, P. L. (2021). Recent developments in physical, biological, chemical, and hybrid treatment techniques for removing emerging contaminants from wastewater. *Journal of Hazardous Materials*, *416*. https://doi.org/10.1016/j.jhazmat.2021.125912

Akhundi, A., & Habibi-Yangjeh, A. (2016). Novel g-C3N4/Ag2SO4 nanocomposites: Fast microwave-assisted preparation and enhanced photocatalytic performance towards degradation of organic pollutants under visible light. *Journal of Colloid and Interface Science*, *482*, 165–174. https://doi.org/10.1016/j.jcis.2016.08.002

Aljuaid, A., Almehmadi, M., Alsaiari, A. A., Allahyani, M., Abdulaziz, O., Alsharif, A., Alsaiari, J. A., Saih, M., Alotaibi, R. T., & Khan, I. (2023). g-C3N4 Based Photocatalyst for the Efficient Photodegradation of Toxic Methyl Orange Dye: Recent Modifications and Future Perspectives. *Molecules 2023, Vol. 28, Page 3199*, *28*(7), 3199. https://doi.org/10.3390/MOLECULES28073199

Alshammari, K., Alakreia, A. S., Aldakhilallah, G. F., Alotaibi, R. B., & Fal, M. (2025). Synthesis and characterization of CdS@g-C_3N_4 catalyst for enhanced hydrogen generation using methanolysis of sodium borohydride. *Journal of Alloys and Compounds*, *1010*. https://doi.org/10.1016/j.jallcom.2024.177590

Ameta, R., Solanki, M. S., Benjamin, S., & Ameta, S. C. (2018). Photocatalysis. *Advanced Oxidation Processes for Wastewater Treatment: Emerging Green Chemical Technology*, 135–175. https://doi.org/10.1016/B978-0-12-810499-6.00006-1

An, W., Sun, K., Hu, J., Cui, W., & Liu, L. (2020). The Z-scheme Ag2CO3@g-C3N4 core-shell structure for increased photoinduced charge separation and stable photocatalytic degradation. *Applied Surface Science*, *504*, 144345. https://doi.org/10.1016/J.APSUSC.2019.144345

Ansari, M. O., Kumar, R., Pervez Ansari, S., Abdel-Wahab Hassan, M. S., Alshahrie, A., & Barakat, M. A. E. F. (2018). Nanocarbon aerogel composites. In *Nanocarbon and its Composites: Preparation, Properties and Applications* (pp. 1–26). Elsevier. https://doi.org/10.1016/B978-0-08-102509-3.00001-8

Arif, A. (2020). Water pollution and industries. *Pure and Applied Biology*, *9*(4). https://doi.org/10.19045/bspab.2020.90237

Arshad Kamran, M., Abbas, A., Ullah, S., Alomar, M., Malik, S., Hammad Aziz, M., & Farwa Bukhari, S. (2024). Boosting electrochemical and photocatalytic performance of Cadmium Sulfide/Zinc Telluride nanocomposites via Nickel doping. *Materials Science and Engineering: B*, *299*, 116932. https://doi.org/10.1016/J.MSEB.2023.116932

Azami, M. S., Jalil, A. A., Aziz, F. F. A., Hassan, N. S., Mamat, C. R., Fauzi, A. A., & Izzudin, N. M. (2022). Exploiting the potential of silver oxo-salts with graphitic carbon nitride/fibrous silica-titania in designing a new dual Z-scheme photocatalyst for photodegradation of 2-chlorophenol. *Separation and Purification Technology*, *292*. https://doi.org/10.1016/j.seppur.2022.120984

Azami, M. S., Jalil, A. A., Hassan, N. S., Hussain, I., Fauzi, A. A., & Aziz, M. A. A. (2021). Green carbonaceous material–fibrous silica-titania composite photocatalysts for enhanced degradation of toxic 2-chlorophenol. *Journal of Hazardous Materials*, *414*, 125524. https://doi.org/10.1016/J.JHAZMAT.2021.125524

Bora, L. V., & Mewada, R. K. (2017). Photocatalytic treatment of dye wastewater and

parametric study using a novel Z-scheme Ag2CO3/SiC photocatalyst under natural sunlight. *Journal of Environmental Chemical Engineering*, *5*(6), 5556–5565. https://doi.org/10.1016/J.JECE.2017.10.037

Brillas, E. (2025). Degradation/mineralization of bisphenol A from aqueous matrices by single and combined electrochemical advanced oxidation processes. A review. *Separation and Purification Technology*, *357*, 130170. https://doi.org/10.1016/J.SEPPUR.2024.130170

Camara, M., Jamil, N. R., & Abdullah, A. F. Bin. (2019). Impact of land uses on water quality in Malaysia: a review. *Ecological Processes*, *8*(1), 1–10. https://doi.org/10.1186/S13717-019-0164-X/FIGURES/4

Cao, W., Chen, L., & Qi, Z. (2015). Microwave-assisted synthesis of Ag/Ag2SO4/ZnO nanostructures for efficient visible-light-driven photocatalysis. *Journal of Molecular Catalysis A: Chemical*, *401*, 81–89. https://doi.org/10.1016/j.molcata.2015.02.023

Chen, Y., Ma, D., He, G., & Pan, S. (2024). Effects of pH on the Photocatalytic Activity and Degradation Mechanism of Rhodamine B over Fusiform Bi Photocatalysts under Visible Light. Water, 16(17), 2389. https://doi.org/10.3390/w16172389

Chen, F., Yang, Q., Wang, Y., Yao, F., Ma, Y., Huang, X., Li, X., Wang, D., Zeng, G., & Yu, H. (2018). Efficient construction of bismuth vanadate-based Z-scheme photocatalyst for simultaneous Cr(VI) reduction and ciprofloxacin oxidation under visible light: Kinetics, degradation pathways and mechanism. *Chemical Engineering Journal*, *348*, 157–170. https://doi.org/10.1016/J.CEJ.2018.04.170

Chen, J., Javaheri, H., Sulaiman, B. A. C., & Dahman, Y. (2016). Synthesis, characterization and applications of nanoparticles. *Fabrication and Self-Assembly of Nanobiomaterials: Applications of Nanobiomaterials*, 1–27. https://doi.org/10.1016/B978-0-323-41533-0.00001-5

Chen, X., Dai, Y., & Wang, X. (2015). Methods and mechanism for improvement of photocatalytic activity and stability of Ag3PO4: A review. *Journal of Alloys and Compounds*, *649*, 910–932. https://doi.org/10.1016/J.JALLCOM.2015.07.174

Cheng, S., Zhao, S., Xing, B., Liu, Y., Zhang, C., & Xia, H. (2022). Preparation of magnetic adsorbent-photocatalyst composites for dye removal by synergistic effect of adsorption and photocatalysis. *Journal of Cleaner Production*, *348*, 131301. https://doi.org/10.1016/J.JCLEPRO.2022.131301

Chimmikuttanda, S. P., Naik, A., Akple, M. S., & Singh, R. (2022). Processing of hybrid

TiO2 semiconducting materials and their environmental application. *Advanced Materials for Sustainable Environmental Remediation: Terrestrial and Aquatic Environments*, 277–300. https://doi.org/10.1016/B978-0-323-90485-8.00011-4

Choo, H. S., Lam, S. M., Sin, J. C., & Mohamed, A. R. (2016). An efficient Ag2SO4-deposited ZnO in photocatalytic removal of indigo carmine and phenol under outdoor light irradiation. *Desalination and Water Treatment*, *57*(30), 14227–14240. https://doi.org/10.1080/19443994.2015.1067833

Crini, G., & Lichtfouse, E. (2019). Advantages and disadvantages of techniques used for wastewater treatment. *Environmental Chemistry Letters*, *17*(1), 145–155. https://doi.org/10.1007/S10311-018-0785-9/METRICS

Deng, F., Lu, X., Luo, Y., Wang, J., Che, W., Yang, R., Luo, X., Luo, S., & Dionysiou, D. D. (2019). Novel visible-light-driven direct Z-scheme CdS/CuInS2 nanoplates for excellent photocatalytic degradation performance and highly-efficient Cr(VI) reduction. *Chemical Engineering Journal*, *361*, 1451–1461. https://doi.org/10.1016/j.cej.2018.10.176

Deng, H., Wu, Y., Li, L., jiang, X., Wang, P., Fang, K., Li, J., Hao, D., Zhu, H., Wang, Q., & Li, Q. (2025). Synergistic mechanisms for efficient and safe antibiotic removal: Effective adsorption and photocatalytic degradation using aerogels. *Separation and Purification Technology*, *354*, 129455. https://doi.org/10.1016/J.SEPPUR.2024.129455

Dewil, R., Mantzavinos, D., Poulios, I., & Rodrigo, M. A. (2017). New perspectives for Advanced Oxidation Processes. In *Journal of Environmental Management* (Vol. 195, pp. 93–99). Academic Press. https://doi.org/10.1016/j.jenvman.2017.04.010

Dimitropoulos, M., Aggelopoulos, C. A., Sygellou, L., Tsantis, S. T., Koutsoukos, P. G., & Yannopoulos, S. N. (2024). Unveiling the photocorrosion mechanism of zinc oxide photocatalyst: Interplay between surface corrosion and regeneration. *Journal of Environmental Chemical Engineering*, *12*(2), 112102. https://doi.org/10.1016/J.JECE.2024.112102

Dostanić, J., Lončarević, D., Đorđević, V., Ahrenkiel, S. P., & Nedeljković, J. M. (2017). The photocatalytic performance of silver halides – Silver carbonate heterostructures. *Journal of Photochemistry and Photobiology A: Chemistry*, *336*, 1–7. https://doi.org/10.1016/J.JPHOTOCHEM.2016.12.019

Ebihara, M., Ikeda, T., Okunaka, S., Tokudome, H., Domen, K., & Katayama, K.

(2021). Charge carrier mapping for Z-scheme photocatalytic water-splitting sheet via categorization of microscopic time-resolved image sequences. Nature Communications, 12(1). https://doi.org/10.1038/s41467-021-24061-4

Fang, S., Ding, C., Liang, Q., Li, Z., Xu, S., Peng, Y., & Lu, D. (2016). In-situ precipitation synthesis of novel BiOCl/Ag2CO3 hybrids with highly efficient visible-light-driven photocatalytic activity. *Journal of Alloys and Compounds*, *684*, 230–236. https://doi.org/10.1016/J.JALLCOM.2016.05.168

Farag, M., El-Dafrawy, S. M., & Hassan, S. M. (2024). ZnO and C/ZnO Catalysts Synthesized via Plant Mediated Extracts for Photodegradation of Crystal Violet and Methyl Orange Dyes. *Journal of Inorganic and Organometallic Polymers and Materials*, *34*(3), 930–943. https://doi.org/10.1007/S10904-023-02811-9/FIGURES/14

Fatah, N. A. A., Triwahyono, S., Jalil, A. A., Salamun, N., Mamat, C. R., & Majid, Z. A. (2017). n-Heptane isomerization over molybdenum supported on bicontinuous concentric lamellar silica KCC-1: Influence of phosphorus and optimization using response surface methodology (RSM). *Chemical Engineering Journal*, *314*, 650–659. https://doi.org/10.1016/J.CEJ.2016.12.028

Fu, Y., Xu, Y., Mao, Y., Tan, M., He, Q., Mao, H., Du, H., Hao, D., & Wang, Q. (2023). Multi-functional Ag/Ag3PO4/AgPMo with S-scheme heterojunction for boosted photocatalytic performance. *Separation and Purification Technology*, *317*, 123922. https://doi.org/10.1016/J.SEPPUR.2023.123922

Gan, J., Wang, H., Hu, H., Su, M., Chen, F., & Xu, H. (2021). Efficient synthesis of tunable band-gap CuInZnS decorated g-C3N4 hybrids for enhanced CO2 photocatalytic reduction and near-infrared-triggered photodegradation performance. *Applied Surface Science*, *564*, 150396. https://doi.org/10.1016/J.APSUSC.2021.150396

Garrido-Cardenas, J. A., Esteban-García, B., Agüera, A., Sánchez-Pérez, J. A., & Manzano-Agugliaro, F. (2020). Wastewater treatment by advanced oxidation process and their worldwide research trends. *International Journal of Environmental Research and Public Health*, *17*(1). https://doi.org/10.3390/ijerph17010170

Ghazi, S., Rhouta, B., Tendero, C., & Maury, F. (2023). Synthesis, characterization and properties of sulfate-modified silver carbonate with enhanced visible light photocatalytic performance. *RSC Advances*, *13*(33), 23076–23086.

https://doi.org/10.1039/d3ra03120a

Ghosh, A., Pramanik, A., Pal, S., & Sarkar, P. (2024). Emergence of Z-Scheme Photocatalysis for Total Water Splitting: An Improvised Route to High Efficiency. The Journal of Physical Chemistry Letters, 15(26), 6841–6851. https://doi.org/10.1021/acs.jpclett.4c01162

Gkika, D. A., Mitropoulos, A. C., Lambropoulou, D. A., Kalavrouziotis, I. K., & Kyzas, G. Z. (2022). Cosmetic wastewater treatment technologies: a review. *Environmental Science and Pollution Research*, *29*(50), 75223–75247. https://doi.org/10.1007/S11356-022-23045-1/FIGURES/5

Glassmeyer, S. T., Burns, E. E., Focazio, M. J., Furlong, E. T., Gribble, M. O., Jahne, M. A., Keely, S. P., Kennicutt, A. R., Kolpin, D. W., Medlock Kakaley, E. K., & Pfaller, S. L. (2023). Water, Water Everywhere, but Every Drop Unique: Challenges in the Science to Understand the Role of Contaminants of Emerging Concern in the Management of Drinking Water Supplies. *GeoHealth*, *7*(12). https://doi.org/10.1029/2022gh000716

Goodarzi, N., Ashrafi-Peyman, Z., Khani, E., & Moshfegh, A. Z. (2023). Recent Progress on Semiconductor Heterogeneous Photocatalysts in Clean Energy Production and Environmental Remediation. *Catalysts 2023, Vol. 13, Page 1102*, *13*(7), 1102. https://doi.org/10.3390/CATAL13071102

Hanafi, M. F., & Sapawe, N. (2020). Effect of initial concentration on the photocatalytic degradation of remazol brilliant blue dye using nickel catalyst. Materials Today: Proceedings, 31, 318–320. https://doi.org/10.1016/j.matpr.2020.06.066

Haleem, A., Shafiq, A., Chen, S. Q., & Nazar, M. (2023). A Comprehensive Review on Adsorption, Photocatalytic and Chemical Degradation of Dyes and Nitro-Compounds over Different Kinds of Porous and Composite Materials. *Molecules 2023, Vol. 28, Page 1081*, *28*(3), 1081. https://doi.org/10.3390/MOLECULES28031081

Halepoto, H., Gong, T., & Memon, H. (2022). Current status and research trends of textile wastewater treatments—A bibliometric-based study. *Frontiers in Environmental Science*, *10*. https://doi.org/10.3389/fenvs.2022.1042256

Hasni, M., Bouazzi, D., Cherif, I., Lefi, N., Caccamo, M. T., Magazù, S., & Badraoui, B. (2026). Tailoring surface and textural properties of magnesium-substituted hydroxyapatite for enhanced methyl orange adsorption: A combined experimental and Hirshfeld surface analysis. Materials Chemistry and Physics:

Sustainability and Energy, 7, 100063. https://doi.org/10.1016/j.macse.2026.100063

He, G., Yang, W., Zheng, W., Gong, L., Wang, X., An, Y., & Tian, M. (2019). Facile controlled synthesis of Ag 3 PO 4 with various morphologies for enhanced photocatalytic oxygen evolution from water splitting. *RSC Advances*, *9*(32), 18222–18231. https://doi.org/10.1039/C9RA01306G

Heiba, Z. K., Ahmed, M. A., Hassan, M., Badawi, A., El-naggar, A. M., & Mohamed, M. B. (2023). Sonochemical synthesis of Ag2CO3/CeO2 p-n heterojunction for decomposition of rhodamine B dye. *Optical Materials*, *141*, 113945. https://doi.org/10.1016/J.OPTMAT.2023.113945

Hojjati-Najafabadi, A., Farahbakhsh, E., Gholamalian, G., Feng, P., Davar, F., Aminabhavi, T. M., Vasseghian, Y., Kamyab, H., & Rahimi, H. (2024). Controllable synthesis of nanostructured flower-like cadmium sulfides for photocatalytic degradation of methyl orange under different light sources. *Journal of Water Process Engineering*, *59*. https://doi.org/10.1016/j.jwpe.2024.105002

Hou, C., Li, Y., Niu, M., Liu, Y., Kong, X., Zhang, M., & Wang, L. (2022). Construction of an all-solid-state Z-scheme Ag@Ag3PO4/TiO2-(F2) heterostructure with enhanced photocatalytic activity, photocorrosion resistance and mechanism insight. *Journal of Alloys and Compounds*, *925*, 166765. https://doi.org/10.1016/J.JALLCOM.2022.166765

Huang, G., Zeng, D., Ke, P., & Chen, Y. (2024). Preparation and characterization of Ag3PO4@g-C3N4 photocatalysts for dye wastewater treatment under visible-light irradiation. *Inorganic Chemistry Communications*, *160*. https://doi.org/10.1016/j.inoche.2023.111889

Huang, Y., Li, M., Zhang, X., Xing, B., Ye, Y., Liu, X., & Zeng, Y. (2024). Enhanced photocatalytic performance of 3d flower-like Ag@Ag2CO3/Bi2O2CO3 all-solid-state Z-scheme heterojunction. *Journal of Alloys and Compounds*, *976*, 173186. https://doi.org/10.1016/J.JALLCOM.2023.173186

Hussain, I., Jalil, A. A., Mamat, C. R., Siang, T. J., Rahman, A. F. A., Azami, M. S., & Adnan, R. H. (2019). New insights on the effect of the H2/CO ratio for enhancement of CO methanation over metal-free fibrous silica ZSM-5: Thermodynamic and mechanistic studies. *Energy Conversion and Management*, *199*, 112056. https://doi.org/10.1016/J.ENCONMAN.2019.112056

Iqbal, M., Ali, A., Nahyoon, N. A., Majeed, A., Pothu, R., Phulpoto, S., & Thebo, K. H. (2019). Photocatalytic degradation of organic pollutant with nanosized cadmium sulfide. *Materials Science for Energy Technologies*, *2*(1), 41–45. https://doi.org/10.1016/J.MSET.2018.09.002

Ismael, M. (2021). Latest progress on the key operating parameters affecting the photocatalytic activity of TiO2-based photocatalysts for hydrogen fuel production: A comprehensive review. *Fuel*, *303*, 121207. https://doi.org/10.1016/J.FUEL.2021.121207

Jabbar, Z. H., & Graimed, B. H. (2022). Recent developments in industrial organic degradation via semiconductor heterojunctions and the parameters affecting the photocatalytic process: A review study. *Journal of Water Process Engineering*, *47*, 102671. https://doi.org/10.1016/J.JWPE.2022.102671

Jayam Somasundaram, A., Elanthamilan, E., Wang, S.-F., & Sharmila Lydia, I. (2024). *Construction of magnetic Ag3PO4/Fe3O4/Chitosan polymer composite with enhanced visible-light-driven photocatalytic activity for the Methylene blue dye degradation*. https://doi.org/10.21203/rs.3.rs-4568116/v1

Jia, X., Tahir, M., Pan, L., Huang, Z. F., Zhang, X., Wang, L., & Zou, J. J. (2016). Direct Z-scheme composite of CdS and oxygen-defected CdWO4: An efficient visible-light-driven photocatalyst for hydrogen evolution. *Applied Catalysis B: Environmental*, *198*, 154–161. https://doi.org/10.1016/J.APCATB.2016.05.046

Jiang, C., Moniz, S. J. A., Wang, A., Zhang, T., & Tang, J. (2017). Photoelectrochemical devices for solar water splitting-materials and challenges. *Chemical Society Reviews*, *46*(15), 4645–4660. https://doi.org/10.1039/C6CS00306K

Jiang, H. J., Mei, Y. L., Liu, W. M., & Wu, Z. J. (2025). Enhanced piezo-photocatalytic activity of oxygen-deficient ZnO nanoparticles prepared by facile precipitation. *Applied Surface Science*, *708*, 163770. https://doi.org/10.1016/J.APSUSC.2025.163770

Jiang, W., Zong, X., An, L., Hua, S., Miao, X., Luan, S., Wen, Y., Tao, F. F., & Sun, Z. (2018). Consciously Constructing Heterojunction or Direct Z-Scheme Photocatalysts by Regulating Electron Flow Direction. *ACS Catalysis*, *8*(3), 2209–2217. https://doi.org/10.1021/ACSCATAL.7B04323/SUPPL_FILE/CS7B04323_SI_001.PDF

Jourshabani, M., Lee, B. K., & Shariatinia, Z. (2020). From Traditional Strategies to Z-

scheme Configuration in Graphitic Carbon Nitride Photocatalysts: Recent Progress and Future Challenges. *Applied Catalysis B: Environmental*, *276*, 119157. https://doi.org/10.1016/J.APCATB.2020.119157

Jubeer, E. M., Manthrammel, M. A., Subha, P. A., Shkir, M., Biju, K. P., & AlFaify, S. A. (2023). Defect engineering for enhanced optical and photocatalytic properties of ZnS nanoparticles synthesized by hydrothermal method. *Scientific Reports*, *13*(1), 16820. https://doi.org/10.1038/S41598-023-43735-1

Kader, S., Al-Mamun, M. R., Suhan, M. B. K., Shuchi, S. B., & Islam, M. S. (2022). Enhanced photodegradation of methyl orange dye under UV irradiation using MoO3 and Ag doped TiO2 photocatalysts. *Environmental Technology & Innovation*, *27*, 102476. https://doi.org/10.1016/J.ETI.2022.102476

Kamble, M. M., Rondiya, S. R., Bade, B. R., Kore, K. B., Nasane, M. P., Dzade, N. Y., Funde, A. M., & Jadkar, S. R. (2020). Optical, structural and morphological study of CdS nanoparticles: role of sulfur source. *Nanomaterials and Energy*, *9*(1), 72–81. https://doi.org/10.1680/JNAEN.19.00041

Khan, M. D., Singh, A., Khan, M. Z., Tabraiz, S., & Sheikh, J. (2023). Current perspectives, recent advancements, and efficiencies of various dye-containing wastewater treatment technologies. *Journal of Water Process Engineering*, *53*, 103579. https://doi.org/10.1016/J.JWPE.2023.103579

Khan, W. U., Ahmed, S., Dhoble, Y., & Madhav, S. (2023). A critical review of hazardous waste generation from textile industries and associated ecological impacts. *Journal of the Indian Chemical Society*, *100*(1), 100829. https://doi.org/10.1016/J.JICS.2022.100829

Kiani, M., Bagherzadeh, M., Kaveh, R., Rabiee, N., Fatahi, Y., Dinarvand, R., Jang, H. W., Shokouhimehr, M., & Varma, R. S. (2020). Novel Pt-Ag3PO4/CdS/Chitosan Nanocomposite with Enhanced Photocatalytic and Biological Activities. *Nanomaterials 2020, Vol. 10, Page 2320*, *10*(11), 2320. https://doi.org/10.3390/NANO10112320

Kishor, R., Purchase, D., Saratale, G. D., Romanholo Ferreira, L. F., Hussain, C. M., Mulla, S. I., & Bharagava, R. N. (2021). Degradation mechanism and toxicity reduction of methyl orange dye by a newly isolated bacterium Pseudomonas aeruginosa MZ520730. *Journal of Water Process Engineering*, *43*, 102300. https://doi.org/10.1016/J.JWPE.2021.102300

Kite, S. V., Kadam, A. N., Sathe, D. J., Patil, S., Mali, S. S., Hong, C. K., Lee, S., &

Garadkar, K. M. (2021). Nanostructured TiO2 Sensitized with MoS2 Nanoflowers for Enhanced Photodegradation Efficiency toward Methyl Orange. *ACS Omega*. https://doi.org/10.1021/ACSOMEGA.1C02194

Krupińska, I. (2020). Impact of the Oxidant Type on the Efficiency of the Oxidation and Removal of Iron Compounds from Groundwater Containing Humic Substances. Molecules, 25(15), 3380. https://doi.org/10.3390/molecules25153380

Kostjukov, V. (2026). Excitation of three forms of methyl orange dye in aqueous solution: A comparative theoretical analysis. Journal of Photochemistry and Photobiology A: Chemistry, 478, 117205. https://doi.org/10.1016/j.jphotochem.2026.117205

Kulkarni, R. C., Koujalagi, P. S., & Kulkarni, R. M. (2023). Self-cleaning ceramic coatings. *Advanced Ceramic Coatings for Emerging Applications*, 43–69. https://doi.org/10.1016/B978-0-323-99624-2.00014-0

Kurosawa, R., Takeuchi, M., & Ryu, J. (2021). Fourier-transform infrared and X-ray diffraction analyses of the hydration reaction of pure magnesium oxide and chemically modified magnesium oxide. RSC Advances, 11(39), 24292–24311. https://doi.org/10.1039/d1ra04290d

Kumar, K. V., Porkodi, K., & Rocha, F. (2008). Langmuir–Hinshelwood kinetics – A theoretical study. *Catalysis Communications*, *9*(1), 82–84. https://doi.org/10.1016/J.CATCOM.2007.05.019

Kumar, N., Yadav, S., Mittal, A., & Kumari, K. (2021). Photocatalysis by zinc oxide-based nanomaterials. *Nanostructured Zinc Oxide: Synthesis, Properties and Applications*, 393–457. https://doi.org/10.1016/B978-0-12-818900-9.00005-X

Kumar, S., & Sharma, J. K. (2016). Stable phase CdS nanoparticles for optoelectronics: A study on surface morphology, structural and optical characterization. *Materials Science- Poland*, *34*(2), 368–373. https://doi.org/10.1515/MSP-2016-0033

Kumar, V., & Shah, M. P. (2021). Advanced oxidation processes for complex wastewater treatment. *Advanced Oxidation Processes for Effluent Treatment Plants*, 1–31. https://doi.org/10.1016/B978-0-12-821011-6.00001-3

Kumari, H., Sonia, Suman, Ranga, R., Chahal, S., Devi, S., Sharma, S., Kumar, S., Kumar, P., Kumar, S., Kumar, A., & Parmar, R. (2023). A Review on Photocatalysis Used For Wastewater Treatment: Dye Degradation. In *Water, Air, and Soil Pollution* (Vol. 234, Issue 6). Institute for Ionics.

https://doi.org/10.1007/s11270-023-06359-9

LaRose, D. (2017, April 5). Carmen Busquets. Carmen Busquets. https://www.carmenbusquets.com/journal/post/fashion-waste-water

Langa, Nomso C Hintsho-Mbita (2023*), Plant and bacteria mediated synthesis of TiO2 NPs for dye degradation in water. A review*. Chemical Physics Impact, 7 (100293), 2667-0224, https://doi.org/10.1016/j.chphi.2023.100293.

Le, A. T., Duy, T., Le, H., Nguyen, H., & Tuan, A. (n.d.). *Photoluminescence and photocatalytic activities of Ag/ZnO metal-semiconductor heterostructure You may also like Enhanced photocatalytic activity of Ag/ZnO nanocomposite immobilized on kanthal coils*. https://doi.org/10.1088/1742-6596/765/1/012023

Lei, D., Xue, J., Bi, Q., Tang, C., & Zhang, L. (2020). 3D/2D direct Z-scheme photocatalyst Zn2SnO4/CdS for simultaneous removal of Cr(VI) and organic pollutant. *Applied Surface Science*, *517*, 146030. https://doi.org/10.1016/J.APSUSC.2020.146030

Li, X., Xu, P., Chen, M., Zeng, G., Wang, D., Chen, F., Tang, W., Chen, C., Zhang, C., & Tan, X. (2019). Application of silver phosphate-based photocatalysts: Barriers and solutions. Chemical Engineering Journal, 366, 339–357. https://doi.org/10.1016/j.cej.2019.02.083

Li, J. Y., Li, Y. H., Qi, M. Y., Lin, Q., Tang, Z. R., & Xu, Y. J. (2020). Selective Organic Transformations over Cadmium Sulfide-Based Photocatalysts. *ACS Catalysis*, *10*(11), 6262–6280. https://doi.org/10.1021/ACSCATAL.0C01567/ASSET/IMAGES/LARGE/CS0C01567_0005.JPEG

Li, J., Yuan, H., Zhang, W., Jin, B., Feng, Q., Huang, J., & Jiao, Z. (2022). Advances in Z-scheme semiconductor photocatalysts for the photoelectrochemical applications: A review. In *Carbon Energy* (Vol. 4, Issue 3, pp. 294–331). John Wiley and Sons Inc. https://doi.org/10.1002/cey2.179

Li, M., Shah, N. H., Zhang, P., Chen, P., Cui, Y., Jiang, Y., & Wang, Y. (2023). Mechanism, modification and application of silver-based photocatalysts. *Materials Today Sustainability*, *22*, 100409. https://doi.org/10.1016/J.MTSUST.2023.100409

Li, X., Wang, J., Zhang, J., Zhao, C., Wu, Y., & He, Y. (2022). Cadmium sulfide modified zinc oxide heterojunction harvesting ultrasonic mechanical energy for efficient decomposition of dye wastewater. *Journal of Colloid and Interface*

Science, *607*, 412–422. https://doi.org/10.1016/J.JCIS.2021.09.004

Li, X., Xu, P., Chen, M., Zeng, G., Wang, D., Chen, F., Tang, W., Chen, C., Zhang, C., & Tan, X. (2019). Application of silver phosphate-based photocatalysts: Barriers and solutions. *Chemical Engineering Journal*, *366*, 339–357. https://doi.org/10.1016/J.CEJ.2019.02.083

Liao, G., Li, C., Li, X., & Fang, B. (2021). Emerging polymeric carbon nitride Z-scheme systems for photocatalysis. *Cell Reports Physical Science*, *2*(3), 100355. https://doi.org/10.1016/J.XCRP.2021.100355

Lin, L., Yang, H., & Xu, X. (2022). Effects of Water Pollution on Human Health and Disease Heterogeneity: A Review. *Frontiers in Environmental Science*, *10*, 880246. https://doi.org/10.3389/FENVS.2022.880246/BIBTEX

Liqiang, J., Yichun, Q., Baiqi, W., Shudan, L., Baojiang, J., Libin, Y., Wei, F., Honggang, F., & Jiazhong, S. (2006). Review of photoluminescence performance of nano-sized semiconductor materials and its relationships with photocatalytic activity. *Solar Energy Materials and Solar Cells*, *90*(12), 1773–1787. https://doi.org/10.1016/J.SOLMAT.2005.11.007

Liu, H., Li, X., Zhang, X., Coulon, F., & Wang, C. (2023). Harnessing the power of natural minerals: A comprehensive review of their application as heterogeneous catalysts in advanced oxidation processes for organic pollutant degradation. *Chemosphere*, *337*, 139404. https://doi.org/10.1016/J.CHEMOSPHERE.2023.139404

Liu, H. Y., Liang, C., Niu, C. G., Huang, D. W., Du, Y. B., Guo, H., Zhang, L., Yang, Y. Y., & Zeng, G. M. (2019). Facile assembly of g-C 3 N 4 /Ag 2 CO 3 /graphene oxide with a novel dual Z-scheme system for enhanced photocatalytic pollutant degradation. *Applied Surface Science*, *475*, 421–434. https://doi.org/10.1016/j.apsusc.2019.01.018

Liu, Y., Fang, L., Lu, H., Liu, L., Wang, H., & Hu, C. (2012). Highly efficient and stable Ag/Ag3PO4 plasmonic photocatalyst in visible light. *Catalysis Communications*, *17*, 200–204. https://doi.org/10.1016/J.CATCOM.2011.11.001

Liu, Y., Kong, J., Yuan, J., Zhao, W., Zhu, X., Sun, C., & Xie, J. (2018). Enhanced photocatalytic activity over flower-like sphere Ag/Ag2CO3/BiVO4 plasmonic heterojunction photocatalyst for tetracycline degradation. *Chemical Engineering Journal*, *331*, 242–254. https://doi.org/10.1016/J.CEJ.2017.08.114

Liu, Y., Song, L., Du, L., Gao, P., Liang, N., Wu, S., Minami, T., Zang, L., Yu, C., & Xu, X. (2020). Preparation of Polyaniline/Emulsion Microsphere Composite for Efficient Adsorption of Organic Dyes. *Polymers 2020, Vol. 12, Page 167*, *12*(1), 167. https://doi.org/10.3390/POLYM12010167

Low, J., Dai, B., Tong, T., Jiang, C., & Yu, J. (2019). In Situ Irradiated X-Ray Photoelectron Spectroscopy Investigation on a Direct Z-Scheme TiO2/CdS Composite Film Photocatalyst. *Advanced Materials*, *31*(6), 1802981. https://doi.org/10.1002/ADMA.201802981

Low, J., Jiang, C., Cheng, B., Wageh, S., Al-Ghamdi, A. A., & Yu, J. (2017). A Review of Direct Z-Scheme Photocatalysts. *Small Methods*, *1*(5), 1700080. https://doi.org/10.1002/SMTD.201700080

Luo, L., Li, Y., Hou, J., & Yang, Y. (2014). Visible photocatalysis and photostability of Ag3PO4 photocatalyst. *Applied Surface Science*, *319*(1), 332–338. https://doi.org/10.1016/J.APSUSC.2014.04.154

Lv, X., Zhang, D., & Wang, J. (2021). Coupling system of silver carbonate nanoparticles and bismuth oxyiodide nanosheets with enhanced photocatalytic properties. In *Indian Journal of Chemical Technology* (Vol. 28).

Makota, O., Dutková, E., Briančin, J., Bednarcik, J., Lisnichuk, M., Yevchuk, I., & Melnyk, I. (2024). Advanced Photodegradation of Azo Dye Methyl Orange Using H2O2-Activated Fe3O4@SiO2@ZnO Composite under UV Treatment. *Molecules 2024, Vol. 29, Page 1190*, *29*(6), 1190. https://doi.org/10.3390/MOLECULES29061190

Mandade, P. (2021). Introduction, basic principles, mechanism, and challenges of photocatalysis. In *Handbook of Nanomaterials for Wastewater Treatment: Fundamentals and Scale up Issues* (pp. 137–154). Elsevier. https://doi.org/10.1016/B978-0-12-821496-1.00016-7

Mao, J., Xu, W., & Seo, S. (2024). Exploring the dual phases of cadmium sulfide: synthesis, properties, and applications of hexagonal wurtzite and cubic zinc blende crystal structures. Journal of Materials Chemistry A, 12(35), 23218–23242. https://doi.org/10.1039/d4ta03496a

Mehra, S., Saroha, J., Rani, E., Sharma, V., Goswami, L., Gupta, G., Srivastava, A. K., & Sharma, S. N. (2023). Development of visible light-driven SrTiO3 photocatalysts for the degradation of organic pollutants for waste-water treatment: Contrasting behavior of MB & MO dyes. *Optical Materials*, *136*,

113344. https://doi.org/10.1016/J.OPTMAT.2022.113344

Merdoud, R., Aoudjit, F., Mouni, L., Honavar, V., Moghadam, R. P., Palabathuni, M., & Ranade, V. V. (2025). Methyl Orange Degradation Using Ag-Doped TiO2, H2O2, and Hydrodynamic Cavitation. ACS Omega, 10(21), 21377–21390. https://doi.org/10.1021/acsomega.5c00034

Mo, G., Jin, Y., Deng, Y., Zhang, C., Liu, J., Niu, Q., Gao, X., Bi, Y., Chen, H., & Li, P. (2026). Band-Gap Engineering of Isoreticular Hydrogen-Bonded Organic Frameworks for Boosting Photocatalytic Hydrogen Evolution. Angewandte Chemie International Edition. https://doi.org/10.1002/anie.202525987

Moghaddam, M., Naderi, N., Hosseinifard, M., & Kazemzadeh, A. (2020). Improved optical and structural properties of cadmium sulfide nanostructures for optoelectronic applications. *Ceramics International*, *46*(6), 7388–7395. https://doi.org/10.1016/J.CERAMINT.2019.11.234

Mohan, H., Ramalingam, V., Karthi, N., Malathidevi, S., Shin, T., Venkatachalam, J., & Seralathan, K. K. (2021). Enhanced visible light-driven photocatalytic activity of reduced graphene oxide/cadmium sulfide composite: Methylparaben degradation mechanism and toxicity. *Chemosphere*, *264*, 128481. https://doi.org/10.1016/J.CHEMOSPHERE.2020.128481

Murcia, J. J., Hernández, J. S., Rojas, H., Moreno-Cascante, J., Sánchez-Cid, P., Hidalgo, M. C., Navío, J. A., & Jaramillo-Páez, C. (2020). Evaluation of Au–ZnO, ZnO/Ag2CO3 and Ag–TiO2 as Photocatalyst for Wastewater Treatment. *Topics in Catalysis*, *63*(11–14), 1286–1301. https://doi.org/10.1007/s11244-020-01232-z

Nandiyanto, A. B. D., Zaen, R., & Oktiani, R. (2020). Correlation between crystallite size and photocatalytic performance of micrometer-sized monoclinic WO3 particles. *Arabian Journal of Chemistry*, *13*(1), 1283–1296. https://doi.org/10.1016/J.ARABJC.2017.10.010

Nasir, J. A., Rehman, Z. U., Shah, S. N. A., Khan, A., Butler, I. S., & Catlow, C. R. A. (2020). Recent developments and perspectives in CdS-based photocatalysts for water splitting. *Journal of Materials Chemistry A*, *8*(40), 20752–20780. https://doi.org/10.1039/D0TA05834C

Osiemo, M. M., Ogendi, G. M., & M'Erimba, C. (2019). Microbial Quality of Drinking Water and Prevalence of Water-Related Diseases in Marigat Urban Centre, Kenya. *Environmental Health Insights*, *13*.

https://doi.org/10.1177/1178630219836988

Panda, D., Venkatesh, N., & Sakthivel, P. (2022). MXene-based materials for remediation of environmental pollutants. *MXenes and Their Composites: Synthesis, Properties and Potential Applications*, 553–594. https://doi.org/10.1016/B978-0-12-823361-0.00014-9

Parwaz Khan, A. A., Singh, P., Raizada, P., & M Asiri, A. (2021). Converting Ag3PO4/CdS/Fe doped C3N4 based dual Z-scheme photocatalyst into photo-Fenton system for efficient photocatalytic phenol removal. *Journal of Industrial and Engineering Chemistry*, *98*, 148–160. https://doi.org/10.1016/j.jiec.2021.04.007

Pavlović, J., Tušar, N. N., & Rajić, N. (2024). The Synthesis and Photocatalytic Efficacy of Distinct Nano-Oxides in the Breakdown of Organic Contaminants. *Catalysts 2024, Vol. 14, Page 771*, *14*(11), 771. https://doi.org/10.3390/CATAL14110771

Petala, A., Nasiou, A., Mantzavinos, D., & Frontistis, Z. (2020). Photocatalytic evaluation of Ag2CO3 for ethylparaben degradation in different water matrices. *Water (Switzerland)*, *12*(4). https://doi.org/10.3390/W12041180

Porcu, S., Secci, F., & Ricci, P. C. (2022). Advances in Hybrid Composites for Photocatalytic Applications: A Review. *Molecules*, *27*(20). https://doi.org/10.3390/MOLECULES27206828

Pourshaban-Mazandarani, M., & Nasiri, A. (2024). Photocatalytic Degradation of Tetracycline in Wastewater with Bio-based Matrix Magnetic Heterogeneous Nanocatalyst: Performance and Mechanism Study. *Journal of Polymers and the Environment*, 1–25. https://doi.org/10.1007/S10924-024-03340-3/METRICS

Priya, B. S., Avula, B., Palanisamy, A. K., Kumaravel, S., Balu, K., Oh, T. H., Ramasundaram, S., Aldossari, S. A., Kaliyamoorthy, S., & Shanthi, M. (2024). Hydrothermal synthesis of cadmium sulfide decorated reduced graphene oxide photocatalyst for the degradation of photostable naphthol blue black dye. *Diamond and Related Materials*, *148*. https://doi.org/10.1016/j.diamond.2024.111513

Quan, Y., Li, R., Yang, Y., Ding, S., Chen, R., Huang, J., Ng, Y. H., & Lai, Y. (2026). Interface engineered Type-II heterojunction ZnIn2S4/SCN for enhanced photocatalytic H2O2 synthesis from pure water. Acta Physico-Chimica Sinica, 100237. https://doi.org/10.1016/j.actphy.2026.100237

Raeisi-Kheirabadi, N., & Nezamzadeh-Ejhieh, A. (2020). A Z-scheme g-

C3N4/Ag3PO4 nanocomposite: Its photocatalytic activity and capability for water splitting. *International Journal of Hydrogen Energy*, *45*(58), 33381–33395. https://doi.org/10.1016/J.IJHYDENE.2020.09.028

Rajesh, G., Kumar, P. S., Akilandeswari, S., Rangasamy, G., Mandal, A., Shankar, V. U., Ramya, M., Nirmala, K., & Thirumalai, K. (2023). A synergistic consequence of catalyst dosage, pH solution and reactive species of Fe-doped CdAl2O4 nanoparticles on the degradation of toxic environmental pollutants. Chemosphere, 318, 137919. https://doi.org/10.1016/j.chemosphere.2023.137919

Rafaie, H. A., Ramli, N. I. T., Khusaimi, Z., Mohd Sarjidan, M. A., Dulyaseree, P., & Hir, Z. A. M. (2023). Ag2CO3-Based Photocatalyst with Enhanced Photocatalytic Activity for Endocrine-Disrupting Chemicals Degradation: A Review. In *Catalysts* (Vol. 13, Issue 3). MDPI. https://doi.org/10.3390/catal13030540

Rafiq, A., Ikram, M., Ali, S., Niaz, F., Khan, M., Khan, Q., & Maqbool, M. (2021). Photocatalytic degradation of dyes using semiconductor photocatalysts to clean industrial water pollution. *Journal of Industrial and Engineering Chemistry*, *97*, 111–128. https://doi.org/10.1016/J.JIEC.2021.02.017

Rani, M., Keshu, & Shanker, U. (2023). Efficient visible light photocatalytic organic colorants elimination performance induced by biosynthesized titanium dioxide coupled cadmium sulfide nanostructures. *International Journal of Environmental Science and Technology*, *20*(5), 5491–5508. https://doi.org/10.1007/S13762-022-04255-Z/METRICS

Raninga, M., Mudgal, A., Patel, V. K., Patel, J., & Kumar Sinha, M. (2023). Modification of activated carbon-based adsorbent for removal of industrial dyes and heavy metals: A review. *Materials Today: Proceedings*, *77*, 286–294. https://doi.org/10.1016/J.MATPR.2022.11.358

Rey, C., Renugopalakrishman, V., Collins, B., & Glimcher, M. J. (1991). Fourier transform infrared spectroscopic study of the carbonate ions in bone mineral during aging. *Calcified Tissue International*, *49*(4), 251–258. https://doi.org/10.1007/BF02556214

Roškaric, M., Žerjav, G., Zavašnik, J., & Pintar, A. (2022). The influence of synthesis conditions on the visible-light triggered photocatalytic activity of g-C3N4/TiO2 composites used in AOPs. *Journal of Environmental Chemical Engineering*,

10(3), 107656. https://doi.org/10.1016/J.JECE.2022.107656

Roy, M., & Saha, R. (2020). Dyes and their removal technologies from wastewater: A critical review. In *Intelligent Environmental Data Monitoring for Pollution Management* (pp. 127–160). Elsevier. https://doi.org/10.1016/B978-0-12-819671-7.00006-3

Sabzehmeidani, M. M., Ghaedi, M., & Karimi, H. (2021). Photocatalytic activity based on electrospun nanofibers. *Interface Science and Technology*, *32*, 625–672. https://doi.org/10.1016/B978-0-12-818806-4.00014-0

Saeed, M., Muneer, M., Haq, A. ul, & Akram, N. (2021). Photocatalysis: an effective tool for photodegradation of dyes—a review. *Environmental Science and Pollution Research 2021 29:1*, *29*(1), 293–311. https://doi.org/10.1007/S11356-021-16389-7

Saint, U. K., Chandra Baral, S., Sasmal, D., Maneesha, P., Datta, S., Naushin, F., & Sen, S. (2025). Effect of pH on photocatalytic degradation of methylene blue in water by facile hydrothermally grown TiO2 nanoparticles under natural sunlight. *JCIS Open*, *19*, 100150. https://doi.org/10.1016/j.jciso.2025.100150

Saravanan, R., Gracia, F., & Stephen, A. (2017). *Basic Principles, Mechanism, and Challenges of Photocatalysis* (pp. 19–40). https://doi.org/10.1007/978-3-319-62446-4_2

Semnani, D. (2017). Geometrical characterization of electrospun nanofibers. *Electrospun Nanofibers*, 151–180. https://doi.org/10.1016/B978-0-08-100907-9.00007-6

Serpone, N., Borgarello, E., & Grätzel, M. (1984). Visible light induced generation of hydrogen from H2S in mixed semiconductor dispersions; improved efficiency through inter-particle electron transfer. *Journal of the Chemical Society, Chemical Communications*, *6*, 342–344. https://doi.org/10.1039/C39840000342

Shah, N., Li, M., Zhang, P., Cui, Y., & Wang, Y. (2023). Enhanced Photocatalytic Activities of Ag2WO4 Modified Ag6Si2O7 through a Comprehensive p-n Heterojunction S-Scheme Process. Crystals, 13(4), 633. https://doi.org/10.3390/cryst13040633

Shabbir, A., Sardar, S., & Mumtaz, A. (2024). Mechanistic investigations of emerging type-II, Z-scheme and S-scheme heterojunctions for photocatalytic applications – A review. *Journal of Alloys and Compounds*, *1003*, 175683. https://doi.org/10.1016/J.JALLCOM.2024.175683

Shao, B., Liu, X., Liu, Z., Zeng, G., Liang, Q., Liang, C., Cheng, Y., Zhang, W., Liu, Y., & Gong, S. (2019). A novel double Z-scheme photocatalyst Ag3PO4/Bi2S3/Bi2O3 with enhanced visible-light photocatalytic performance for antibiotic degradation. *Chemical Engineering Journal*, *368*, 730–745. https://doi.org/10.1016/J.CEJ.2019.03.013

Sharma, S., Dutta, V., Raizada, P., Hosseini-Bandegharaei, A., Singh, P., & Nguyen, V. H. (2020). Tailoring cadmium sulfide-based photocatalytic nanomaterials for water decontamination: a review. *Environmental Chemistry Letters 2020 19:1*, *19*(1), 271–306. https://doi.org/10.1007/S10311-020-01066-X

Shetty, S. S., D, D., S, H., Sonkusare, S., Naik, P. B., Kumari N, S., & Madhyastha, H. (2023). Environmental pollutants and their effects on human health. *Heliyon*, *9*(9), e19496. https://doi.org/10.1016/J.HELIYON.2023.E19496

Sinar Mashuri, S. I., Kasim, M. F., Mohd Kaus, N. H., Tan, Y. H., Islam, A., Rashid, U., Asikin-Mijan, N., Andas, J., Taufiq-Yap, Y. H., Yaakob, M. K., Wan Ismail, W. I. N., & Ibrahim, M. L. (2023). Photo-response range extension of Z-scheme ZnO/CdS for LED-light-driven photo-active catalyst. *Renewable and Sustainable Energy Reviews*, *184*, 113602. https://doi.org/10.1016/J.RSER.2023.113602

Singh, S., Parveen, S., Clarizia, L., & Kumar, P. (2026). An insight into photo-catalytic degradation mechanism of persistent pollutants with transition metal oxides and their composites: Photocatalysis mechanism, rate affecting parameters, and removal pathways. Catalysis Reviews, 68(1), 220–268. https://doi.org/10.1080/01614940.2024.2440664

Singh, S., Atri, A. K., Qadir, I., Sharma, S., Manhas, U., & Singh, D. (2023). Role of Different Fuels and Sintering Temperatures in the Structural, Optical, Magnetic, and Photocatalytic Properties of Chromium-Containing Nickel Ferrite: Kinetic Study of Photocatalytic Degradation of Rhodamine B Dye. *ACS Omega*, *8*(7), 6302–6317. https://doi.org/10.1021/acsomega.2c06249

Sudha, D., Radha, R., Unnisa, C. N., Jamesh, M., Revathi, A., Hsu, H., & Kirubavathy, S. J. (2026). Evaluation of Physicochemical, Optical, Morphological, and Photocatalytic Properties of Metal Oxide Nanostructures Derived From Metal Organic Hybrids. ChemistrySelect, 11(9). https://doi.org/10.1002/slct.202505333

Tada, H., Mitsui, T., Kiyonaga, T., Akita, T., & Tanaka, K. (2006). All-solid-state Z-

scheme in CdS–Au–TiO2 three-component nanojunction system. *Nature Materials 2006 5:10*, *5*(10), 782–786. https://doi.org/10.1038/nmat1734

Tang, B., Lv, B., Yu, G., Zhang, M., Luo, Q., Li, K., Yin, Z., & Zhang, Z. (2023). Non-noble metal based nickel phosphate decorated CdS nanorods for persistent and efficient solar-to-hydrogen conversion. *Surfaces and Interfaces*, *41*, 103325. https://doi.org/10.1016/j.surfin.2023.103325

Tang, H., Chang, S., Tang, G., & Liang, W. (2017). AgBr and g-C3N4 co-modified Ag2CO3 photocatalyst: A novel multi-heterostructured photocatalyst with enhanced photocatalytic activity. *Applied Surface Science*, *391*, 440–448. https://doi.org/10.1016/J.APSUSC.2016.07.021

Tang, S., Yang, S., Chen, Y., Yang, Y., Li, Z., Zi, L., Liu, Y., Wang, Y., Li, Z., Fu, Z., & Li, Y. (2023). Ionothermally synthesized S-scheme isotype heterojunction of carbon nitride with significantly enhanced photocatalytic performance for hydrogen evolution and carbon dioxide reduction. *Carbon*, *201*, 815–828. https://doi.org/10.1016/J.CARBON.2022.09.071

Teng, C., Chen, Y., Tang, Z., Yuan, W., Zhang, L., Guo, Y., Li, F., & Huang, Q. (2024a). Synthesis of Ag2CO3/TiO2/SiC with pH stability and chloride ion boosted for efficient photodegrading tetracycline under visible light. *Chemical Engineering Journal*, *488*, 150983. https://doi.org/10.1016/J.CEJ.2024.150983

Teng, C., Chen, Y., Tang, Z., Yuan, W., Zhang, L., Guo, Y., Li, F., & Huang, Q. (2024b). Synthesis of Ag2CO3/TiO2/SiC with pH stability and chloride ion boosted for efficient photodegrading tetracycline under visible light. *Chemical Engineering Journal*, *488*, 150983. https://doi.org/10.1016/J.CEJ.2024.150983

Tian, N., Huang, H., He, Y., Guo, Y., & Zhang, Y. (2015). Organic–inorganic hybrid photocatalyst g-C3N4/Ag2CO3 with highly efficient visible-light-active photocatalytic activity. *Colloids and Surfaces A: Physicochemical and Engineering Aspects*, *467*, 188–194. https://doi.org/10.1016/J.COLSURFA.2014.11.049

Tupikina, E. Yu., Korostelev, V. O., Krutin, D. V., & Tolstoy, P. M. (2023). Evolution of vibrational bands upon gradual protonation/deprotonation of arsinic acid H2As(O)OH in media of different polarity. Physical Chemistry Chemical Physics, 25(12), 8664–8675. https://doi.org/10.1039/d2cp06060d

Uddin, F. (2021). Environmental hazard in textile dyeing wastewater from local textile industry. *Cellulose*, *28*(17), 10715–10739. https://doi.org/10.1007/S10570-021-

04228-4/METRICS

Vaya, D., & Surolia, P. K. (2020). Semiconductor based photocatalytic degradation of pesticides: An overview. In *Environmental Technology and Innovation* (Vol. 20). Elsevier B.V. https://doi.org/10.1016/j.eti.2020.101128

Veerasingam, S., & Venkatachalapathy, R. (2014). Estimation of carbonate concentration and characterization of marine sediments by Fourier Transform Infrared Spectroscopy. *Infrared Physics & Technology*, *66*, 136–140. https://doi.org/10.1016/J.INFRARED.2014.06.005

Verre, F., Kumar, K., Berndtsson, R., & Hashemi, H. (2026). Redefining water scarcity through the integrated water strategic resilience index amid climate and conflict pressures. Scientific Reports, 16(1). https://doi.org/10.1038/s41598-026-42170-2

Wang, Y., Du, K., Xu, R., Cui, D., Shi, Y., Hao, W., & Du, Y. (2023). Bismuth-based semiconductor heterostructures for photocatalytic pollution gases removal. Current Opinion in Green and Sustainable Chemistry, 41, 100824. https://doi.org/10.1016/j.cogsc.2023.100824

Wang, J., Xia, Y., Zhao, H., Wang, G., Xiang, L., Xu, J., & Komarneni, S. (2017). Oxygen defects-mediated Z-scheme charge separation in g-C3N4/ZnO photocatalysts for enhanced visible-light degradation of 4-chlorophenol and hydrogen evolution. *Applied Catalysis B: Environmental*, *206*, 406–416. https://doi.org/10.1016/J.APCATB.2017.01.067

Wang, S., Li, D., Sun, C., Yang, S., Guan, Y., & He, H. (2014). Highly efficient photocatalytic treatment of dye wastewater via visible-light-driven AgBr–Ag3PO4/MWCNTs. *Journal of Molecular Catalysis A: Chemical*, *383–384*, 128–136. https://doi.org/10.1016/J.MOLCATA.2013.12.001

Wang, S., Zhu, B., Liu, M., Zhang, L., Yu, J., & Zhou, M. (2019). Direct Z-scheme ZnO/CdS hierarchical photocatalyst for enhanced photocatalytic H2-production activity. *Applied Catalysis B: Environmental*, *243*, 19–26. https://doi.org/10.1016/J.APCATB.2018.10.019

Wang, Y., Yang, X., Ma, Q., Kong, J., Jia, H., Wang, Z., & Yu, M. (2015). Preparation of flower-like CdS with SDBS as surfactant by hydrothermal method and its optical properties. *Applied Surface Science*, *340*, 18–24. https://doi.org/10.1016/J.APSUSC.2015.02.104

Warren, Z., Wenk, J., & Mattia, D. (2023). Increased photocorrosion resistance of ZnO

foams via transition metal doping. *RSC Advances*, *13*(4), 2438–2450. https://doi.org/10.1039/d2ra06730g

Wei, P., Yin, S., Zhou, T., Peng, C., Xu, X., Lu, J., Liu, M., Jia, J., & Zhang, K. (2021). Rational design of Z-scheme ZnFe2O4/Ag@Ag2CO3 hybrid with enhanced photocatalytic activity, stability and recovery performance for tetracycline degradation. *Separation and Purification Technology*, *266*, 118544. https://doi.org/10.1016/J.SEPPUR.2021.118544

Wei, T., Gao, S., Wang, Q., Xu, H., Wang, Z., Huang, B., & Dai, Y. (2017). Transformation from Ag@Ag3PO4 to Ag@Ag2SO4 hybrid at room temperature: preparation and its visible light photocatalytic activity. *Journal of Nanoparticle Research*, *19*(2), 1–13. https://doi.org/10.1007/S11051-016-3726-1/METRICS

Wen, Y., Wang, Z., Cai, Y., Song, M., Qi, K., & Xie, X. (2022). S-scheme BiVO4/CQDs/β-FeOOH photocatalyst for efficient degradation of ofloxacin: Reactive oxygen species transformation mechanism insight. *Chemosphere*, *295*, 133784. https://doi.org/10.1016/J.CHEMOSPHERE.2022.133784

Wu, F., Li, X., Liu, W., & Zhang, S. (2017). Highly enhanced photocatalytic degradation of methylene blue over the indirect all-solid-state Z-scheme g-C3N4-RGO-TiO2 nanoheterojunctions. *Applied Surface Science*, *405*, 60–70. https://doi.org/10.1016/J.APSUSC.2017.01.285

Xia, Z., Wang, L., Tan, W., Yuan, L., He, X., Wang, J., Chen, L., Zeng, S., Lu, S., & Jiao, Z. (2024). Visible-Light Photocatalytic Degradation Efficiency of Tetracycline and Rhodamine B Using a Double Z-Scheme Heterojunction Catalyst of UiO-66-NH2/BiOCl/Bi2S3. *Inorganic Chemistry*, *63*(31), 14578–14590. https://doi.org/10.1021/ACS.INORGCHEM.4C01917/ASSET/IMAGES/LARGE/IC4C01917_0010.JPEG

Xie, Z. H., Wen, Y., Yao, H., Liu, Y., Yu, G., & Zhong, C. J. (2025). A Z-scheme g-C3N4/TiO2 heterojunction for enhanced performance in protecting magnesium and nickel couple from galvanic corrosion. *Journal of Alloys and Compounds*, *1010*. https://doi.org/10.1016/j.jallcom.2024.177463

Xu, G., Du, M., Li, T., Guan, Y., & Guo, C. (2021). Facile synthesis of magnetically retrievable Fe3O4/BiVO4/CdS heterojunction composite for enhanced photocatalytic degradation of tetracycline under visible light. *Separation and*

Purification Technology, *275*, 119157. https://doi.org/10.1016/J.SEPPUR.2021.119157

Xu, Q., Zhang, L., Cheng, B., Fan, J., & Yu, J. (2020). S-Scheme Heterojunction Photocatalyst. *Chem*, *6*(7), 1543–1559. https://doi.org/10.1016/J.CHEMPR.2020.06.010

Xu, Q., Zhang, L., Yu, J., Wageh, S., Al-Ghamdi, A. A., & Jaroniec, M. (2018). Direct Z-scheme photocatalysts: Principles, synthesis, and applications. *Materials Today*, *21*(10), 1042–1063. https://doi.org/10.1016/J.MATTOD.2018.04.008

Yang, J., Liang, J., Yang, G., Feng, Y., Ren, G., Ren, C., Han, X., & Wang, X. (2020). Characteristics of Non-Point Source Pollution under Different Land Use Types. *Sustainability 2020, Vol. 12, Page 2012*, *12*(5), 2012. https://doi.org/10.3390/SU12052012

Yang, S., Li, K., Feng, W., Huang, P., Liu, K., Zhuo, Y., Li, W., Yang, Z., & Han, D. (2025). Engineering a ZnO/Ag2CO3/Ag2O Ternary Heterojunction: Dual Z-Scheme Photocatalytic Pathway for Enhanced Pollutants Degradation. *Langmuir*, *41*(15), 9618–9630. https://doi.org/10.1021/ACS.LANGMUIR.4C04526

Yap, C. K., Peng, S. H. T., & Leow, C. S. (2019). Contamination in Pasir Gudang Area, Peninsular Malaysia: What can we learn from Kim Kim River chemical waste contamination? *Journal of Humanities and Education Development*, *1*(2), 82–87. https://doi.org/10.22161/jhed.1.2.4

Yin, H., Liu, J., Shi, H. L., Sun, L., Yuan, X., & Xia, D. (2022). Highly efficient catalytic ozonation for oxalic acid mineralization with Ag2CO3 modified g-C3N4: Performance and mechanism. *Process Safety and Environmental Protection*, *162*, 944–954. https://doi.org/10.1016/J.PSEP.2022.04.060

Yusoff, N. R., Lim, P. W., Azmi, N. A. B., Yusoff, M., & Muhammad, M. (2021). Effect of photocatalyst dosage and air loading in photocatalytic degradation of metamifop. IOP Conference Series: Earth and Environmental Science, 842(1), 012061. https://doi.org/10.1088/1755-1315/842/1/012061

Yu, C., Chen, X., Li, N., Zhang, Y., Li, S., Chen, J., Yao, L., Lin, K., Lai, Y., & Deng, X. (2022). Ag3PO4-based photocatalysts and their application in organic-polluted wastewater treatment. *Environmental Science and Pollution Research*, *29*(13), 18423–18439. https://doi.org/10.1007/S11356-022-18591-7/METRICS

Yu, X., Qiu, H., Wang, B., Meng, Q., Sun, S., Tang, Y., & Zhao, K. (2020). A ternary

photocatalyst of all-solid-state Z-scheme TiO2–Au–BiOBr for efficiently degrading various dyes. *Journal of Alloys and Compounds*, *839*, 155597. https://doi.org/10.1016/J.JALLCOM.2020.155597

Zahedifar, M., Seyedi, N., & Razavi, R. (2024). In situ fabrication of Ag2S/Ag2SO4 on the chitosan NP matrix for enhanced photodegradation of rhodamine B dye contaminant under visible light. *Biomass Conversion and Biorefinery*, *14*(9), 10011–10026. https://doi.org/10.1007/S13399-022-03094-9/METRICS

Zarghami, Z., Maddahfar, M., & Ramezani, M. (2015). Ag@Ag2SO4 nanoparticles: simple microwave-assistance synthesis, characterization and its co-photocatalytic degradation of methylene blue. *Journal of Materials Science: Materials in Electronics*, *26*(9), 6339–6343. https://doi.org/10.1007/s10854-015-3221-y

Zhang, S., Wang, J., Chen, S., Li, R., & Peng, T. (2019). Construction of Ag2S/WO3 Direct Z-Scheme Photocatalyst for Enhanced Charge Separation Efficiency and H2 Generation Activity. Industrial & Engineering Chemistry Research, 58(32), 14802–14813. https://doi.org/10.1021/acs.iecr.9b02335

Zhang, Y., Wang, Y., Wu, X., Li, T., Zhao, F., Tan, J., Liu, M., & Huang, H. (2025). Photocorrosion of metal sulfides: Mechanism, characterization, anti-photocorrosion strategies and solar catalysis applications. Coordination Chemistry Reviews, 545, 217021. https://doi.org/10.1016/j.ccr.2025.217021

Zhang, D., Zhang, X., Xia, D., Li, J., Zhang, W., Liu, D., Lan, Y., Guo, M., & Dong, G. (2025). A novel dual Z-scheme BiOBr/Bi-MOF/AgFeO2 heterojunction for activating peroxymonosulfate toward efficient photocatalytic removal of levofloxacin. *Applied Surface Science*, *710*, 163895. https://doi.org/10.1016/J.APSUSC.2025.163895

Zhang, J., Yang, D., Shi, J., Wang, Z., Zhu, W., Wang, Y., & Chen, Z. (2022). Improving oxygen evolution activity by constructing a perylene imide based Z-scheme heterojunction. *Journal of Materials Chemistry A*, *10*(27), 14513–14528. https://doi.org/10.1039/D2TA01999J

Zhang, M., Yin, H. fei, Yao, J. cheng, Arif, M., Qiu, B., Li, P. fei, & Liu, X. heng. (2020). All-solid-state Z-scheme BiOX(Cl, Br)-Au-CdS heterostructure: Photocatalytic activity and degradation pathway. *Colloids and Surfaces A: Physicochemical and Engineering Aspects*, *602*, 124778. https://doi.org/10.1016/J.COLSURFA.2020.124778

Zhang, W., Xiong, J., Li, S., & Li, W. (2025). 1D-2D Z-scheme junction by coupling CaTiO3 rectangular nanorods with CdS nanosheets enhances photocatalytic hydrogen evolution. *Molecular Catalysis*, *570*. https://doi.org/10.1016/j.mcat.2024.114701

Zhang, Z., Ji, R., Sun, Q., He, J., Chen, D., Li, N., Li, H., Marcomini, A., Xu, Q., & Lu, J. (2023). Enhanced photocatalytic degradation of 2-chlorophenol over Z-scheme heterojunction of CdS-decorated oxygen-doped g-C3N4 under visible-light. *Applied Catalysis B: Environmental*, *324*, 122276. https://doi.org/10.1016/J.APCATB.2022.122276

Zhong, Y., Zhu, H., Xie, X., Yang, L., Shen, Y., Fan, Q., Xie, Z., & Le, Z. (2025). All-Solid-State Z-Scheme CsPbBr3/Au/g-C3N4 Heterojunctions for Enhanced Photocatalytic C–H Oxidation. Inorganic Chemistry, 64(6), 2706–2715. https://doi.org/10.1021/acs.inorgchem.4c04472

Zhu, J., Liao, M., Zhao, C., Liu, M., Han, A., Zhu, C., Sun, Y., Zhao, M., Ye, S., & Cao, H. (2023). A comprehensive review on semiconductor-based photocatalysts toward the degradation of persistent pesticides. *Nano Research*, *16*(5), 6402–6443. https://doi.org/10.1007/S12274-023-5428-6/METRICS

Zhu, X., Qiu, F., Li, X., Rong, X., Wang, J., & Yang, D. (2017). Silver carbonate loaded on activated carbon composite photocatalyst with enhanced photocatalytic activity under visible light irradiation. *Materials Technology*, *32*(1), 38–45. https://doi.org/10.1080/10667857.2015.1116219

Zhu, Z., Murugananthan, M., Gu, J., & Zhang, Y. (2018). Fabrication of a Z-Scheme g-C3N4/Fe-TiO2 Photocatalytic Composite with Enhanced Photocatalytic Activity under Visible Light Irradiation. *Catalysts 2018, Vol. 8, Page 112*, *8*(3), 112. https://doi.org/10.3390/CATAL8030112

Zulfiqar, S., Liu, S., Rahman, N., Tang, H., Shah, S., Yu, X. H., & Liu, Q. Q. (2021). Construction of S-scheme MnO2@CdS heterojunction with core–shell structure as H2-production photocatalyst. *Rare Metals*, *40*(9), 2381–2391. https://doi.org/10.1007/S12598-020-01616-W/METRICS

Zyoud, A., Zyoud, A. H., Zyoud, S. H., Nassar, H., Zyoud, S. H., Qamhieh, N., Hajamohideen, A. R., & Hilal, H. S. (2023). Photocatalytic degradation of aqueous methylene blue using ca-alginate supported ZnO nanoparticles: point of zero charge role in adsorption and photodegradation. *Environmental Science and Pollution Research*, *30*(26), 68435–68449. https://doi.org/10.1007/S11356-023-

APPENDICES

APPENDIX

Calculation of CB and VB Level

The band edge positions of CB and VB can be calculated by using the following equations:

$$E_{CB} = X - E_C - \frac{1}{2} E_g$$
$$E_{VB} = E_{CB} + E_g$$

Where;

X – Electronegativity of the semiconductor

E_c – Energy of the free electrons on the hydrogen scale (~ 4.5eV)

E_g – Band gap of the semiconductor

$X - \frac{1}{2} (E_{EA} + E_{ion})$ Where.

E_{EA} – Electron affinity

E_{ion} – First ionization energy from periodic table

Calculation for: Ag_2CO_3

Ag	C	O
$E_{EA} = \frac{125.6\ kJ/mol}{96.48\ kJ/mol}$	$E_{EA} = \frac{153.9\ kJ/mol}{96.48\ kJ/mol}$	$E_{EA} = \frac{141\ kJ/mol}{96.48\ kJ/mol}$
= 1.30 eV	= 1.59 eV	= 1.46 eV
$E_{ion} = \frac{731\ kJ/mol}{96.48\ kJ/mol}$	$E_{ion} = \frac{1086.45\ kJ/mol}{96.48\ kJ/mol}$	$E_{ion} = \frac{1313.9\ kJ/mol}{96.48\ kJ/mol}$
= 7.58 eV	= 11.26 eV	= 13.62
$X_{Ag} = \frac{1}{2}$ (1.30 + 7.58)	$X_{Ag} = \frac{1}{2}$ (1.59 + 11.26)	$X_{Ag} = \frac{1}{2}$ (1.46 + 13.62)
= 4.44eV	= 6.425eV	= 7.54eV

Determine electronegativity of Ag_2CO_3

$X_{Ag2CO3} = (X_{Ag}^2 \times X_C \times X_O^3)^{1/6}$

$X_{Ag2CO3} = (4.44^2 \times 6.425 \times 7.54^3)^{1/6}$

= 6.15

Determine the CB Level	Determine the VB Level
$E_{CB} = X - E_c - \frac{1}{2} E_g$ $E_{CB} = 6.15 - 4.5 - \frac{1}{2}$ (2.37) E_{CB} = 0.465 eV	$E_{VB} = E_{CB} + E_g$ E_{VB} = 0.465 + 2.37

	= 2.835 eV

Calculation for: CdS

Cd	S
$E_{EA} = \frac{0\ kJ/mol}{96.48\ kJ/mol}$ = 0.00 eV $E_{ion} = \frac{867.8\ kJ/mol}{96.48\ kJ/mol}$ = 8.99 eV X_{Ag} = ½ (0.00 + 8.99) = 4.495eV	$E_{EA} = \frac{-200\ kJ/mol}{96.48\ kJ/mol}$ = - 2.07 eV $E_{ion} = \frac{999.6\ kJ/mol}{96.48\ kJ/mol}$ = 10.36 eV X_{Ag} = ½ (-2.07 + 10.36) = 4.145 eV
Determine electronegativity of CdS $X_{CdS} = (X_{Cd} \times X_s)^{1/2}$ $X_{CdS} = (4.495 \times 4.145)^{1/2}$ = 4.32	
Determine the CB Level $E_{CB} = X - E_c - ½\ E_g$ E_{CB} = 4.32 – 4.5 – ½ (2.19) E_{CB} = -1.275eV	Determine the VB Level $E_{VB} = E_{CB} + E_g$ E_{VB} = -1.275 + 2.19 = 0.915 eV

AUTHOR'S PROFILE

Ommy Madina binti Abdul Halim has successfully graduated with the First Class Honour in Bachelor of Science in Applied Chemistry (2023) from Universiti Teknologi MARA, Campus Arau, Perlis Branch. Presently, she is completing his study MSc in Applied Chemistry (2026) from Universiti Teknologi MARA with the study are of Environmental Chemistry. Specifically, she explored the photocatalyst materials such as silver oxosalts and other catalysts to encounter the wastewater problem such as dye , pharmaceutical waste and organic pollutants. With the experience as Graduate Research Assistant for FRGS Granted, she managed to experience few scientific datasets includes X-Ray diffraction (XRD), transmission-electron microscopy (TEM), Field emission scanning electron microscopy (FESEM), Fourier transform infrared (FTIR) spectroscopy, X-ray photoelectron spectroscopy (XPS) and Ultra-violet visible diffuse reflectance spectroscopy (UV-Vis/DRS), Photoluminescence (PL) and N_2 Physisorption. In addition, she also actively reviewed few journals and paper as the reviewer such as Materials Letter.

LIST OF PUBLICATION

Halim, O. M. A., Mustapha, N. H., Mohd Fudzi, S. N., Azhar, R., Zanal, N. I. N., Nazua, N. F., Nordin, A. H., Mohd Azami, M. S., Mohd Ishak, M. A., Ismail, W. I. N. W., & Ahmad, Z. (2025). A review on modified ZnO for the effective degradation of methylene blue and rhodamine B. Results in Surfaces and Interfaces, 18, 100408. https://doi.org/10.1016/J.RSURFI.2024.100408

Halim, O. M., Haslinda, H. , Ahmad, Z. , Nawawi, W. I. , Tan, K. H. , Jamaluddin, N. , Izzudin, N. M. , Jalil, A. A. , Azmi, A. A. and Azami, M. S. (2025). Preparation of Silver Phosphate/Graphitic Carbon Nitride via Microwave Irradiation for Photodegradation of Rhodamine B. Malaysian Journal of Chemistry, 2025, Vol. 27(3), 38-47. https://doi.org/10.55373/mjchem.v27i3.38

Zanal, N. I. N., Ghani Abdul, N. I., Hamzah, S. R., Mustapha, N. H., Halim Abdul, O. M., Nazua, N. F., Roslan, N. I., Ahmad, Z., Abdullah, M. F., & Wan Ismail, W. I. N. (2024). Immobilised Ag-Tio 2 /Enr/Pvc Using Reversed Photodeposition Method For Photocatalytic Degradation Of Methylene Blue DYE. Malaysian Journal of Analytical Sciences, 28(5), 1169–1183. https://www.researchgate.net/publication/387872163

Suhaimi, N. H. S., Azhar, R., Adzis, N. S., Mohd Ishak, M. A., Ramli, M. Z., Hamzah, M. Y., Ismail, K., & Nawawi, W. I. (2025). Recent updates on TiO2-based materials for various photocatalytic applications in environmental remediation and energy production. Desalination and Water Treatment, 321, 100976. https://doi.org/10.1016/J.DWT.2024.100976

LIST OF CONFERENCE

Halim, O. M., S. N., Azhar, R., Zanal, N. I. N., Nazua, N. F., Nordin, A. H., Mohd Azami, M. S (2023, August 23). Effect of Various Dyes on Pt Doped TiO_2 for Hydrogen Production Under Photo Electrochemistry Process. ISTEC 2023, Bayview Pulau Pinang, Malaysia.

Halim, O. M., S. N., Azhar, R., Zanal, N. I. N., Nazua, N. F., Nordin, A. H., Mohd Azami, M. S. (2024, October 9-10). Structural properties of Ag_2CO_3/CdS for Enhanced Photocatalytic Degradation towards Methyl Orange. I-COSTECH 2024. UiTM Perlis Branch, Perlis, Malaysia

LIST OF INNOVATION AND EXHIBITION

Halim, O. M. A., Azhar, R., Suhaimi, N. H. S., Adzis, N. S., Zanal., N. F., Nordin, A. H., Mohd Azami, M. S., Mohd Ishak, M. A., Ismail, W. I. N. W., & Ahmad, Z.(2025). Z-Catalytex : The Future of Clean Water Starts Here. 7th International Innovation, Design, and Articulation (i-IDeA 2025). UiTM Perlis Branch, Perlis, Malaysia.

Halim, O. M. A., Azhar, R., Suhaimi, N. H. S., Adzis, N. S., Zanal., N. F., Nordin, A. H., Mohd Azami, M. S., Mohd Ishak, M. A., Ismail, W. I. N. W., & Ahmad, Z. (2024). GET: A Smart Wastewater System for Water Remediation. Invention, Innovation, Design and Exposition, IIDEX 2024. UiTM Selangor Branch, Puncak Alam, Malaysia.

Halim, O. M. A., Azhar, R., Suhaimi, N. H. S., Adzis, N. S., Zanal., N. F., Nordin, A. H., Mohd Azami, M. S., Mohd Ishak, M. A., Ismail, W. I. N. W., & Ahmad, Z. (2024). STH: Solar to Hydrogen for Photocatalytic Water Splitting. International Innovation and Invention Competition Through Exhibition, iCOMPEX 2024. Politeknik Sultan Abdul Halim Muadzam Shah, Kedah, Malaysia.

Halim, O. M. A., Azhar, R., Suhaimi, N. H. S., Adzis, N. S., Zanal., N. F., Nordin, A. H., Mohd Azami, M. S., Mohd Ishak, M. A., Ismail, W. I. N. W., & Ahmad, Z. (2024). PEC Process: A Novel Continuous Treatment System for Efficient Wastewater Treatment. Symposium of Innovation and Creativity (SIC 14). UiTM Perlis Branch, Perlis, Malaysia.

Halim, O. M. A., Azhar, R., Suhaimi, N. H. S., Adzis, N. S., Zanal., N. F., Nordin, A. H., Mohd Azami, M. S., Mohd Ishak, M. A., Ismail, W. I. N. W., & Ahmad, Z. (2024). ARAUCAT: A Novel Photocatalyst for Green Hydrogen Production. Symposium of Innovation and Creativity (SIC 14). UiTM Perlis Branch, Perlis, Malaysia.

Halim, O. M. A., Azhar, R., Suhaimi, N. H. S., Adzis, N. S., Zanal., N. F., Nordin, A. H., Mohd Azami, M. S., Mohd Ishak, M. A., Ismail, W. I. N. W., & Ahmad, Z. (2023). ARAUCAT: Novel Hydrogen Production from Water splitting. Thailand Inventor's Day, IPITEX 2023, Bangkok, Thailand.

Halim, O. M. A., Azhar, R., Suhaimi, N. H. S., Adzis, N. S., Zanal., N. F., Nordin, A. H., Mohd Azami, M. S., Mohd Ishak, M. A., Ismail, W. I. N. W., & Ahmad, Z. (2023). Germicidal and Electrocoagulation Treatment (GET). Malaysia Technology Expo. MTE 2023. World Trade Centre, Kuala Lumpur, Malaysia.

Halim, O. M. A., Azhar, R., Suhaimi, N. H. S., Adzis, N. S., Zanal., N. F., Nordin., A. H, Rosli, M.A., Hamzah, S.R., Mohamad., N.A., Mohd Azami, M. S., Mohd Ishak, M. A., Ismail, W. I. N. W., & Ahmad, Z (2023). PECA: A Smart Wastewater Treatment. Penang International Invention, Invention and Design, PIID 2023, UiTM Penang Branch, Permatang Pauh, Malaysia.

Halim, O. M. A., Azhar, R., Suhaimi, N. H. S., Adzis, N. S., Zanal., N. F., Nordin., A. H, Rosli, M.A., Hamzah, S.R., Mohamad., N.A., Mohd Azami, M. S., Mohd Ishak, M. A., Ismail, W. I. N. W., & Ahmad, Z (2023). PECA System: A Synergistic Eco-Friendly Wastewater. SIRIM Invention, Innovation & Technology Expo, SIRIM Penang, Permatang Pauh, Malaysia.